USGS
science for a changing world

Prepared in cooperation with U.S. Bureau of Reclamation and the San Luis and Delta-Mendota Water Authority

Land Subsidence along the Delta-Mendota Canal in the Northern Part of the San Joaquin Valley, California, 2003–10

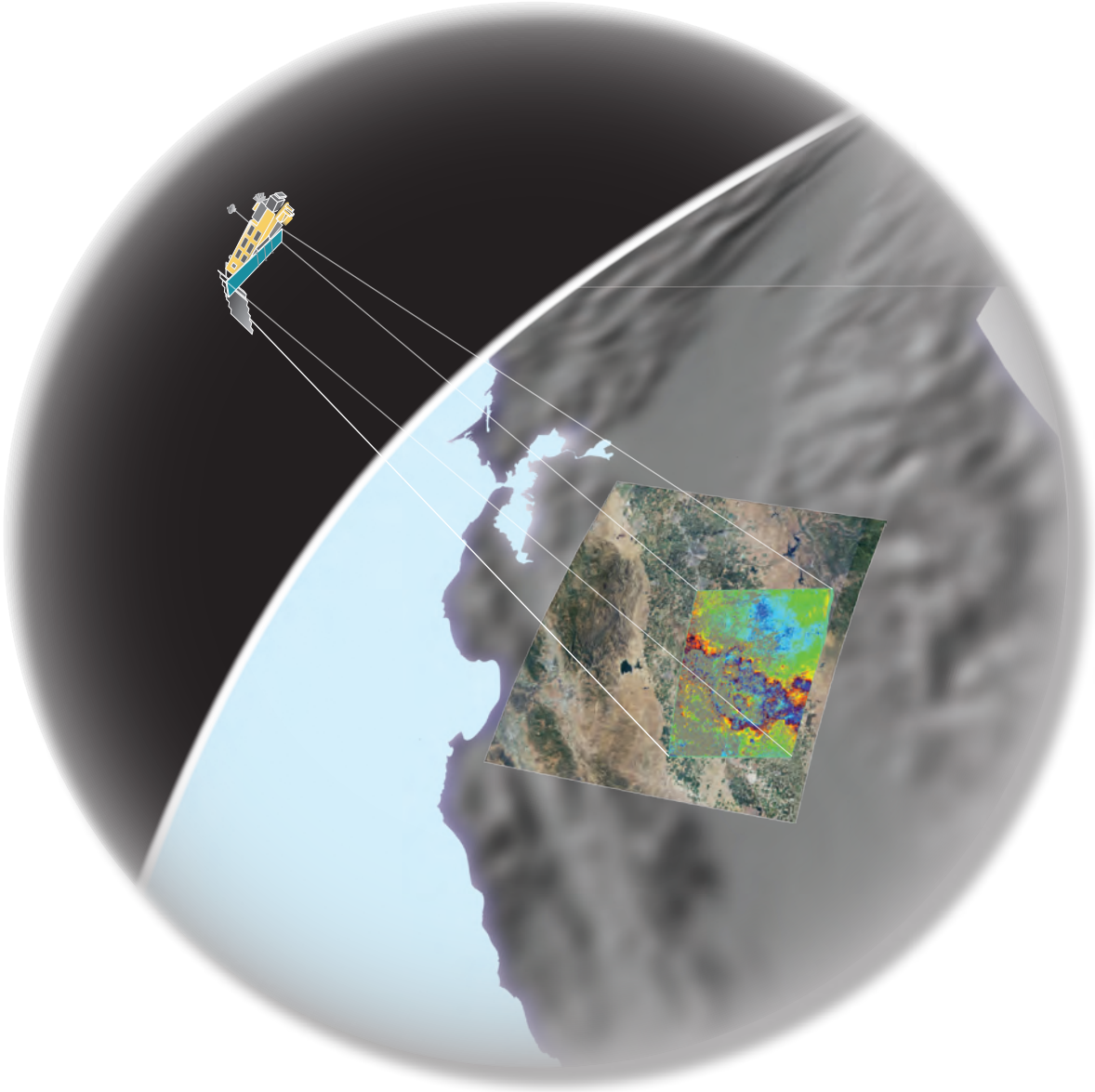

Scientific Investigations Report 2013-5142

U.S. Department of the Interior
U.S. Geological Survey

Cover. Schematic rendering of ENVIronmental SATellite (ENVISAT) data collection from earth orbit.

Land Subsidence along the Delta-Mendota Canal in the Northern Part of the San Joaquin Valley, California, 2003–10

By Michelle Sneed, Justin Brandt, and Mike Solt

Prepared in cooperation with the U.S. Bureau of Reclamation and the San Luis and Delta-Mendota Water Authority

Scientific Investigations Report 2013–5142

U.S. Department of the Interior
U.S. Geological Survey

U.S. Department of the Interior
SALLY JEWELL, Secretary

U.S. Geological Survey
Suzette M. Kimball, Acting Director

U.S. Geological Survey, Reston, Virginia: 2013

Suggested citation:
Sneed, Michelle, Brandt, Justin, and Solt, Mike, 2013, Land subsidence along the Delta-Mendota Canal in the northern part of the San Joaquin Valley, California, 2003–10: U.S. Geological Survey Scientific Investigations Report 2013–5142, 87 p., *http://dx.doi.org/10.3133/sir20135142*

Contents

Contents

Figures

Figures—Continued

Table

Conversion Factors

SI to Inch/Pound

Multiply	By	To obtain
	Length	
millimeter (mm)	0.03937	inch (in.)
meter (m)	3.281	foot (ft)
kilometer (km)	0.6214	mile (mi)
meter (m)	1.094	yard (yd)
	Area	
square kilometer (km^2)	247.1	acre
square kilometer (km^2)	0.3861	square mile (mi^2)
	Flow rate	
millimeter per year (mm/yr)	0.03937	inch per year (in/yr)

Temperature in degrees Celsius (°C) may be converted to degrees Fahrenheit (°F) as follows:

°F=(1.8×°C)+32

Horizontal coordinate information is referenced to the North American Datum of 1983 (NAD 83).

Vertical coordinate information is referenced to the National Geodetic Vertical Datum of 1929 (NGVD 29).

Altitude, as used in this report, refers to distance above the vertical datum.

Abbreviations

ALOS	Advanced Land Observing Satellite
ASAR	Advanced Synthetic Aperture Radar
Caltrans	California Department of Transportation
CCID	Central California Irrigation District
CGPS	Continuous Global Positioning System
DMC	Delta-Mendota Canal
DWR	California Department of Water Resources
ENVISAT	ENVIronmental SATellite
ESA	European Space Agency
GPS	Global Positioning System
InSAR	Interferometric Synthetic Aperture Radar
JAXA	Japanese Aerospace eXploration Agency
MODIS	MODerate resolution Imaging Spectroradiometer
NAIP	National Agriculture Imagery Program
NASA	National Aeronautics and Space Administration
NAVSTAR	Navigation Satellite Timing and Ranging
NGS	National Geodetic Survey
PALSAR	Phased Array L-band Synthetic Aperture Radar
PS	persistent scatterer
PVC	polyvinyl-chloride
Reclamation	U.S. Bureau of Reclamation
SAR	Synthetic Aperture Radar
SLDMWA	San Luis and Delta-Mendota Water Authority
SNARF	Stable North American Reference Frame
UNAVCO	University Navigation Satellite Timing and Ranging Consortium
USGS	U.S. Geological Survey

Well-Numbering System

Wells are identified and numbered according to their location in the rectangular system for the subdivision of public lands. Identification consists of the township number, north or south; the range number, east or west; and the section number. Each section is divided into sixteen 40-acre tracts lettered consecutively (except I and O), beginning with "A" in the northeast corner of the section and progressing in a sinusoidal manner to "R" in the southeast corner. Within the 40-acre tract, wells are sequentially numbered in the order they are inventoried. The final letter refers to the base line and meridian. In California, there are three base lines and meridians; Humboldt (H), Mount Diablo (M), and San Bernardino (S). All wells in the study area are referenced to the Mount Diablo base line and meridian (M). Well numbers consist of 15 characters and follow the format 005S006E23K002M. In this report, well numbers are abbreviated and written 5S/6E-23K2. Wells in the same township and range are referred to only by their section designation, -23K2. The following diagram shows how the number for well 5S/6E-23K2 is derived.

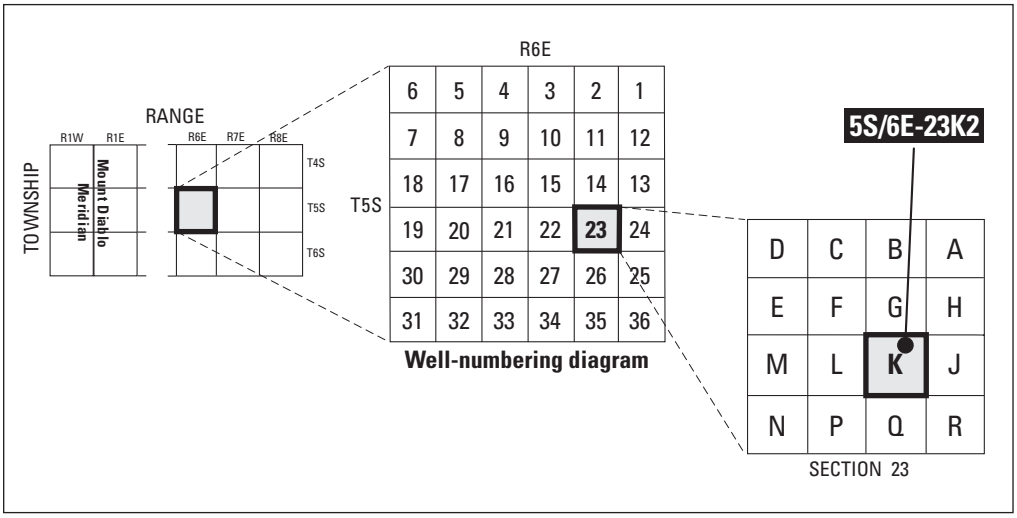

Acknowledgements

This study was done in cooperation with the U.S. Bureau of Reclamation and the San Luis and Delta-Mendota Water Authority; the authors gratefully acknowledge their support and assistance during this study. The authors specifically acknowledge Matt Costa, Pat Nacci, and especially Mark Walsh, all from the San Luis and Delta-Mendota Water Authority, who were instrumental in setting the extensometer steel components, including reference tables, I-beams, and counterweight assemblies. Mark also assisted this project by modifying wellheads, fabricating and installing secure enclosures to house groundwater-level monitoring equipment, and welding steel structures at three extensometer sites. Mark's can-do attitude, ingenuity, and attention to the smallest of details were essential to the success of this project. The authors also gratefully acknowledge Rod Sorenson from California State University, Sacramento, for his innovative fabrication of extensometer components. His thoughtful consideration of project requirements and precise machining of the components resulted in state-of-the-art measurement systems for 50-year-old extensometers.

We thank the University NAVSTAR Consortium (UNAVCO) for allowing free access to continuous GPS data. Radar data used to produce the interferograms shown in this report were acquired by the European Space Agency and the Japanese Aerospace eXploration Agency and distributed by WinSAR, GeoEarthScope, and the Alaska SAR Facility for purposes of research and development. Leveling surveys along Highway 152 were done by Caltrans and published by the National Geodetic Survey (NGS). The GPS surveys along the California Aqueduct were provided by the California Department of Water Resources. Leveling and GPS surveys along the Delta-Mendota Canal were done by the California Department of Water Resources and various private contractors, and provided by Chris White, general manager of the Central California Irrigation District. Fordel extensometer data and water-level data from well 13S/15E-31J6 were provided by Luhdorff & Scalmanini Consulting Engineers. Water-level data for wells MW-1 and MW-3 were provided by the City of Tracy.

This page intentionally left blank.

Land Subsidence along the Delta-Mendota Canal in the Northern Part of the San Joaquin Valley, California, 2003–10

By Michelle Sneed, Justin Brandt, and Mike Solt

Abstract

Extensive groundwater withdrawal from the unconsolidated deposits in the San Joaquin Valley caused widespread aquifer-system compaction and resultant land subsidence from 1926 to 1970—locally exceeding 8.5 meters. The importation of surface water beginning in the early 1950s through the Delta-Mendota Canal and in the early 1970s through the California Aqueduct resulted in decreased pumping, initiation of water-level recovery, and a reduced rate of compaction in some areas of the San Joaquin Valley. However, drought conditions during 1976–77 and 1987–92, and drought conditions and regulatory reductions in surface-water deliveries during 2007–10, decreased surface-water availability, causing pumping to increase, water levels to decline, and renewed compaction. Land subsidence from this compaction has reduced freeboard and flow capacity of the Delta-Mendota Canal, the California Aqueduct, and other canals that deliver irrigation water and transport floodwater.

The U.S. Geological Survey, in cooperation with the U.S. Bureau of Reclamation and the San Luis and Delta-Mendota Water Authority, assessed land subsidence in the vicinity of the Delta-Mendota Canal as part of an effort to minimize future subsidence-related damages to the canal. The location, magnitude, and stress regime of land-surface deformation during 2003–10 were determined by using extensometer, Global Positioning System (GPS), Interferometric Synthetic Aperture Radar (InSAR), spirit leveling, and groundwater-level data. Comparison of continuous GPS, shallow extensometer, and groundwater-level data, combined with results from a one-dimensional model, indicated the vast majority of the compaction took place beneath the Corcoran Clay, the primary regional confining unit.

Land-surface deformation measurements indicated that much of the northern portion of the Delta-Mendota Canal (Clifton Court Forebay to Check 14) was fairly stable or minimally subsiding on an annual basis; some areas showed seasonal periods of subsidence and of uplift that resulted in little or no longer-term elevation loss. Many groundwater levels in this northern area did not reach historical lows during 2003–10, indicating that deformation in this region was primarily elastic.

Although the northern portion of the Delta-Mendota Canal was relatively stable, land-surface deformation measurements indicated the southern portion of the Delta-Mendota Canal (Checks 15–21) subsided as part of a large subsidence feature centered about 15 kilometers northeast of the Delta-Mendota Canal, south of the town of El Nido. Results of InSAR analysis indicated at least 540 millimeters of subsidence near the San Joaquin River and the Eastside Bypass during 2008–10, which is part of a 3,200 square-kilometer area—including the southern part of the Delta-Mendota Canal—affected by 20 millimeters or more of subsidence during the same period. Calculations indicated that the subsidence rate doubled in 2008 in some areas. The GPS surveys done in 2008 and 2010 confirmed the high subsidence rate measured by using InSAR for the same period. Water levels in many shallow and deep wells in this area declined during 2007–10; water levels in many deep wells reached historical lows, indicating that subsidence measured during this period was largely inelastic. InSAR-derived subsidence maps for various periods during 2003–10 showed that the area of maximum active subsidence (that is, the largest rates of subsidence) shifted from its historical (1926–70) location southwest of Mendota to south of El Nido.

Continued groundwater-level and land-subsidence monitoring in the San Joaquin Valley is important because (1) regulatory- and drought-related reductions in surface-water deliveries since 1976 have resulted in increased groundwater pumping and associated land subsidence, and (2) land use and associated groundwater pumping continue to change throughout the valley. The availability of surface water remains uncertain; even during record-setting precipitation years, such as 2010–11, water deliveries have fallen short of requests and groundwater pumping was required to meet the irrigation demand. Due to the expected continued demand for irrigation supply water and the limitations and uncertainty of surface-water supplies, groundwater pumping and associated land subsidence is likely to continue in the future. Spatially detailed information on land subsidence is needed to facilitate minimization of future subsidence-related damages to the Delta-Mendota Canal and other infrastructure in the San Joaquin Valley. The integration of subsidence, deformation, and water-level measurements—particularly continuous measurements—enables the analysis of aquifer-system response to increased groundwater pumping, which in turn, enables identification of the preconsolidation head and calculation of aquifer-system storage properties. This information can be used to improve numerical model simulations of groundwater flow and aquifer-system compaction and allow for consideration of land subsidence in the evaluation of water-resource management alternatives.

Introduction

The San Joaquin Valley, a broad alluviated structural trough constituting the southern two-thirds of the Central Valley of California, is 400 kilometers (km) long, averages 65 km in width, and covers 26,000 square kilometers (km^2), excluding the rolling foothills of the Sierra Nevada, Tehachapi Mountains, and the Coast Ranges that skirt the valley on three sides (fig. 1). The study area includes the part of the valley from Tracy on the north to Huron on the south (fig. 1).

The extensive withdrawal of groundwater from the unconsolidated deposits of the San Joaquin Valley has caused widespread land subsidence—locally exceeding 8.5 meters (m) between 1926 and 1970 (Poland and others, 1975; fig. 2), and reaching 9 m by 1981 (Ireland, 1986). Long-term groundwater-level declines can result in a vast one-time release of "water of compaction" from compacting silt and clay layers (aquitards), which causes land subsidence (Galloway and others, 1999). Land subsidence from groundwater pumping began in the mid-1920s (Poland and others, 1975; Bertoldi and others, 1991; Galloway and Riley, 1999), and by 1970, about half of the San Joaquin Valley, or about 13,500 km^2 had land subsidence of more than 0.3 m (Poland and others, 1975; fig. 2).

Surface-water imports from the Central Valley Project's Delta-Mendota Canal (DMC) since the early 1950s and the State Water Project's California Aqueduct since the early 1970s resulted in a decrease in groundwater pumping in some parts of the valley, which was accompanied by a steady recovery of water levels and a reduced rate of compaction in some areas. During the droughts of 1976–77 and 1987–92, diminished deliveries of imported surface water prompted pumping of groundwater to meet irrigation demands. This increased groundwater pumping resulted in water-level declines and periods of renewed compaction. Following each of these droughts, recovery to pre-drought water levels was rapid and compaction virtually ceased (fig. 3; Swanson, 1998; Galloway and others, 1999).

During 2007–10, groundwater pumping again increased as a result of reduced Central Valley Project and State Water Project surface-water deliveries caused by climatic and regulatory reductions in surface-water deliveries. The climatic drought was terminated by the fairly average 2009–10 winter; however, regulatory drought—the combination of court-mandated reductions in surface-water deliveries for environmental issues and for increasing the diminished reservoir storage from the multi-year climatic drought—resulted in 2010 surface-water deliveries that were 50 percent of requested amounts (*http://www.acwa.com/news/water-supply-challenges/2012-state-water-project-deliveries-increased-65*, accessed October 9, 2012). Because aquifer systems respond to both climatic and regulatory droughts alike, this period is referred to as the 2007–10 drought in this report. Groundwater levels declined during this period in response to increased pumping, approaching historical low levels, which reinitiated compaction, as shown at continuous Global Positioning System (CGPS) station P304 and well 13S/15E-31J6 near Mendota (fig. 4). Surface-water deliveries were limited to 35–60 percent of requested supplies for agricultural, municipal, industrial, and environmental uses during this period. Furthermore, following the historically wet winter of 2010–11, State Water Project surface-water deliveries in 2011 were still only 80 percent of requested supplies (*http://www.acwa.com/news/water-supply-challenges/2012-state-water-project-deliveries-increased-65*, accessed May 31, 2012), indicating that substantial groundwater pumping likely would continue.

Groundwater pumping that results in renewed compaction and land subsidence in the valley could cause serious operational, maintenance, and construction-design problems for the California Aqueduct, the San Luis and Delta-Mendota Canals, and other water-delivery and flood-control canals in the San Joaquin Valley. Subsidence has reduced the flow capacity of several canals that deliver irrigation water to farmers and transport floodwater out of the valley. Several canals managed by the San Luis and Delta-Mendota Water Authority (SLDMWA) and the Central California Irrigation District (CCID) have had reduced freeboard and structural damages that have already required millions of dollars worth of repairs, and more repairs are expected in the future (Bob Martin, SLDMWA and Chris White, CCID, oral commun., 2010).

Purpose and Scope

In 2009, the U.S. Geological Survey (USGS), in cooperation with the U.S. Bureau of Reclamation (Reclamation) and the SLDMWA, initiated a study to assess land subsidence in the vicinity of the DMC as part of an effort to minimize future subsidence-related damages to the canal. The purpose of this report is to present the status of subsidence and water-level trends along the DMC in the northern part of the San Joaquin Valley from 2003 through 2010. Updated water-level, compaction, and subsidence data are presented in a historical context. The focus of this report is subsidence caused by water-level decline and consequent compaction of aquifer systems, which is the dominant mechanism of subsidence in the valley. However, it is possible that some of the subsidence discussed in this report was caused by one or more additional processes, including hydrocompaction of moisture-deficient deposits above the water table, fluid withdrawal from oil and gas fields, deep-seated tectonic movements, and oxidation of peat soils, which is a major factor in the Sacramento-San Joaquin Delta (Galloway and others, 1999).

Subsidence-related data and analyses presented in this report include Global Positioning System (GPS) data, spirit-leveling surveys, extensometer data, and Interferometric Synthetic Aperture Radar (InSAR) analyses. The GPS and spirit-leveling survey data were collected by many parties at various spatial and temporal scales. Four extensometers were refurbished as part of this work; performance-testing data and compaction data collected from these extensometers are presented. The generation of InSAR maps showing land-surface deformation for various time spans is described. Measured groundwater-level changes during 2003–10 were examined and compared with measurements of land subsidence to evaluate their relation.

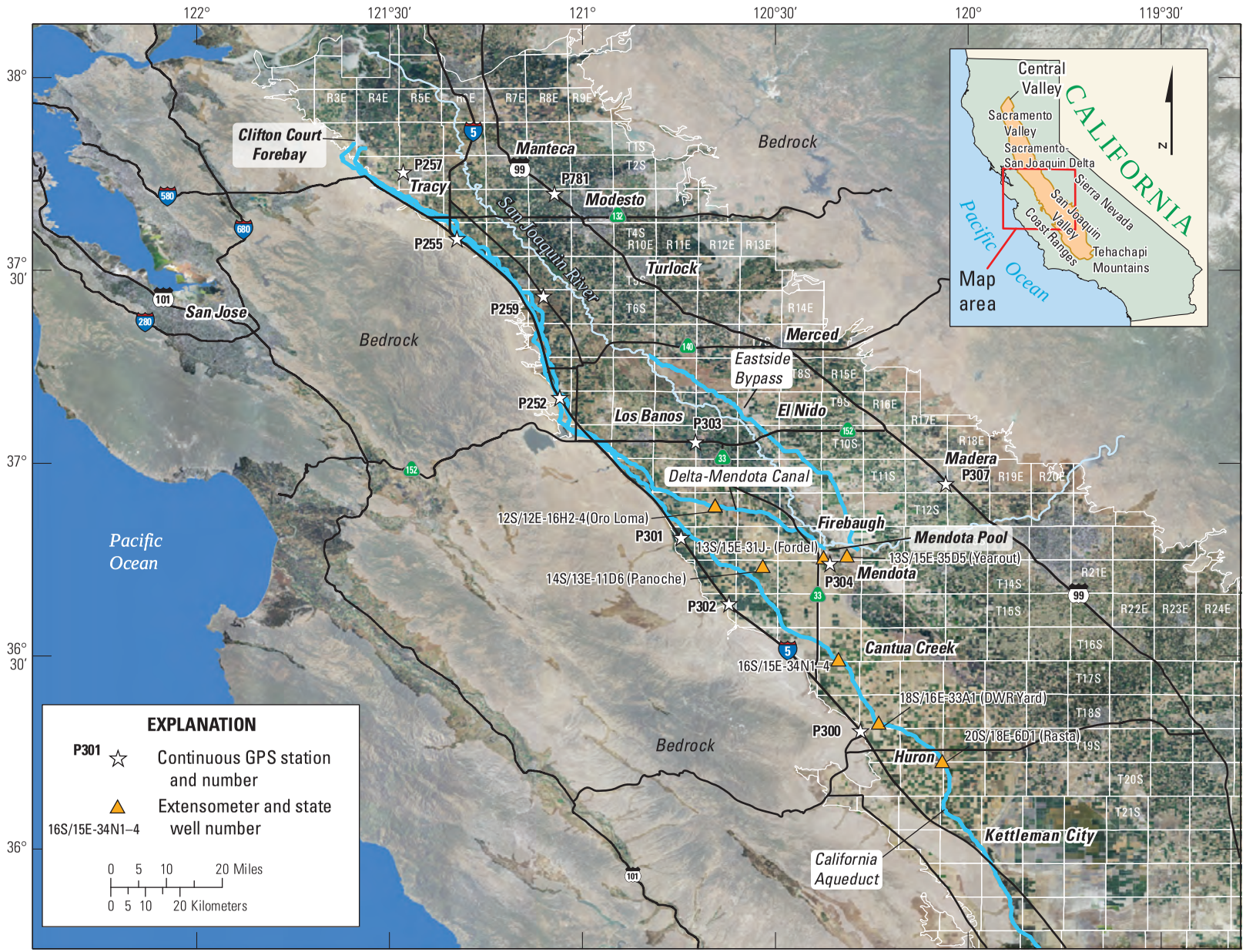

Figure 1. Location and geographic features of the study area, and locations of continuous Global Positioning System (GPS) stations and extensometers, San Joaquin Valley, California.

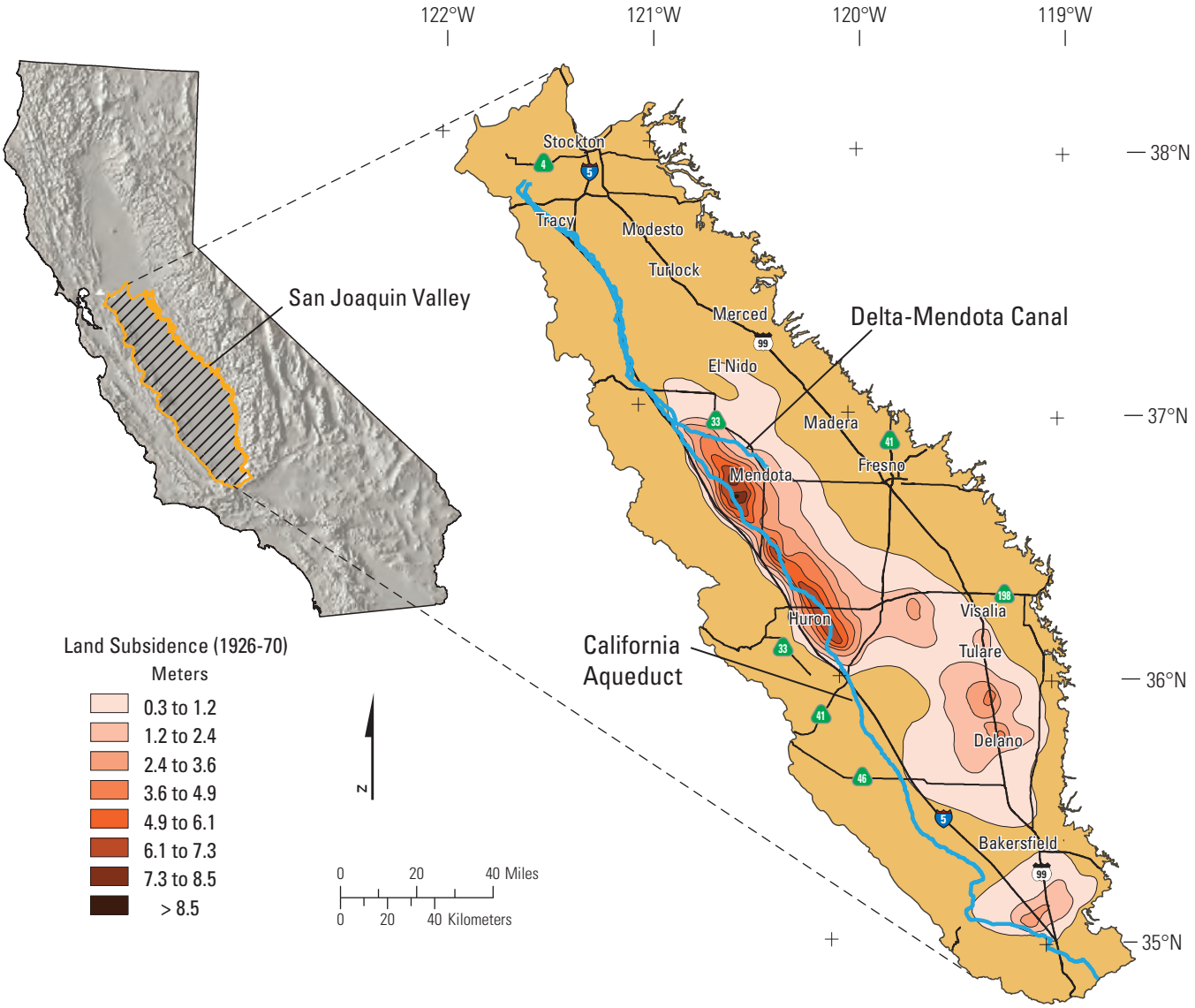

Figure 2. Land subsidence in the San Joaquin Valley, California, 1926–70 (modified from Ireland and others, 1984).

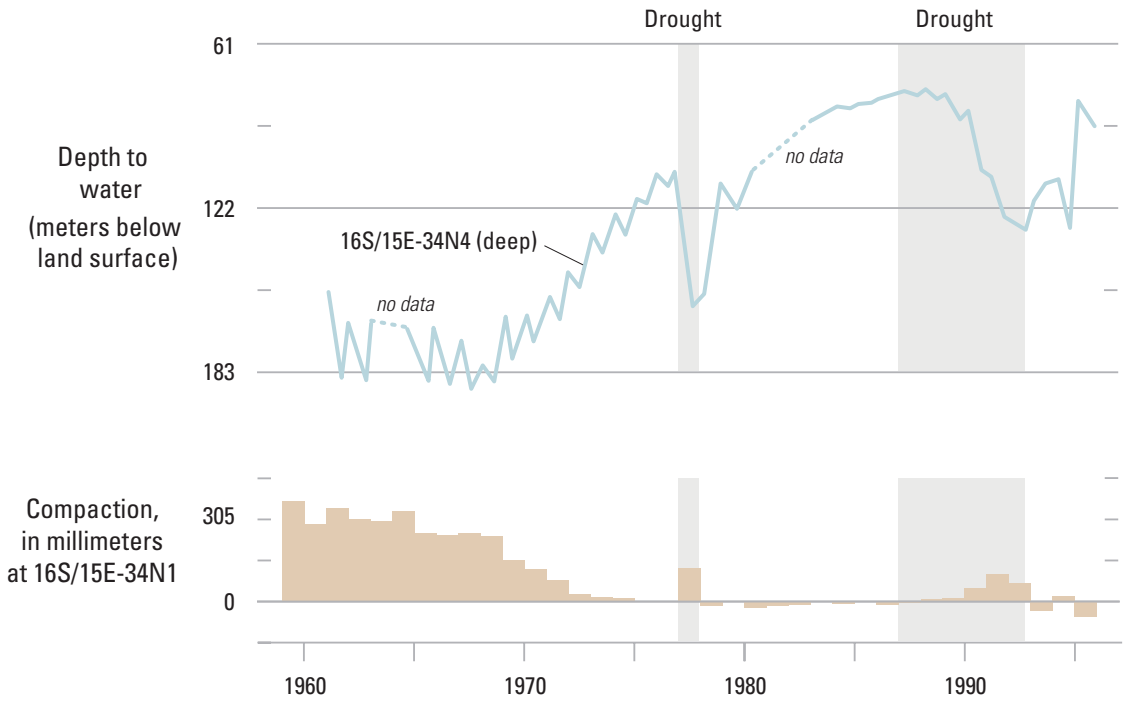

Figure 3. Water levels and compaction in observation well 16S/15E-34N4 and extensometer 16S/15E-34N1, respectively, near Cantua Creek, 1960s–90s (modified from Swanson, 1998; Galloway and others, 1999). See figure 1 for location.

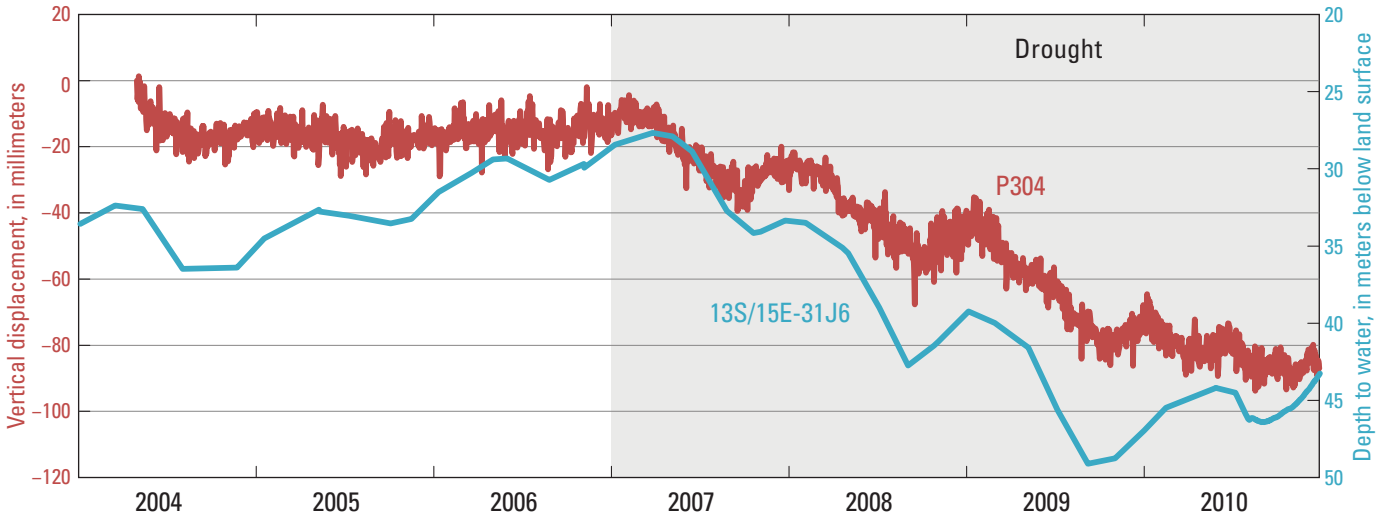

Figure 4. Discrete measurements of water levels in well 13S/15E-31J6, screened below the Corcoran Clay Member, and vertical displacement at continuous Global Positioning System (GPS) station P304 near Mendota, California, 2004–10. 13S/15E-31J6 data before May 1, 2010, were obtained from Glenn Browning, Luhdorff and Scalmanini Consulting Engineers, and 13S/15E-31J6 data after May 1, 2010, were obtained from the U.S. Geological Survey. P304 daily data were obtained from the University NAVSTAR Consortium.

Description of Study Area

The San Joaquin Valley of California covers about 26,000 km^2 and represents the southern part of the Central Valley, also known as the Great Valley of California. Centrally located in California, the San Joaquin Valley is bounded by the Sacramento-San Joaquin Delta and Sacramento Valley on the north, the Sierra Nevada on the east, the Tehachapi Mountains on the south, and the Coast Ranges on the west, and is a vast agricultural region drained by the San Joaquin River (fig. 1). Generally, the land surface has low relief; its configuration is the result of millions of years of alluvial and fluvial deposition of sediments derived from the bordering mountain ranges. Most of the valley lies close to sea level, but elevation increases along the valley margins; along the eastern edge, the land surface is about 150 m above sea level, and most of the western boundary ranges from 15 to 110 m above sea level (Faunt, 2009). The geographic area of focus in this report is the part of the San Joaquin Valley that is traversed by the DMC, but also includes some neighboring areas (fig. 1). The area of focus contains several significant population centers, the largest of which are the cities of Tracy (population 83,000) and Los Banos (population 36,000), and many smaller communities are distributed throughout the region. More than two-thirds of the region, however, is dominated by agricultural land uses, including permanent and seasonal crops.

Climate in the study area is arid-to-semiarid and is characterized by hot, dry summers and damp, mild winters, when the area frequently is covered by a ground fog known regionally as "tule fog" (Faunt, 2009). Precipitation during an average year ranges from 125 to 500 mm (Climate Source, 2006). Dramatic deviations from average climatic conditions are manifested as droughts or floods, and most of the San Joaquin Valley is prone to flooding. About 85 percent of the precipitation falls during November through April and half of it falls during December through February on average (Climate Source, 2006).

Surface water is used in the San Joaquin Valley when it is available; essentially all natural flows in area streams are diverted for agricultural and municipal use (Moore and others, 1990; Faunt, 2009). The valley also relies heavily on groundwater, which accounts for about 30 percent of the annual supply for agricultural and urban purposes (California Department of Water Resources, 2003; Faunt, 2009). Percentages of surface water and groundwater that constitute the annual supply are not well understood in the study area; however, during periods of drought, the groundwater usage increases.

Previous Land-Subsidence Studies

Land subsidence in the San Joaquin Valley was documented in the many reports generated as part of the cooperative subsidence program during 1956–86 by the USGS and the California Department of Water Resources (DWR). These reports include the widely cited USGS Professional Paper Series 437 A–I (Bull, 1964; Lofgren and Klausing, 1969; Bull, 1972; Lofgren, 1975; Bull and Miller, 1975; Bull, 1975; Bull and Poland, 1975; Poland and others, 1975; Ireland and others, 1984), collectively referred to as "the Poland Reports," after Dr. Joseph F. Poland, who led the program, and Series 497 A–E and G (Johnson and others, 1968; Meade, 1964; Meade, 1967; Meade, 1968; Miller and others, 1971; Riley, 1970). An additional report was published as part of the proceedings from the "Dr. Joseph F. Poland Symposium on Land Subsidence," held in 1995; this report (Swanson, 1998) provides a brief update of land subsidence in the San Joaquin Valley from the early 1980s through 1995, when subsidence data collection in the valley was sharply reduced; the downscaled monitoring effort focused on selected extensometers and surveys along the California Aqueduct and other important canals. These previous reports described three areas of subsidence: (1) Los Banos-Kettleman City, (2) Tulare-Wasco, and (3) Arvin-Maricopa. This report focuses on an area very similar to the Los Banos-Kettleman City area, but extends the northern boundary to near Tracy, and includes an area to the east, in the vicinity of Madera. A report describing hydraulic and mechanical properties affecting groundwater flow and aquifer-system compaction in the San Joaquin Valley (Sneed, 2001) was produced to constrain Reclamation's WESTSIM model, which was used to evaluate potential land subsidence under selected hydrologic conditions (Quinn and Faghih, 2008). Subsidence detected by InSAR was described for selected areas and periods during the 1990s (Brandt and others, 2005). A report by Faunt (2009) documented a numerical model of the hydrologic landscape and groundwater flow within the Central Valley and also incorporated subsidence observations to constrain the subsidence simulations.

Hydrogeologic Framework

Geology and Aquifer System

The San Joaquin Valley is a major northwest-southeast structural trough. Throughout Late Cretaceous (Mesozoic Era) and Tertiary (Cenozoic Era) Periods of geologic time, thousands of meters of shallow-water marine sediments were deposited in this down-warping fore-arc basin. Overlying these marine deposits are continental deposits of late Cenozoic age. In aggregate, these marine and continental deposits form an immense wedge that thickens from east to west and from north to south. At the extreme southern end of the valley, the thickness of sediments exceeds 8,500 m (Lofgren, 1976; Sneed, 2001).

The valley was formed chiefly by tectonic movement during late Cenozoic (late Tertiary Period and Quaternary Period) that included westward tilting of the Sierra Nevada block. Quaternary deformation has been principally along the southern and western borders of the valley, where the marine and continental rocks are tightly faulted and folded and the stream terraces are conspicuously elevated (Lofgren, 1976). A detailed discussion of the geology of the Central Valley is given by Page (1986).

The sediments of the San Joaquin Valley compose an aquifer system comprising unconfined, semi-confined, and confined aquifers. Three distinct groundwater bodies exist in much of the study area (fig. 5). In downward succession, these include (1) a body of unconfined to semi-confined freshwater in alluvial deposits overlying a widespread lacustrine confining bed—the Corcoran Clay Member of the Tulare Formation (referred to in this report as the Corcoran Clay); (2) an extensive reservoir of freshwater confined beneath the Corcoran Clay in alluvial and lacustrine deposits; and (3) a body of saline water, contained primarily in marine sediments, that underlies the freshwater body throughout the area (Page, 1986).

Numerous lenses of fine-grained sediments, which are highly compressible and account for nearly all aquifer-system compaction and resultant land subsidence, are distributed throughout the San Joaquin Valley and generally constitute more than 50 percent of the total thickness of the valley fill (Williamson and others, 1989). Generally, these lenses are not vertically extensive or laterally continuous; an exception is the Corcoran Clay, which was deposited during the Pleistocene when as much as 17,100 km^2 of the San Joaquin Valley was inundated by lakes (Page and Bertoldi, 1983; Farrar and Bertoldi, 1988). This diatomaceous clay is a low-permeability, areally extensive, lacustrine deposit (Johnson and others, 1968) that is as much as 60 m thick (Davis and others, 1959; Page, 1986). A detailed description of sediment texture in the Central Valley aquifer system is given in Faunt (2009).

Groundwater Levels and Movement

Groundwater levels and associated movement have responded to changes in the groundwater budget associated with development (fig. 5). Prior to development, natural discharge from the aquifer system within the San Joaquin Valley was in a long-term dynamic equilibrium with natural recharge, and longer-term changes in groundwater storage were negligible (Planert and Williams, 1995). Groundwater from recharge areas along mountain fronts flowed downward and laterally toward the valley trough, where it flowed upward to areas of discharge along rivers and marshes (fig. 5*A*; Planert and Williams, 1995; Faunt, 2009). Precipitation that fell on the valley floor, which was not consumed by evapotranspiration, infiltrated and followed a similar path. During the early years of groundwater development, wells drilled into the deep aquifer in low-lying areas near rivers and marshes flowed, owing to higher hydraulic head in the confined parts of the aquifer system (Faunt, 2009).

Large-scale groundwater development since about 1860 for both agricultural and urban uses has modified the groundwater levels and flow patterns from predevelopment conditions throughout the Central Valley (fig. 5*B*; Faunt, 2009). Groundwater levels have declined and groundwater flow has become more rapid and complex. Groundwater pumpage and recharge from irrigation has resulted in a steepening of downward hydraulic gradients, a general reversal of upward gradients, and shortened flow paths between sources and sinks (Faunt, 2009). Total flow through the Central Valley aquifer system has increased more than six-fold as a result of increased pumpage and recharge (Faunt, 2009).

Well depths in the San Joaquin Valley are determined by the locations of permeable aquifer materials and by the local groundwater quality. In some areas, wells are screened in the lower part of the aquifer system because of the low permeability and poor water quality of the upper parts of the aquifer system (Planert and Williams, 1995). The construction of thousands of irrigation wells, many of which have long intervals of screened casing, has increased the hydraulic connections between zones within the aquifer system than during the predevelopment flow regime (Bertoldi and others, 1991). Where these wells are open above and below the Corcoran Clay, flow occurs through the boreholes between the unconfined, semi-confined, and confined parts of the aquifer system.

Groundwater withdrawal and the lowering of hydraulic heads in the confined parts of the aquifer system by as much as about 150 m have reversed the predevelopment flow regime between the upper and lower parts of the aquifer system (Bull and Miller, 1975; Poland and others, 1975; Ireland and others, 1984; Williamson and others, 1989; Galloway and Riley, 1999; Faunt, 2009). Furthermore, by the 1960s, irrigation had become the dominant source of recharge; this recharge generally maintained or raised the water table, resulting in increased downward flow in the system. Groundwater-level measurements and simulations (Faunt, 2009) indicated that seasonal fluctuations in the confined part of the aquifer system exceeded 100 m in places, whereas those at the water table generally were less than 1.5 m.

Surface-water imports began in the early 1950s through the DMC, and in the late 1960s and early 1970s through the California Aqueduct. Importation of surface water through these canals resulted in significantly reduced reliance on groundwater in some areas. The combined effect of increased availability of imported surface water and decreased groundwater pumping was a large-scale, rapid recovery of the water levels in the confined part of the aquifer system (Faunt, 2009). In some parts of the western San Joaquin Valley, groundwater levels in the confined part of the aquifer system recovered to pre-1960 levels, while groundwater levels in the unconfined system remained fairly high. Since the early 1970s, this water-level recovery has been interrupted, primarily during periods when surface-water deliveries were curtailed as a result of climatic or regulatory drought, such as during 1976–77, 1987–92, and 2007–10. During these periods, groundwater levels declined quickly with the onset of pumping, partly as a result of reduced aquifer-system storage capacity, which is described in the section "Mechanics of Pumping-Induced Land Subsidence" (figs. 3 and 4; Faunt, 2009). A detailed history of changes in groundwater levels and movement is found in Faunt (2009).

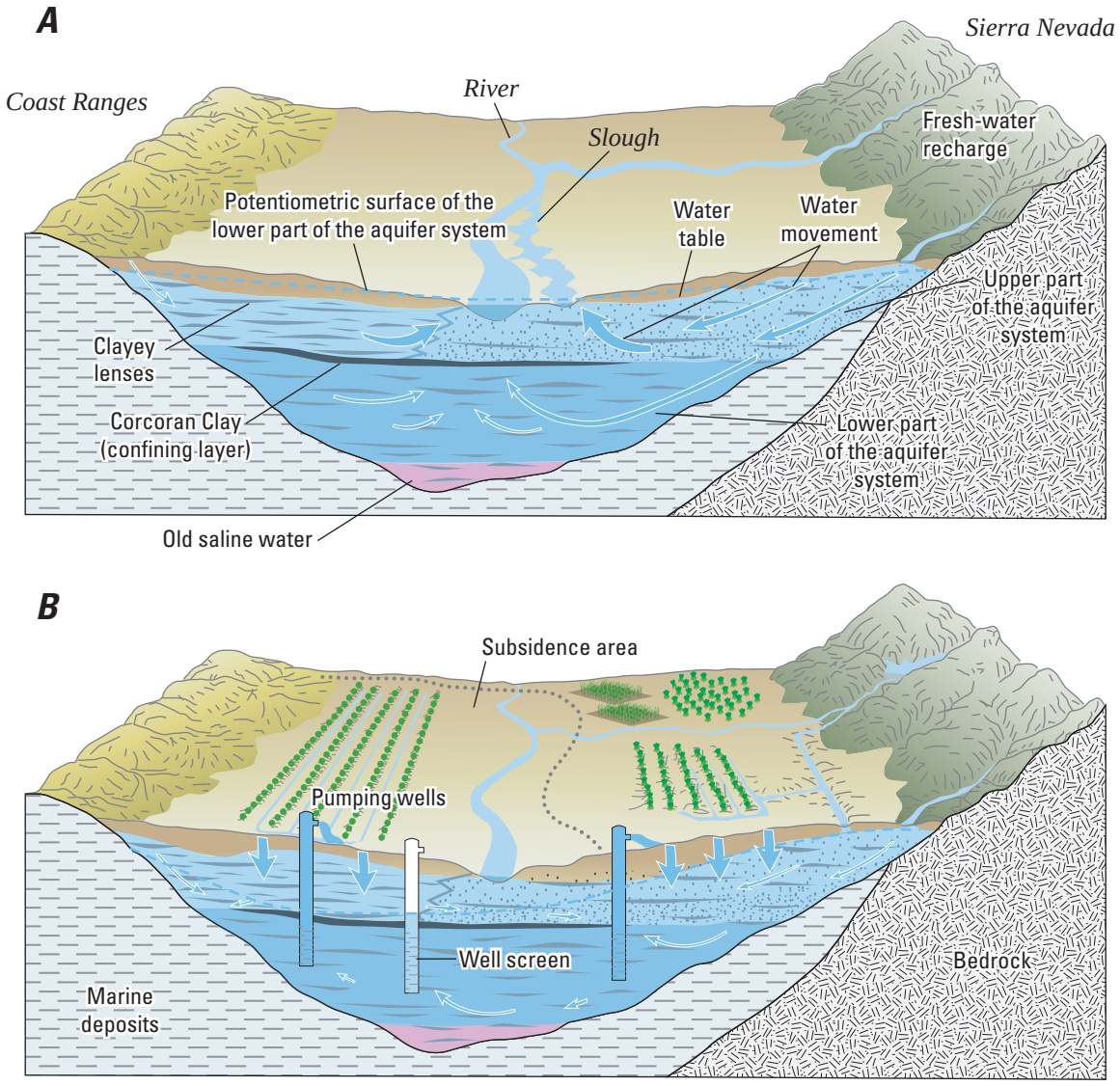

Figure 5. Relation of the Corcoran Clay to younger and older alluvium and aquifers and groundwater-flow regimes in the San Joaquin Valley, California, for *A*, pre-development and *B*, post-development (modified from Belitz and Heimes, 1990; Galloway and others, 1999; Faunt, 2009).

Land Subsidence

The extensive withdrawal of groundwater from the unconsolidated deposits of the San Joaquin Valley has caused widespread land subsidence—locally exceeding 8.5 m between 1926 and 1970 (fig. 2; Poland and others, 1975) and reaching 9 m by 1981 (Ireland, 1986). Long-term groundwater-level declines can result in a vast one-time release of "water of compaction" from compacting silt and clay layers (aquitards), which causes land subsidence (Galloway and others, 1999). There are several additional types of subsidence in the San Joaquin Valley, including subsidence related to the hydrocompaction of moisture-deficient deposits above the water table, subsidence related to fluid withdrawal from oil and gas fields, subsidence caused by deep-seated tectonic movements, and subsidence caused by the oxidation of peat soils that is a major factor in the Sacramento-San Joaquin Delta. However, aquifer-system compaction caused by groundwater pumpage, the focus of this report, causes the largest magnitude and areal extent of land subsidence in the San Joaquin Valley (Poland and others, 1975; Ireland and others, 1984; Farrar and Bertoldi, 1988; Bertoldi and others, 1991; Galloway and Riley, 1999).

Land subsidence from groundwater pumping began in the mid-1920s (Poland and others, 1975; Bertoldi and others, 1991; Galloway and Riley, 1999), and, by 1970, there had been more than 0.3 m of land subsidence in about half of the San Joaquin Valley, or about 13,500 km^2 (Poland and

others, 1975). The San Joaquin Valley contains three principal areas of subsidence caused by groundwater withdrawals as defined in the Poland Reports: (1) 6,215 km^2 in the Los Banos-Kettleman City area, (2) 3,680 km^2 in the Tulare-Wasco area, and (3) 1,815 km^2 in the Arvin-Maricopa area (Poland and others, 1975; Thomas and Phoenix, 1976; Ireland and others, 1984). The study area for this report is similar to the Los Banos-Kettleman City area. In the Los-Banos-Kettleman City area, hydraulic head declines of more than 120 m in the confined part of the aquifer system caused the inelastic (permanent) compaction of the clayey beds, yielding a one-time release of "water of compaction"—this resulted in 9 m of land subsidence during 1926–81 and an associated loss of aquifer-system storage (fig. 2; Poland and others, 1975; Ireland and others, 1984; Ireland, 1986; Galloway and Riley, 1999). This one-time release of water of compaction was substantial; it is estimated that by the mid-1970s, about one-third of the volume of water pumped from storage in this area came from compaction of fine-grained beds (Poland and others, 1975; Faunt, 2009). Although the largest body of clay is the Corcoran Clay, a relatively insignificant volume of water has been released from storage in the Corcoran Clay (Faunt, 2009), likely because of its large thickness and low permeability.

Subsidence was greatly slowed or arrested in the Los Banos-Kettleman City area after the importation of surface water (particularly through the California Aqueduct beginning in the early 1970s) and subsequent recovery of groundwater levels. The droughts of 1976–77, 1987–92, and 2007–10 resulted in diminished deliveries of imported water, increased pumping, rapid lowering of groundwater levels, and re-initiation of subsidence (figs. 3 and 4; Swanson, 1998; Galloway and Riley, 1999).

In addition to the loss of water and storage capacity from inelastic compaction, subsidence in the Central Valley has caused damage to structures including aqueducts, roads, bridges, buildings, and well casings. Important and expensive damages and repairs include the loss of conveyance capacity in canals that deliver water or remove floodwaters, the realignment of canals as their constant gradient becomes variable, the raising of infrastructure such as canal check stations, and the releveling of furrowed fields, many of which are laser-leveled for maximum irrigation efficiency. The effects of a sag in a channel profile are increased flow velocity in the upstream end, decreased velocity in the middle, and loss of flow capacity immediately downstream of the sag. If the channel is unlined, such as the Eastside Bypass and the lower reaches of the DMC, erosion will occur in the upstream end and deposition will occur in the subsided area. If the sag is deep, filling the channel with water to the top of the levee in the sag will not raise the water level enough to maintain the flow capacity downstream of the subsided reach. In addition, subsidence has increased the potential for flooding in low lying areas (Bertoldi, 1989; Faunt, 2009).

Mechanics of Pumping-Induced Land Subsidence

Land subsidence attributed to groundwater pumping takes place in many aquifer systems that are, at least in part, composed of unconsolidated fine-grained sediments and that have undergone extensive groundwater development (Poland, 1984). The relation between changes in pore-fluid pressure and compression of the aquifer system is based on the principle of effective stress (Terzaghi, 1925):

$$\sigma_e = \sigma_T - \rho \tag{1}$$

where effective or intergranular stress (σ_e) is the difference between total stress or geostatic load (σ_T) and the pore-fluid pressure (ρ; fig. 6).

The pore structure of a sedimentary aquifer system is supported by the granular skeleton of the aquifer system and the pore-fluid pressure of the groundwater that fills the intergranular pore space (Meinzer, 1928). If total stress remains constant and groundwater is withdrawn in quantities that result in reduced pore-fluid pressure (manifested as water-level declines in wells), the intergranular stress, or effective stress, on the granular skeleton will increase. A change in effective stress deforms the skeleton: an increase in effective stress compresses it, and a decrease in effective stress causes it to expand. The vertical component of this deformation sometimes results in non-recoverable compaction of the aquifer system and a permanent reduction in aquifer-system storage capacity (fig. 6). An aquifer-system skeleton consisting of primarily fine-grained sediments, such as silt and clay, is much more compressible than one consisting of primarily coarse-grained sediments, such as sand and gravel. Inelastic (non-recoverable) compaction of coarse-grained sediment is negligible (Ireland and others, 1984; Hanson, 1989; Sneed and Galloway, 2000).

Aquifer-system deformation is elastic (recoverable) if the stress imposed on the skeleton is smaller than any previous effective stress (Leake and Prudic, 1991). The largest historical effective stress imposed on the aquifer system—sometimes the result of the lowest groundwater level—is the "preconsolidation stress," and the corresponding (lowest) groundwater level is the "preconsolidation head." If the effective stress exceeds the preconsolidation stress, the pore structure of the granular matrix of the fine-grained sediments is rearranged; this new configuration results in a reduction of pore volume and, thus, inelastic (largely irreversible) compaction of the aquifer system. Furthermore, the compressibility of the fine-grained sediments constituting the aquitards, and any resulting compaction under stresses exceeding the preconsolidation stress, is 20 to more than 100 times greater than under stresses less than the preconsolidation stress (Riley, 1998).

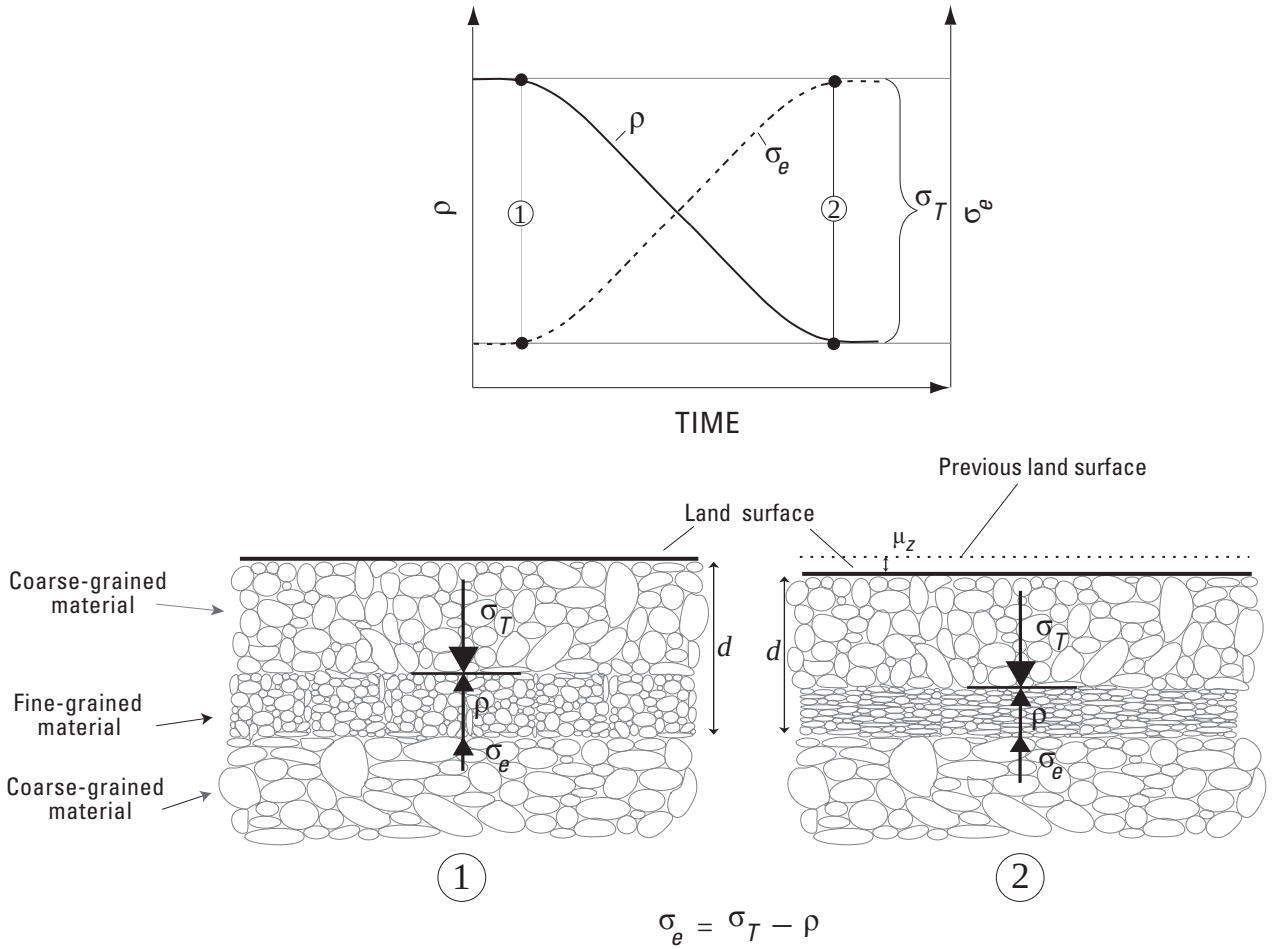

Figure 6. Principle of effective stress, as applied to land subsidence. Vertical displacement (μ_z) of land surface as a result of a decrease in pore-fluid pressure (ρ) and resultant increase in effective stress (σ_e) exerted on a horizontal plane located at depth (d) below land surface in fine-grained material under conditions of total stress (σ_T) in a one-dimensional, fluid-saturated geologic medium (modified from Sneed and Galloway, 2000).

This is a simplified explanation that does not always hold in practice because of the temporal aspect of compaction. For a developed aquifer system with an appreciable thickness of fine-grained sediments, a significant part of the total compaction can be residual compaction (Sneed and Galloway, 2000), which is compaction that occurs in thick aquitards as heads in the aquitards equilibrate with heads in the adjacent aquifers (Terzaghi, 1925). Depending on the thickness and the vertical hydraulic diffusivity of a thick aquitard, fluid-pressure equilibration—and thus compaction—lags behind pressure (or hydraulic head) declines in the adjacent aquifers; concomitant compaction can require decades or centuries to approach completion. Thus, if pore pressure exceeds the preconsolidation stress for a relatively short period, the preconsolidation stress is not necessarily reset to the new low value; pore pressures only slightly below the original preconsolidation head could trigger permanent compaction (fig. 3; Phillips and others, 2003). The time constant of an aquitard, τ, is the time required for about 93 percent of the excess pore pressure to dissipate, and therefore about 93 percent of the ultimate compaction to occur, following an instantaneous decrease in stress. The time constant is directly proportional to the inverse of the vertical hydraulic diffusivity, and for a doubly draining aquitard, to the square of the half-thickness of the aquitard:

$$\tau = S'_s \left(b'/2\right)^2 / K'_v \qquad (2)$$

where

S'_s is the specific storage of the aquitard,
b' is the aquitard thickness,
K'_v is the vertical hydraulic conductivity of the aquitard, and
S'_s / K'_v is the inverse of the vertical hydraulic diffusivity (Riley, 1969).

Ireland and others (1984) estimated that the time constants for aquifer systems at 15 sites in the San Joaquin Valley ranged from 5 to 1,350 years. Terzaghi (1925) described this delay in his theory of hydrodynamic consolidation. Numerical modeling based on Terzaghi's theory has been used to simulate complex histories of compaction caused by known water-level fluctuations (Helm, 1978; Hanson, 1989; Sneed and Galloway, 2000).

The concepts reviewed in this section collectively form the aquitard-drainage model, which provides the theoretical basis of many subsidence studies related to the production of groundwater, oil, and gas. For a review of the history of the aquitard-drainage model, see Holzer (1998); for a more complete description of aquifer-system compaction, see Poland (1984); and, for a review and selected case studies of land subsidence caused by aquifer-system compaction in the United States, see Galloway and others (1999).

Measurements and Methods

In this report, measurements of elevations, aquifer-system compaction, and water levels are presented, interpreted, and integrated to improve understanding of the processes responsible for land-surface elevation changes. The sources of original data and processing techniques (if any) are described in this section of this report; data are presented, interpreted, and integrated in the "Land Subsidence and Aquifer-System Compaction" section.

Elevation and Elevation Change

Elevation and change in elevation have been measured at selected locations or along transportation and water-conveyance routes using InSAR, CGPS, campaign GPS surveying, and spirit-leveling surveying by agencies and groups including USGS, DWR, SLDMWA, CCID, California Department of Transportation (Caltrans), National Geodetic Survey (NGS), University NAVSTAR (Navigation Satellite Timing and Ranging) Consortium (UNAVCO), and various private contractors.

InSAR

InSAR is a satellite-based remote sensing technique that can detect centimeter level ground-surface deformation under favorable conditions over hundreds of square kilometers at a spatial resolution (pixel size) of 90 m or less (Bawden and others, 2003). Synthetic Aperture Radar (SAR) imagery is produced by reflecting radar signals off a target area and measuring the two-way travel time back to the satellite. SAR imagery has two components; amplitude and phase. The amplitude is the measure of the radar signal intensity returned to the satellite, and the varying reflective properties delineate features of the landscape such as roads, mountains, structures, and other features. The phase component is proportional to the line-of-sight distance from the ground to the satellite (range) and is the component used to measure land-surface displacement (subsidence and uplift).

There are two primary forms of interferometric processing: conventional and persistent scatterer (PS) InSAR. The conventional InSAR technique uses two SAR scenes of the same area taken at different times and differences the phase portion of the SAR signal, resulting in maps called interferograms that show relative ground-elevation change (range change) between the two SAR acquisition dates. If the ground has moved away from the satellite (subsidence), a more distal phase portion of the waveform is reflected back to the satellite. Conversely, if the ground has moved closer to the satellite (uplift), a more proximal phase portion of the waveform is reflected back to the satellite (Sneed and Brandt, 2013). The phase difference, or shift, between the two SAR images is then calculated, relative to a selected reference point, for each pixel within the image extent.

The PS InSAR technique is similar to the conventional technique, but usually requires 20 or more SAR images that are processed simultaneously to determine, in part, the amplitude variance of all the SAR images at each pixel. Pixels that have relatively high variance in amplitude among the many SAR images are filtered from the data set, resulting in a data set containing "stable" pixels. The differential phase is then calculated in a manner identical to that of conventional InSAR, except that the differential phase is calculated only for each "stable" pixel, rather than for every pixel within the image extent. A differential phase regression model is then calculated for selected interferometric pairs, which defines a linear dependence of interferometric phase on the difference in satellite geometry of the two SAR images composing the interferometric pair. This linear relationship leads to a digital-elevation model height-correction factor. The regression analysis also considers the linear dependence of phase with regard to time and can lead to a linear deformation rate, relative to a selected reference point (Werner and others, 2003; Strozzi and others, 2005).

InSAR signal quality is dependent on topography, satellite orbit geometry, ground cover, atmospheric artifacts, land-use practices, time span of the interferogram, and other factors. Areas with high topographic relief can result in blocked radar signals in the line-of-sight (shadows). Strict satellite orbit control is required for successful application of the InSAR technique because repeat satellite passes must view the same point on the ground from very similar positions and angles in order to minimize the parallax effect. The parallax effect is typically minimized by selecting SAR images for interferometric processing for which the perpendicular baseline, or horizontal distance between two satellite passes, is less than about 200 m (Sneed and Brandt, 2013). However, the relatively flat topography of the study area allowed inclusion of SAR image pairs with perpendicular baselines as long as about 560 m without adversely affecting the ability to interpret the interferograms.

In the San Joaquin Valley, the principal sources of error in the InSAR method result from atmospheric artifacts and agricultural land-use practices, both of which have deleterious effects on interferograms. Atmospheric artifacts are caused by non-uniform atmospheric water vapor in the form of clouds and tule fog; water vapor slows the radar signal, causing a phase shift that can lead to erroneous deformation interpretations (Zebker and others, 1997). Agricultural land-use practices, including the tilling, plowing, or flooding of farm fields, cause large and non-uniform ground-surface changes that

affect the amount of radar signal reflected back to the satellite; the magnitude of these changes cannot be resolved by using InSAR. Interferograms spanning long time spans (generally 2 or more years) often have poor signal quality because more non-uniform change is likely to have occurred in both urban and non-urban areas (Sneed and Brandt, 2013). The PS InSAR technique is less affected by the land-use and time-span dependent effects, since pixels with relatively high variance in amplitude are removed early in the processing, leaving only the relatively "good" quality pixels for processing.

Atmospheric artifacts can be identified by using multiple independent interferogram pairs or by stacking interferograms, and time-span dependent errors can be reduced by stacking interferograms. The term "independent interferograms" refers to two or more interferograms that do not share a common SAR scene. The process of "stacking interferograms" involves summing two or more interferograms. Stacking two interferograms that share a common SAR image that contains atmospheric artifacts will remove those artifacts in the resulting stacked interferogram. Stacking also is beneficial in reducing time-span dependent errors. Stacking two or more interferograms that span shorter periods, which have less timespan-dependent errors, can result in more coherent longer-term interferograms.

For this study, SAR data acquired between 2003 and 2010 from the European Space Agency's (ESA) ENVIronmental SATellite (ENVISAT) and the Japanese Aerospace eXploration Agency's (JAXA) Advanced Land Observing Satellite (ALOS) were used for InSAR analysis. For this period, the side-looking C-band (56-mm wavelength) ENVISAT satellite orbited the Earth at an altitude of approximately 800 km and had a 35-day repeat cycle with a vertical resolution as small as 5 mm. The L-band (240-mm wavelength) ALOS satellite orbited the Earth at an altitude of approximately 700 km and had a 46-day repeat cycle with a vertical resolution as small as 20 mm. Although the longer wavelength Phased Array L-band Synthetic Aperture Radar (PALSAR) instrument aboard ALOS is less sensitive to atmosphere and agricultural land-use changes than the shorter-wavelength Advanced Synthetic Aperture Radar (ASAR) instrument aboard ENVISAT, it also is about four times less sensitive to range changes, or deformation (Sandwell and others, 2008). The lower sensitivity of L-band data permitted application of the conventional InSAR processing technique to these data, and the greater sensitivity to atmospheric conditions and agricultural land uses of C-band interferometry required processing with the PS InSAR technique. Interferograms processed using PS InSAR also were restricted to about a 1-year time span in order to reduce time-span dependent errors.

Two primary methods were used to evaluate InSAR image quality for this study. First, a visual correlation analysis of each image was done to qualify image quality. For L-band data, the entire image was analyzed visually to qualify correlation. For C-band data, the mountainous areas were analyzed visually for correlation because the high density of persistent scatterer pixels in mountainous areas facilitated detection of spatial decorrelation in comparison to the low density of persistent scatterers on the valley floor, and because fewer potential sources of artifacts exist in mountainous areas compared to the valley floor. When the InSAR imagery was determined to be decorrelated or otherwise degraded in the fairly stable mountainous areas, it was considered likely that the valley floor also was decorrelated, and the image was either rejected or only conditionally accepted for analysis. Second, visible spectrum imagery from the MODerate resolution Imaging Spectroradiometer (MODIS) instrument aboard the National Aeronautics and Space Administration (NASA) TERRA and AQUA satellites was used to make qualitative assessments of atmospheric moisture throughout the study area on each day of C-band SAR acquisition. This was a fairly simple means to identify clouds or fog over the study area, and to reject, accept, or conditionally accept the C-band imagery, which can be greatly affected by such conditions. MODIS data were not used to analyze the L-band data because L-band is much less prone to atmospheric degradation because of its much longer wavelength.

A total of 64 ENVISAT SAR images on 2 separate tracks (T299 and T435) extending from about the City of Tracy to Kettleman City (fig. 7) were acquired and processed using the PS INSAR technique to produce 331 interferograms. Of these interferograms, 83 were of sufficient quality for analysis, with time spans ranging from 35 to 385 days between July 3, 2003, and July 26, 2010 (table 1). A subset of these 83 interferograms was used for time-series generation, stacking to produce interferograms that span seasonal and annual periods between July 3, 2003, and July 26, 2010, or both to allow for deformation analysis over shorter and longer periods (table 1; appendices A–C). Any deformation that may have occurred during periods of gaps in the time series or stacks was not estimated.

A total of 41 ALOS SAR images on 4 separate tracks (T219, T220, T221, T545; fig. 7) were acquired and processed, resulting in 100 ALOS interferograms using the conventional InSAR processing technique, 15 of which were of sufficient quality for interpretation (table 1). Although ALOS data are more limited, the data were instrumental for defining maximum subsidence locations where ENVISAT and terrestrial survey data were not available.

Ordinary kriging was applied to PS InSAR data to interpolate ground-surface elevation change between the stable pixels identified by using the PS InSAR technique. The kriged data were then used to interpret PS InSAR data at specific locations. To improve kriging computational run-times, the volume of PS InSAR data was reduced by arbitrarily selecting 1 percent of the original points generated by the PS InSAR process on the basis of spatial location. R statistical software (The R Center for Statistical Computing, 2008) was used to calculate the interpolated values and assess the degree of spatial correlation; an initial range of 30 km defined the tolerance for semivariogram calculations. A spherical model was fit to the estimated semivariogram to optimize the output of the deformation values generated by the kriging calculations. The ordinary kriging calculations were then applied to a predefined

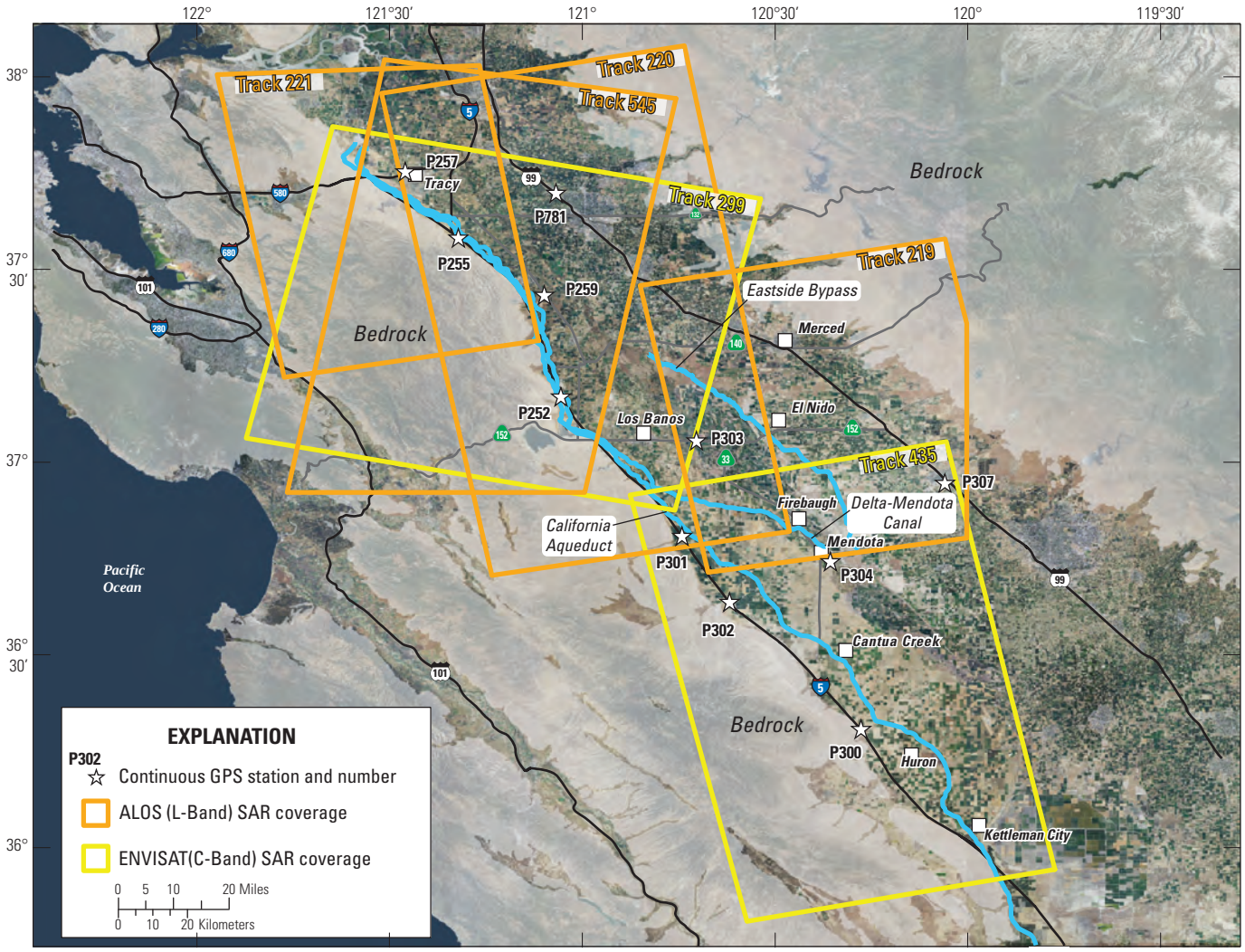

Figure 7. Locations of continuous Global Positioning System (GPS) stations and extents of ENVIronmental SATellite (ENVISAT) and Advanced Land Observing Satellite (ALOS) Synthetic Aperture Radar (SAR) coverage, San Joaquin Valley, California. Extents of ENVISAT SAR coverage were obtained from the European Space Agency, and the extents of ALOS SAR coverage were obtained from the Japanese Aerospace eXploration Agency.

Table 1. Interferograms interpreted for this report. See appendices A–C for selected interferograms used in time series and stacked interferograms shown in this report.

[**Abbreviations**: ALOS, Advanced Land Observing Satellite; ENVISAT, ENVIronmental SATellite; mm/dd/yyyy, month/day/year; SAR, Synthetic Aperture Radar; *, used in deformation time series and/or in stacked interferograms]

Index number	Track	1st SAR acquisition (mm/dd/yyyy)	2nd SAR acquisition (mm/dd/yyyy)	Time span of SAR pair, in days
ENVISAT Interferograms				
1*	T435	07/03/2003	05/13/2004	315
2*	T435	05/13/2004	11/04/2004	175
3	T435	05/13/2004	12/09/2004	210
4	T435	09/30/2004	11/04/2004	35
5	T435	09/30/2004	03/24/2005	175
6*	T435	11/04/2004	01/13/2005	70
7	T299	11/29/2004	01/03/2005	35
8	T299	11/29/2004	11/14/2005	350
9	T435	12/09/2004	02/17/2005	70
10*	T435	01/13/2005	03/24/2005	70
11	T435	02/17/2005	02/02/2006	350
12	T299	11/14/2005	05/08/2006	175
13	T435	12/29/2005	03/09/2006	70
14	T435	02/02/2006	03/09/2006	35
15	T435	02/02/2006	05/18/2006	105
16*	T435	03/09/2006	01/18/2007	315
17	T435	04/13/2006	05/18/2006	35
18	T435	05/18/2006	10/05/2006	140
19	T435	05/18/2006	02/22/2007	280
20	T435	06/22/2006	07/27/2006	35
21	T435	08/31/2006	10/05/2006	35
22	T435	08/31/2006	01/18/2007	140
23	T435	10/05/2006	02/22/2007	140
24*	T435	01/18/2007	11/29/2007	315
25	T435	10/25/2007	11/29/2007	35
26	T435	10/25/2007	01/03/2008	70
27	T435	11/29/2007	01/03/2008	35
28*	T435	11/29/2007	04/17/2008	140
29*	T299	12/24/2007	03/03/2008	70
30*	T299	12/24/2007	09/29/2008	280
31	T299	01/28/2008	04/07/2008	70
32*	T299	03/03/2008	05/12/2008	70
33	T299	03/03/2008	09/29/2008	210
34	T299	04/07/2008	05/12/2008	35
35	T299	04/07/2008	06/16/2008	70
36	T299	04/07/2008	07/21/2008	105
37	T299	04/07/2008	09/29/2008	175
38	T299	04/07/2008	01/12/2009	280
39	T299	04/07/2008	03/23/2009	350
40	T299	04/07/2008	04/27/2009	385
41*	T435	04/17/2008	05/22/2008	35
42*	T299	05/12/2008	07/21/2008	70
43	T299	05/12/2008	08/25/2008	105
44	T299	05/12/2008	01/12/2009	245
45	T299	05/12/2008	02/16/2009	280
46	T299	06/16/2008	07/21/2008	35
47	T299	06/16/2008	08/25/2008	70
48*	T299	07/21/2008	08/25/2008	35
49	T299	07/21/2008	01/12/2009	175
50	T299	07/21/2008	04/27/2009	280
ENVISAT Interferograms—Continued				
51*	T435	07/03/2003	05/13/2004	35
52*	T299	08/25/2008	04/27/2009	245
53	T299	08/25/2008	07/06/2009	315
54	T299	09/29/2008	01/12/2009	105
55*	T299	09/29/2008	02/16/2009	140
56	T299	09/29/2008	07/06/2009	280
57	T299	09/29/2008	08/10/2009	315
58	T299	01/12/2009	09/14/2009	245
59	T299	02/16/2009	04/27/2009	70
60	T299	02/16/2009	06/01/2009	105
61*	T299	02/16/2009	07/06/2009	140
62	T299	03/23/2009	02/01/2010	315
63*	T299	04/27/2009	06/01/2009	35
64	T299	04/27/2009	08/10/2009	105
65	T299	04/27/2009	11/23/2009	210
66	T299	04/27/2009	12/28/2009	245
67*	T299	06/01/2009	12/28/2009	210
68	T299	06/01/2009	05/17/2010	350
69*	T299	07/06/2009	11/23/2009	140
70	T299	07/06/2009	06/21/2010	350
71	T299	08/10/2009	11/23/2009	105
72	T299	08/10/2009	06/21/2010	315
73	T299	10/19/2009	07/26/2010	280
74	T299	11/23/2009	12/28/2009	35
75*	T299	11/23/2009	02/01/2010	70
76	T299	11/23/2009	05/17/2010	175
77*	T299	12/28/2009	06/21/2010	175
78	T299	02/01/2010	04/12/2010	70
79	T299	02/01/2010	05/17/2010	105
80*	T299	02/01/2010	06/21/2010	140
81	T299	04/12/2010	05/17/2010	35
82	T299	05/17/2010	07/26/2010	70
83*	T299	06/21/2010	07/26/2010	35
ALOS Interferograms				
84	P221	12/24/2006	03/26/2007	92
85	P219	05/23/2007	01/08/2008	230
86	P219	11/23/2007	02/23/2008	92
87	P219	01/08/2008	02/23/2008	46
88*	P219	01/08/2008	01/13/2010	736
89	P221	02/11/2008	03/28/2008	46
90	P219	02/23/2008	04/09/2008	46
91	P219	02/23/2008	01/13/2010	690
92	P545-South	11/01/2008	11/04/2009	368
93	P545-North	11/01/2008	11/04/2009	368
94	P221	11/13/2008	12/29/2008	46
95	P221	11/13/2008	03/31/2009	138
96	P221	12/29/2008	03/31/2009	92
97	P220-South	03/14/2009	12/15/2009	276
98	P220-North	03/14/2009	12/15/2009	276

grid by using the log of the PS InSAR values and the semivariogram parameters to calculate interpolated range-change values every 500 m. For a general description of kriging theory, see appendix D.

Continuous Global Positioning System Network

The CGPS data for this study were obtained from the UNAVCO Plate Boundary Observatory (PBO) network of continuously operating GPS stations. The PBO is the geodetic component of UNAVCO, a consortium of research institutions whose focus is measuring vertical and horizontal plate boundary deformation across the North American and Pacific Plates in the western United States using high-precision measurement techniques. Daily CGPS position time series were downloaded from the PBO website (*http://pbo.unavco.org/*, accessed 6/7/2012) using the Stable North American Reference Frame (SNARF). Day-to-day CGPS height solutions vary by as much as about 35 mm, likely due to variable atmospheric conditions, random walk noise, and other effects not directly related to land-surface-elevation change (Zerbini and others, 2001; Williams and others, 2004; Langbein, 2008). To minimize this high-frequency noise and to enable better correlation between changes in GPS heights and InSAR range-change measurements, a 31-day moving average was applied to the CGPS data (fig. 8). The removal of the fairly large day-to-day variations in GPS heights minimized potential error without removing seasonal (figs. 8*A* and 8*C*) or long-term deformation trends (figs. 8*B* and 8*C*), and permitted more meaningful comparison with InSAR data. In addition to comparing the CGPS height data to range-change measurements from PS InSAR data, the locations of the relatively stable CGPS stations P257 and P300 also were used as the selected reference points to calculate the relative range change of the PS InSAR data from ENVISAT tracks T299 and T435, respectively. Data from nine additional CGPS sites were used for InSAR error analysis.

Campaign GPS and Spirit Level Surveying

Published and unpublished data from previously completed spirit-level and GPS surveys in the study area were obtained and used for analysis of land-surface change for this study. Published subsidence contours of a large portion of the San Joaquin Valley from 1926–70, constructed using topographic maps and spirit-level surveys (Poland and others, 1975), were used to compare areas of historical subsidence to areas of more recent subsidence. Published elevation data for selected bench marks along Highway 152 surveyed during 1972, 1988, and 2004 (National Geodetic Survey archives) were used to compute changes in elevation between the survey dates (Marti Ikehara, National Geodetic Survey, written commun., 2012). Similarly, elevation data for selected bench marks along the California Aqueduct surveyed during 2000, 2006, and 2009 were used to compute changes in elevation between the survey dates (Forrest Smith, California

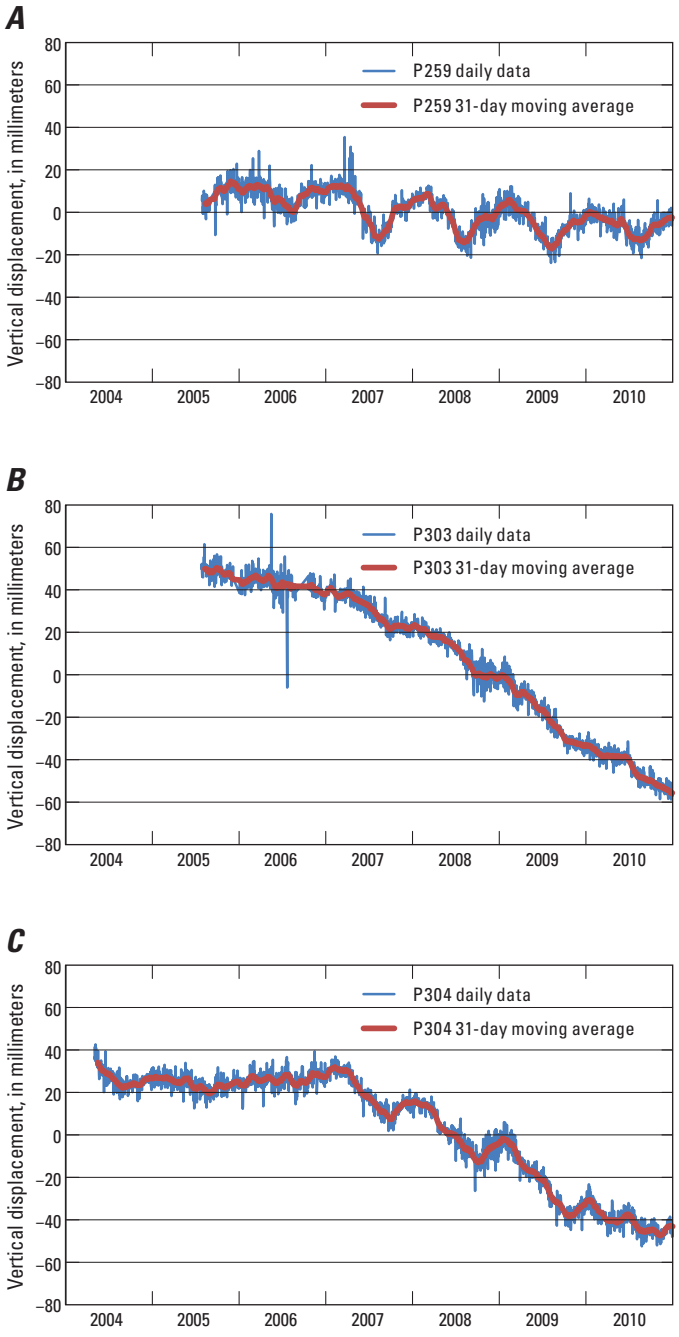

Figure 8. Daily and averaged (31-day moving) continuous Global Positioning System (CGPS) data from three selected CGPS stations in the San Joaquin Valley, California, which are representative of *A*, seasonally dominated displacement with little long-term displacement (P259); *B*, long-term-dominated displacement with little seasonal displacement (P303); and *C*, long-term and seasonal displacement (P304). CGPS data were obtained from the University NAVSTAR Consortium.

Department of Water Resources, written commun., 2009). Elevation data from leveling surveys in 1935, 1953, 1957, 1984, and 1996, and annual GPS and spirit-level survey data from along the Delta-Mendota Canal for 1997–2001, obtained from SLDMWA and CCID, were used to compute changes in elevation between the survey dates (Bob Martin, San Luis and Delta-Mendota Water Authority and Chris White, Central California Irrigation District, written commun., 2010).

Aquifer-System Compaction Measurements Using Borehole Extensometers

Aquifer-system compaction has been monitored at selected locations for various periods with borehole extensometers by different agencies, including the USGS, DWR, SLDMWA, and CCID, and by Luhdorff and Scalmanini Consulting Engineers. A total of 35 extensometers have been monitored in the San Joaquin Valley, with most of the monitoring occurring in the 1950s and 1960s (fig. 9*A*). For a detailed description about extensometer construction and measurement of aquifer-system compaction, see Lofgren (1961), Poland (1984), and Freeman (1996).

Most of the borehole extensometers constructed in the San Joaquin Valley in the 1950s and 1960s (fig. 9*A*) have not been actively monitored since the early 1980s (fig. 9*B*). When this study was initiated in 2009, only four of these extensometers were being actively monitored in the study area: 13S/15E-31J- (Fordel), 13S/15E-35D5 (Yearout), 12S/12E-16H2 (Oro Loma Deep), and 12S/12E-16H3 (Oro Loma Shallow) (figs. 1 and 9*C*). Except for Oro Loma Deep which is anchored 305 m below land surface, the remaining extensometers are anchored above or near the top of the Corcoran Clay (less than 150 m below land surface); consequently, only a small fraction of the total aquifer-system thickness is monitored by those extensometers. The two Oro Loma extensometers and the Yearout extensometer are cable extensometers built in the 1950s and 1960s, respectively. The Fordel extensometer is a pipe extensometer; data collection began in 1999 (fig. 9*C*).

In an effort to increase the number of active monitoring locations and to improve the frequency, precision, and depth range of aquifer-system compaction measurements, 12 existing extensometers identified by DWR as possible candidates for refurbishment (Al Steele, California Department of Water Resources, written commun., 2009) were assessed to determine their suitability for refurbishment. The assessment criteria included site locations and distributions, access, extensometer depth, aquifer-system compaction and subsidence history, and estimated costs for data-quantity and quality improvements. Four cable-type extensometers (fig. 10) were selected for refurbishment in consultation with Reclamation and the SLDMWA: 12S/12E-16H2 (Oro Loma Deep, 305-m depth), 14S/13E-11D6 (Panoche, 414-m depth), 18S/16E-33A1 (DWR Yard, 314-m depth), and 20S/18E-6D1 (Rasta, 264-m depth; figs. 1 and 9*C*).

To improve the quality of aquifer-system compaction measurements, the existing reference tables and associated counterbalance systems at three sites (Oro Loma Deep, Panoche, and DWR Yard), which sit atop the concrete pads, were replaced with new reference tables and counterbalance systems that are decoupled from the concrete pads and constructed to minimize the effects of near-surface deformation caused by processes including the wetting and drying of near-surface materials, and air temperature variations (Riley, 1986; fig. 11). Properly installed extensometer reference tables facilitate measurement of the deeper aquifer-system processes that are the focus of this study. Triangular reference tables were mounted on three 3-inch diameter steel legs, each of which was cemented only at the base of holes bored to depths of about 5.5 m below land surface. To minimize the effect of shallow sediment movement on the extensometer measurements, each table leg was encased in 4-inch polyvinyl-chloride (PVC) casing. Cardboard forms were placed around the table legs to decouple them from the concrete pads, which were expanded from the existing dimensions to include the table legs (fig. 11). At the fourth site (Rasta), a new reference table was not constructed because overhead power lines restricted drill-rig access. Instead, the original reference table was modified to enable instrumentation (described below) to be installed (fig. 12). Insulated and secure metal shelters were constructed atop the concrete foundations to protect the equipment against vandalism and environmental variables (extreme temperatures, pests, rain, wind, and so on).

To increase the number of measurements of aquifer-system compaction and water levels at the extensometer sites, each site was instrumented with a data logger to record hourly data from a linear potentiometer (figs. 11 and 12) and one or more submersible pressure transducers. An analog dial gauge also was installed at each extensometer site to provide data continuity in cases of power, data logger, or potentiometer failure, and also to provide verification and calibration of the potentiometer data (figs. 11 and 12). Because the Panoche, DWR Yard, and Rasta extensometers also were constructed as observation wells with screened intervals below the Corcoran Clay (345–365 m; 262–326 m; and dual screens 232–255 m and 259–266 m, respectively; Ireland and others, 1984), submersible pressure transducers were installed to measure water levels representing these intervals. The Oro Loma Deep extensometer was not constructed as an observation well; two water-level observation wells—12S/12E-16H5 and 12S/12E-16H6—with screened intervals below the Corcoran Clay (204–217 m and 235–277 m, respectively) were constructed in individual boreholes at the Oro Loma site (Ireland and others, 1984). Both wells were instrumented with submersible pressure transducers and data loggers.

The refurbishment of the four selected extensometers was completed in early 2012. Since then, the sites have been maintained by USGS personnel who download the data, make manual dial-gauge and water-level measurements for quality control, and adjust equipment. Preliminary data collected at the refurbished extensometer sites are presented in appendix E.

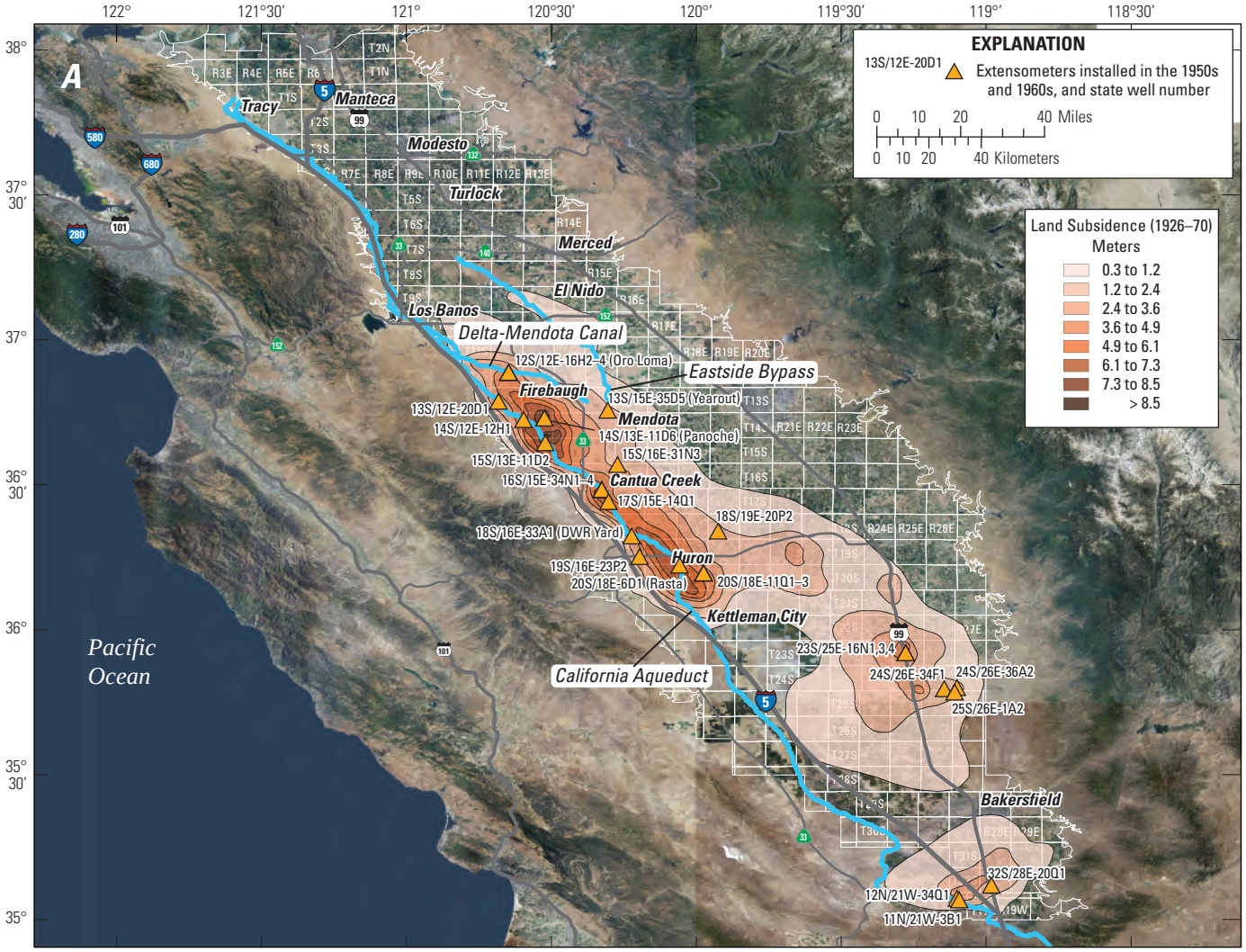

Figure 9. Land-subsidence monitoring locations and methods in the San Joaquin Valley, California, in the *A*, 1960s; *B*, 1980s; and *C*, 2010s. Land-subsidence contours shown in *A* were modified from Ireland and others, 1984. Land-subsidence contours shown in *C* were produced as a part of this study.

Figure 9. Continued.

Figure 9. Continued.

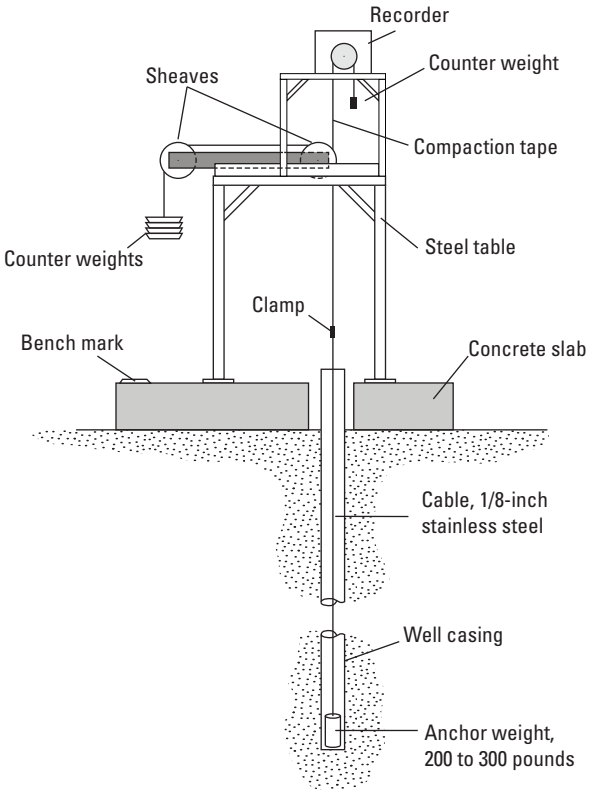

Figure 10. Construction details of a typical San Joaquin Valley cable-type borehole extensometer (modified from Lofgren, 1961; Bull, 1975).

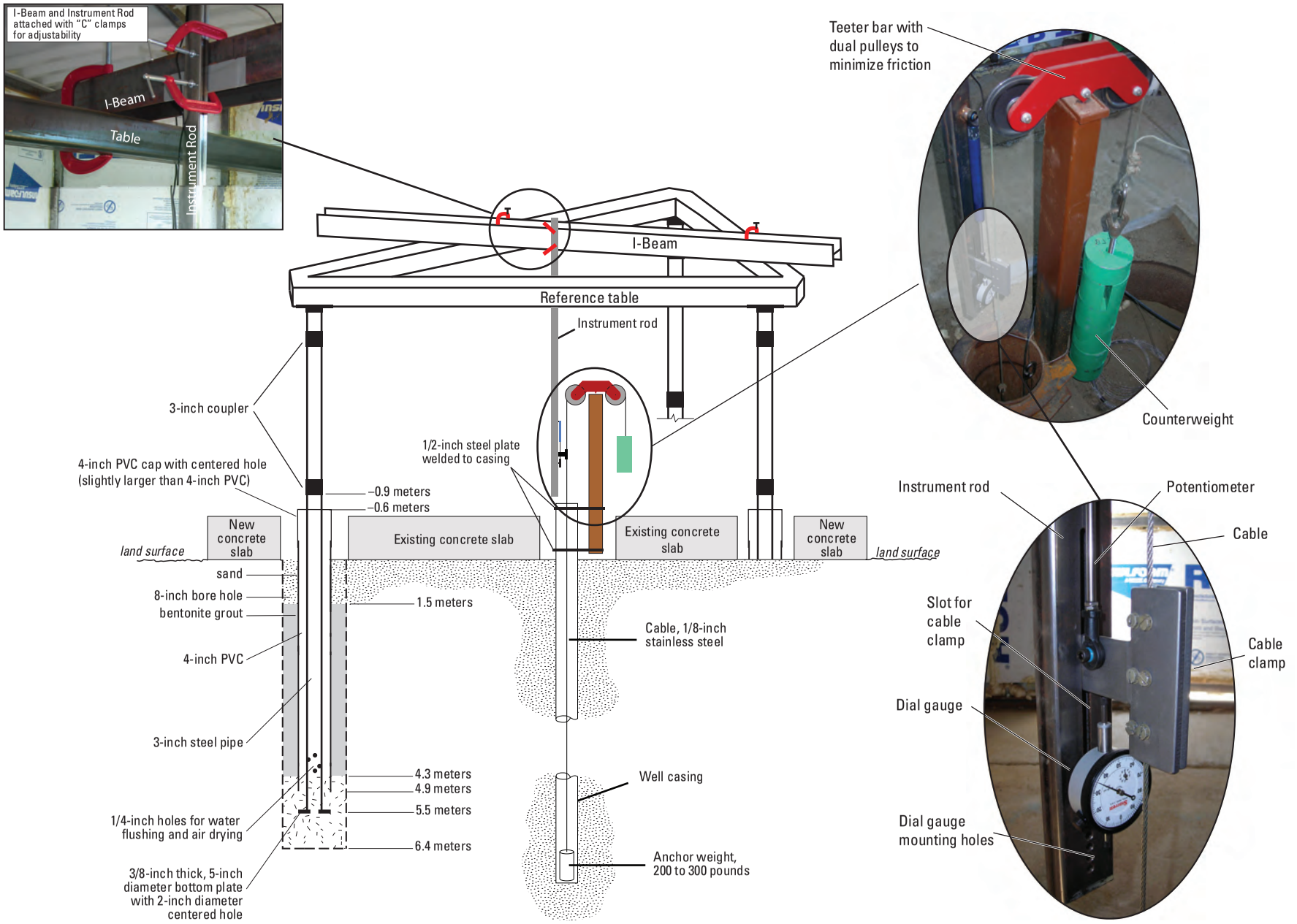

Figure 11. New reference table and counterbalance system constructed as part of extensometer refurbishment at sites 12S/12E-16H2 (Oro Loma Deep), 14S/13E-11D6 (Panoche), and 18S/16E-33A1 (DWR Yard), and potentiometer and dial gauge instrumentation installed at all four refurbished extensometers, San Joaquin Valley, California.

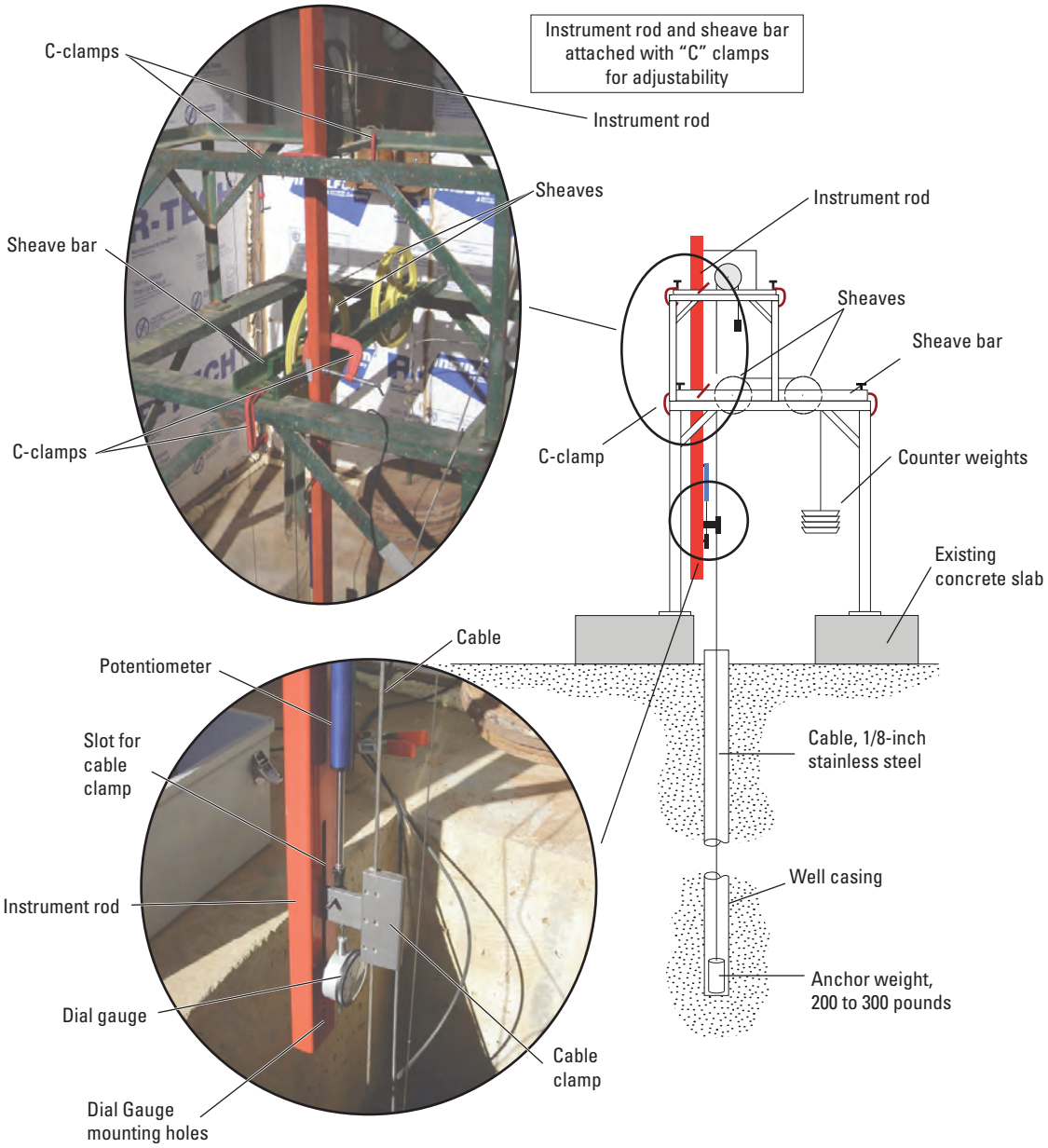

Figure 12. Modified reference table and instrumentation at 20S/18E-6D1 (Rasta), San Joaquin Valley, California.

Water Levels

Measurements of groundwater levels in wells within the study area (fig. 13) were obtained from USGS and DWR databases, and the City of Tracy. These data were analyzed to determine the degree of correlation between vertical changes in land surface and changes in groundwater levels. Hydrographs were generated to display groundwater-level elevations through time for the unconfined to semi-confined parts of the aquifer system (above the Corcoran Clay) and for the confined parts of the aquifer system (below the Corcoran Clay).

Hydrographs were generated for selected deforming and stable areas and for each check station along the DMC. A check station is a structure built to control the water-surface level and flow in a canal. Wells for which screen intervals were known were categorized as either above the Corcoran Clay (shallow) or below the Corcoran Clay (deep). For wells with unknown screen intervals, water-level elevations from that well were compared to water-level elevations from nearby wells with known screen intervals. If a correlation between the water levels from the well with unknown screen intervals and water levels from the wells with known screen intervals could be made with a high degree of confidence, the well was categorized as shallow or deep accordingly. In areas where multiple wells were present, representative hydrographs were selected based on availability of construction information, location, similarity to hydrographs from nearby wells, measurement frequency, and period of record. Wells with screen intervals both above and below the Corcoran Clay were not (knowingly) used.

Land Subsidence and Aquifer-System Compaction

The PS InSAR and ALOS interferograms and CGPS data showed that during 2003–10, some areas within the study area had significant land-surface elevation changes, and others were relatively stable. A combination of individual and stacked interferograms were used to examine the characteristics of shorter- and longer-term deformation, respectively. For this report, "shorter-term" refers to periods of less than 1 year, and "longer-term" refers to periods of 1 year or longer. Following the calculation of PS InSAR range change data, relative to the selected reference points of CGPS P257 and P300, the interferograms were interpreted for nine additional CGPS sites in order to analyze PS InSAR-measurement quality and precision (fig. 14). This comparative analysis showed that nearly all of the PS InSAR interferogram-derived range-change values were within 10 mm of the vertical deformation values calculated from the CGPS measurements. This indicated a resolution of the PS InSAR (C-band) data of 10 mm or better. Note that 5 of the 11 CGPS stations shown in figure 14 (P255, P252, P301, P302, and P300) are on the fringes of the valley (fig. 7) where the aquifer system is fairly thin and bedrock is shallow; measurements from these stations likely include land-surface deformation unrelated to aquifer-system compaction, such as uplift of the Coast Ranges. These CGPS sites were useful in characterizing the quality of the InSAR data, but were not used in the subsidence analysis. Because the resolution of L-band data is 20 mm, which is lower in resolution than the CGPS data, the L-band InSAR results were not compared to CGPS data.

Selected PS InSAR interferograms constructed with data collected during 2003–10 are presented to show detailed land-surface deformation patterns along the northern and southern reaches of the DMC for the periods 2007–10 and 2003–08, respectively (figs. 15, 16, and appendices A–C). The ALOS interferogram for January 8, 2008 to January 13, 2010 was contoured at a 120-mm contour interval, where data permitted, to show detailed land-deformation patterns in areas not covered by the PS InSAR interferograms (fig. 17).

Current (2003–10) Pattern of Land Subsidence

The current (2003–10) pattern of land subsidence in the study area is discussed in this section of the report by four areas showing similar land-deformation patterns (in space and time): (1) Clifton Court Forebay-Check 6-Turlock, (2) Checks 7–9, (3) Checks 10–14, and (4) Check 15-P304 (fig. 13). Interferogram selection criteria to generate the time-series graphs were based on the land-surface elevation peaks (early in the year) and troughs (early fall) shown by CGPS data (fig. 14), which can be combined to show year-to-year elevation changes. However, because of limited data availability that was further restricted by quality, these peaks and troughs likely were not captured by the interferograms, possibly resulting in conservative estimates of seasonal elevation changes.

Clifton Court Forebay-Check 6-Turlock

The Clifton Court Forebay-Check 6-Turlock area includes Clifton Court Forebay, Checks 1–6, CGPS P257 and P781, and the towns of Tracy, Modesto, and Turlock (Area 1 in figure 13). Land-surface elevations within this area generally were either stable or subsided only small amounts from December 2007 through July 2010 (figs. 15, 18*A* and 19; appendices A and C); at some locations, shorter periods of uplift and subsidence occurred during this period (figs. 14 and 18*A*). InSAR-generated time series from the end of 2007 through July 2010 indicated Clifton Court Forebay subsided about 20 mm and nearby Tracy subsided about 5 mm (fig. 18*A*). The slightly greater subsidence magnitudes toward the Clifton Court Forebay (fig. 15) could result from peat oxidation, which is the dominant process causing land subsidence in the Sacramento-San Joaquin Delta (Galloway and others, 1999). InSAR-generated time series from the end of 2007 through July 2010 indicated Turlock subsided about 25 mm (fig. 18*A*). This region fluctuated seasonally: the land surface uplifted during fall and winter and subsided during spring

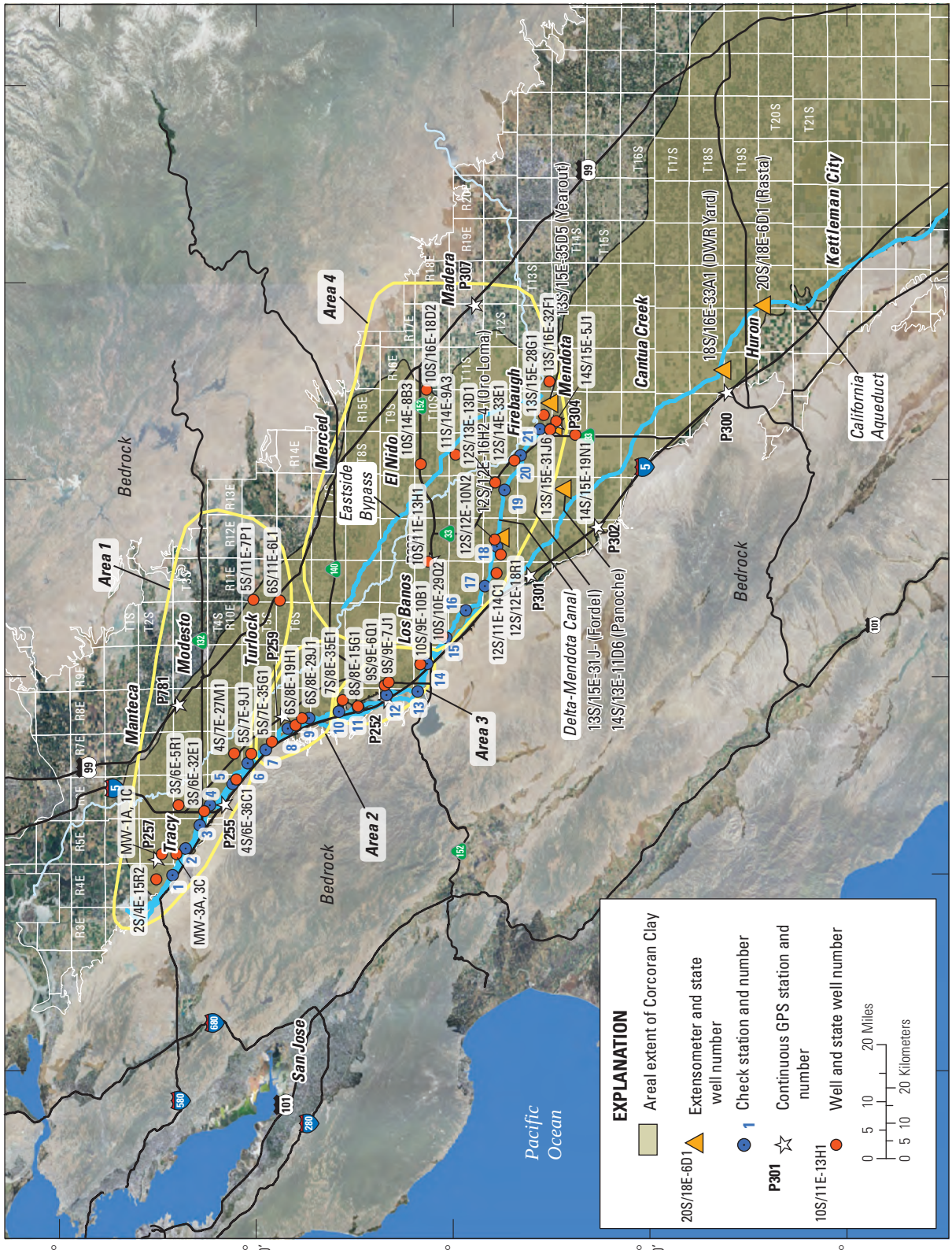

Figure 13. Check stations, continuous Global Positioning System (CGPS) stations, and wells used to generate groundwater-elevation hydrographs, and four areas showing similar land-surface deformation patterns, San Joaquin Valley, California (areal extent of Corcoran Clay obtained from Faunt, 2009).

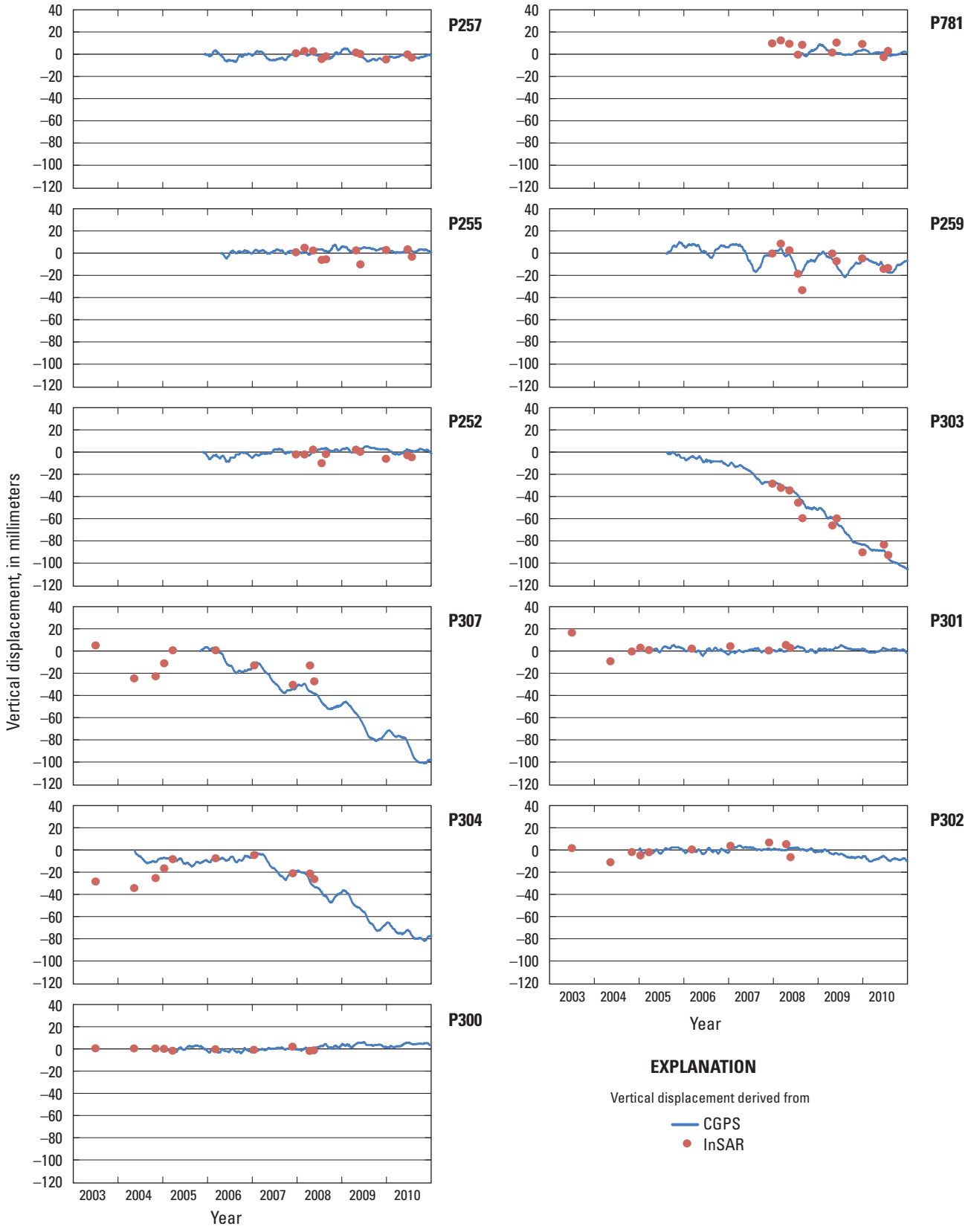

Figure 14. Continuous Global Positioning System (CGPS) time series and Interferometric Synthetic Aperture Radar (InSAR) time series at the 11 CGPS station locations in the San Joaquin Valley for periods during 2003–10. CGPS data were obtained from the University NAVSTAR Consortium. See figure 7 for locations of CGPS stations. See appendices A and B for interferograms used to construct the InSAR time series.

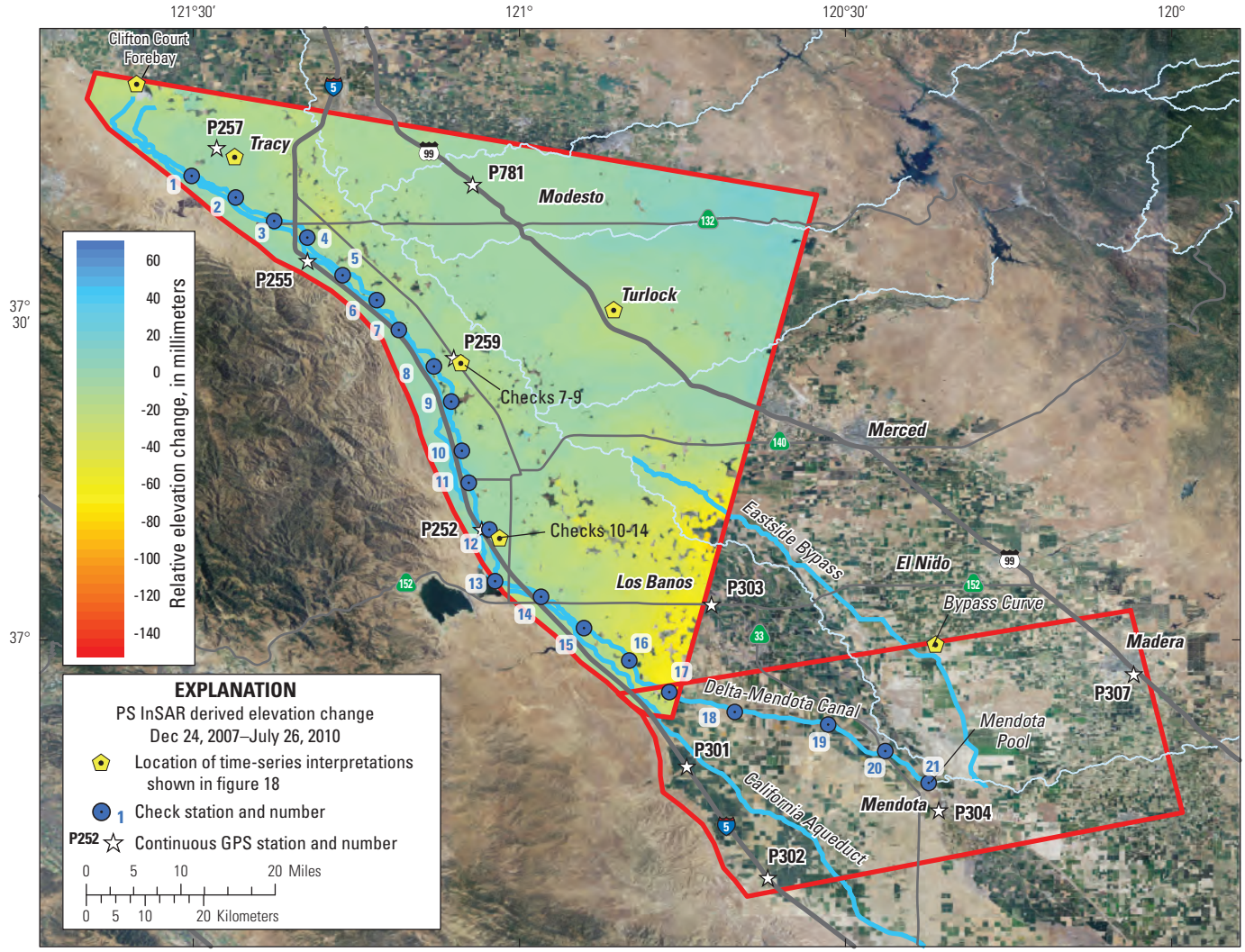

Figure 15. Elevation changes for the northern reaches of the Delta-Mendota Canal, ENVIronmental SATellite (ENVISAT) track 299, interpreted from stacked persistent scatterer Interferometric Synthetic Aperture Radar (PS InSAR) interferograms, December 24, 2007–July 26, 2010, San Joaquin Valley, California. Negative values indicate subsidence, and positive values indicate uplift. See appendix A for the individual interferograms used to produce this stacked interferogram.

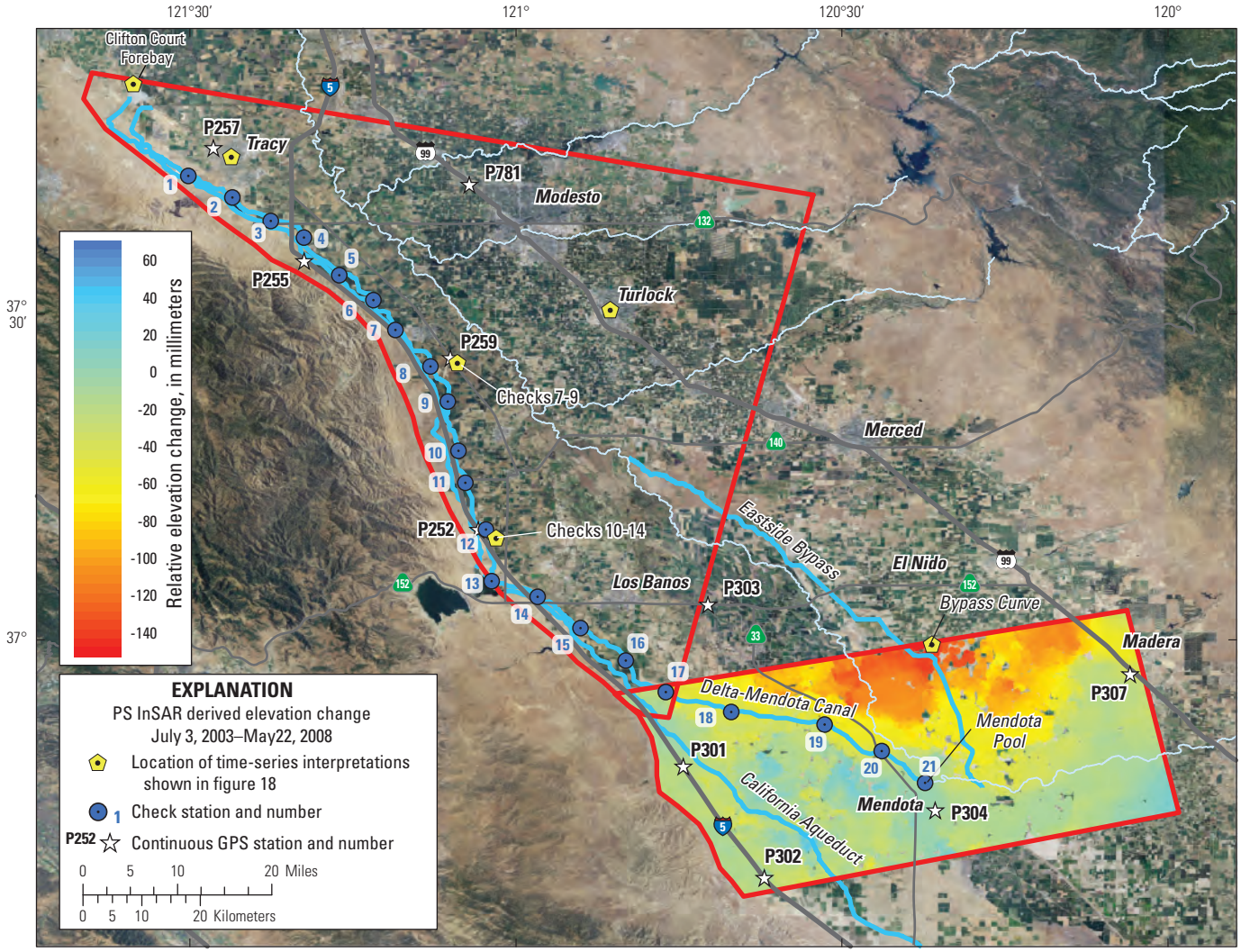

Figure 16. Elevation changes for the southern reaches of the Delta-Mendota Canal, ENVIronmental SATellite (ENVISAT) track 435, interpreted from stacked persistent scatterer Interferometric Synthetic Aperture Radar (PS InSAR) interferograms, July 3, 2003–May 22, 2008, San Joaquin Valley, California. Negative values indicate subsidence, and positive values indicate uplift. See appendix B for the individual interferograms used to produce this stacked interferogram.

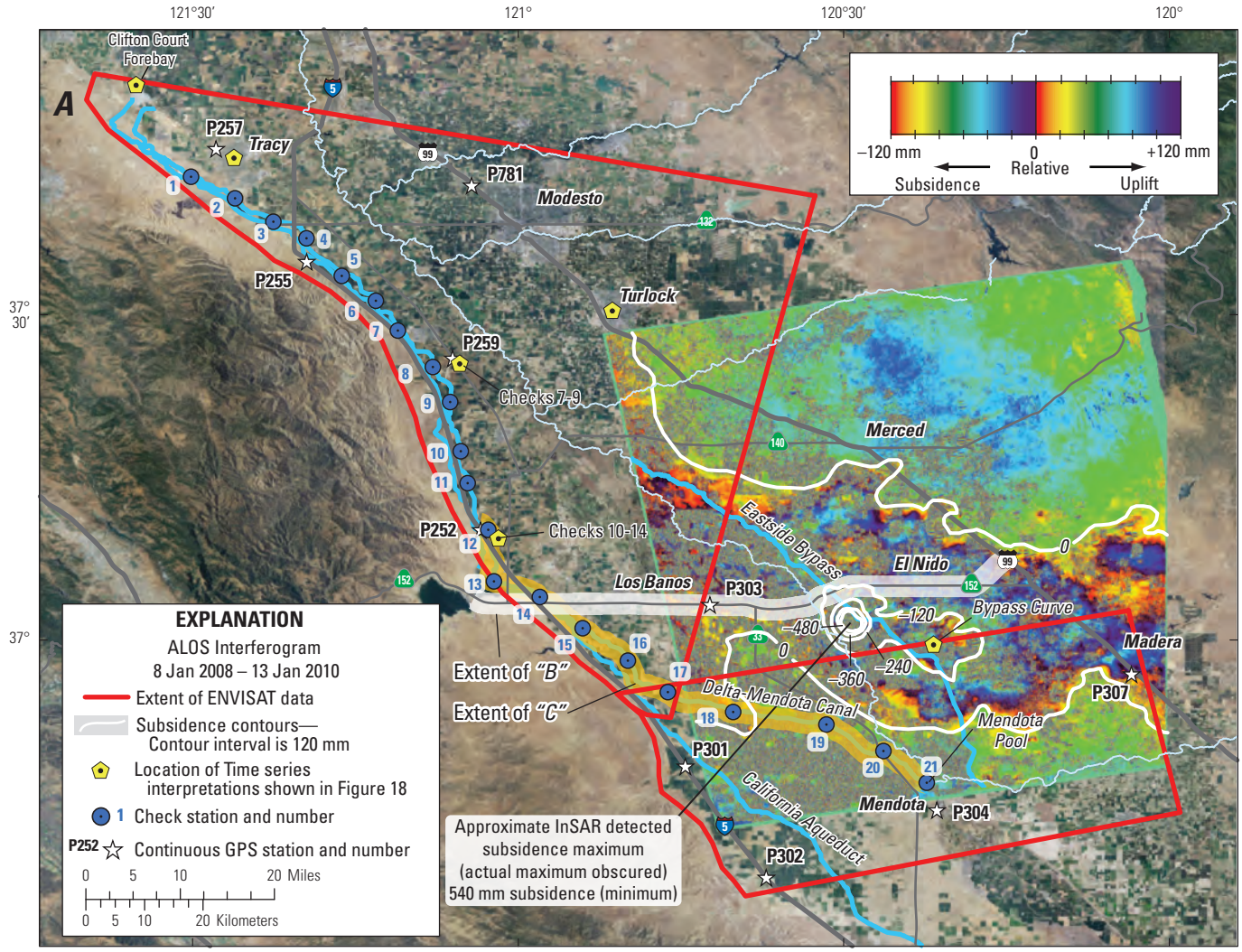

Figure 17. *A,* Advanced Land Observing Satellite (ALOS) interferogram with subsidence contours showing vertical changes in land surface in the central San Joaquin Valley area, California, during January 8, 2008–January 13, 2010; *B,* elevation changes computed from repeat geodetic surveys along Highway 152 for 1972–2004; and *C,* elevation changes computed from repeat geodetic surveys along the Delta-Mendota Canal for 1935–2001. Subsidence data along Highway 152 were computed from published National Geodetic Survey elevations. Subsidence graph along the Delta-Mendota Canal was obtained from the San Luis and Delta-Mendota Water Authority and the Central California Irrigation District.

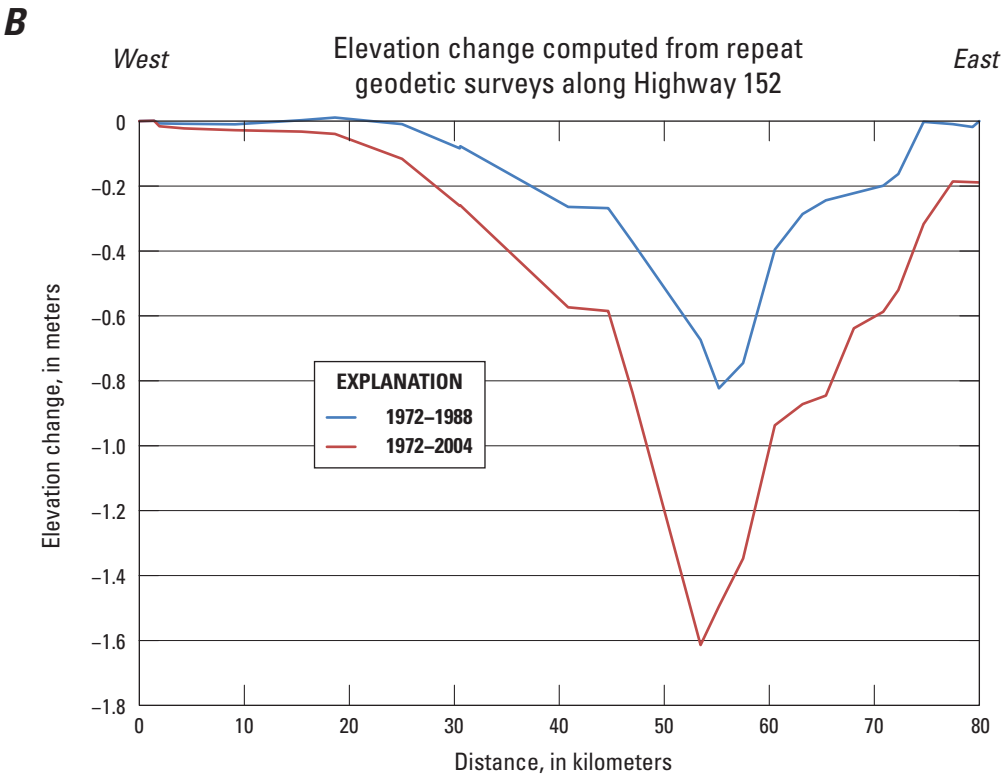

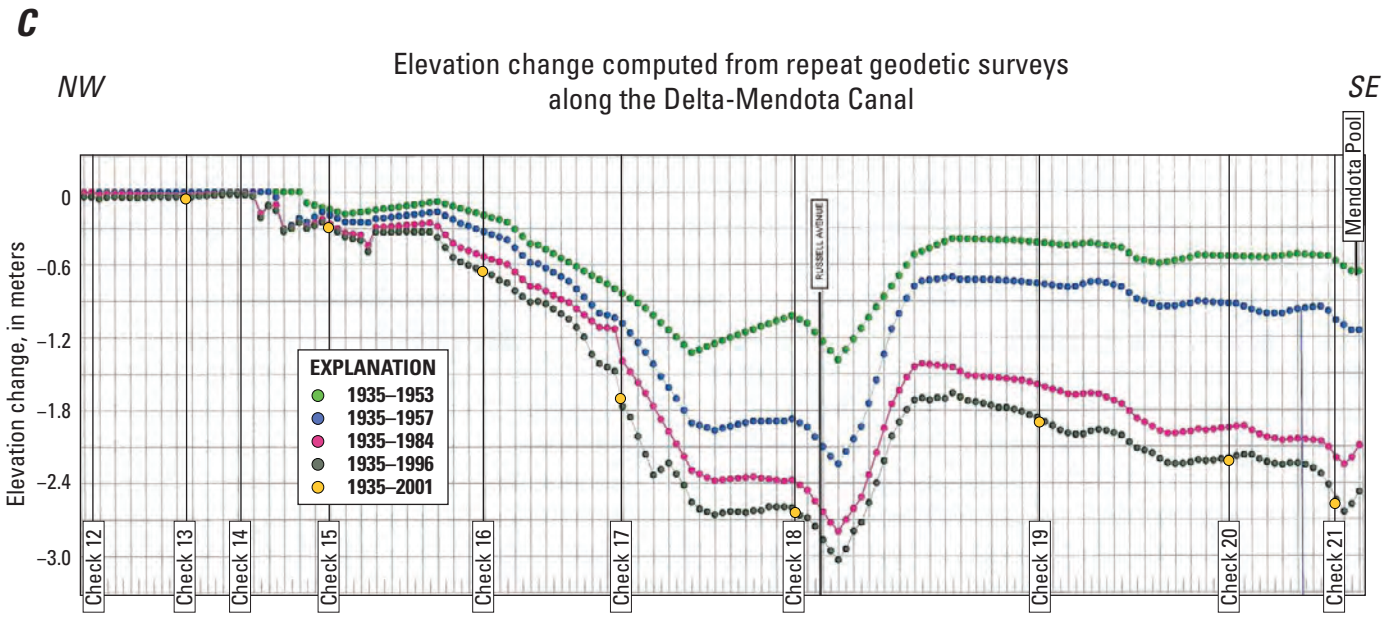

Figure 17. Continued.

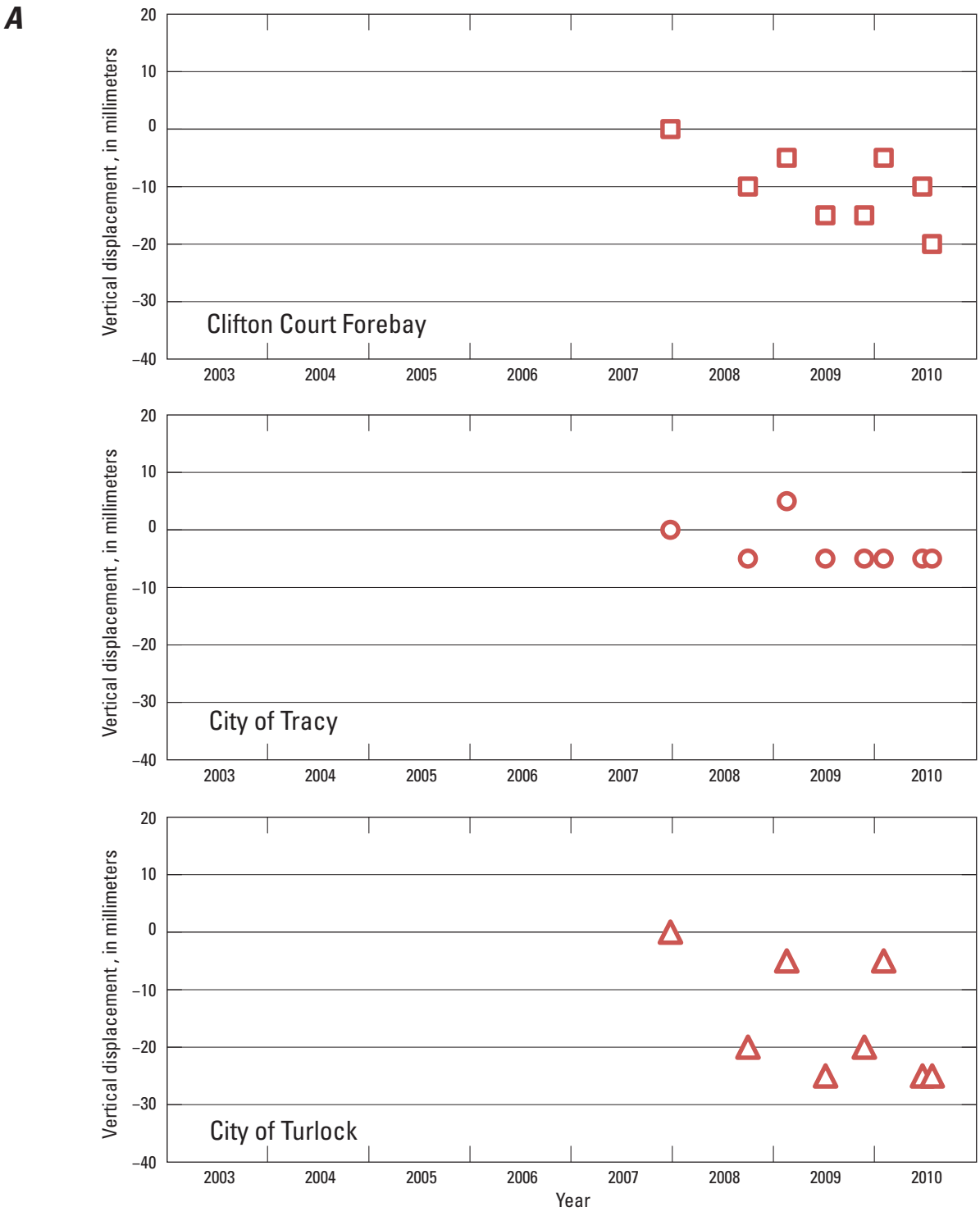

Figure 18. Interferometric Synthetic Aperture Radar (InSAR) calculated vertical displacements between December 2007–July 2010 for *A,* Clifton Court Forebay, Tracy, and Turlock; *B,* Checks 7–9; *C,* Checks 10–14; and *D,* Bypass Curve, San Joaquin Valley, California. See appendices A–C for interferograms used to construct the time series.

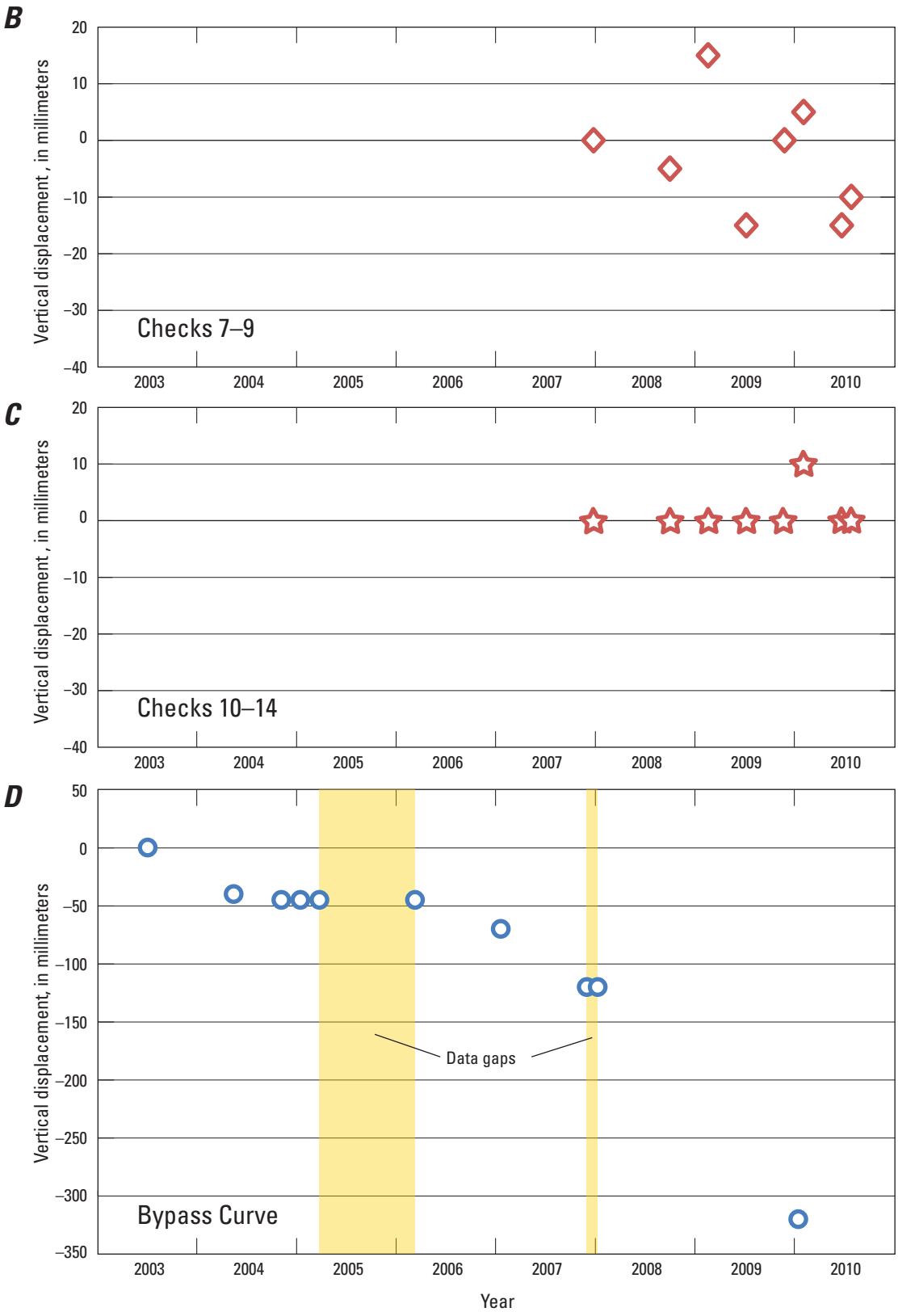

Figure 18. Continued.

and summer (fig. 18*A*). Turlock seasonally fluctuated as much as 20 mm, while Clifton Court Forebay and Tracy fluctuated 10 mm or less (fig. 18*A*). The CGPS stations (fig. 15) in Tracy (P257) and near Modesto (P781) also showed shorter-term elevation fluctuations superimposed on relatively longer-term elevation stability (fig. 14).

PS InSAR-calculated vertical-displacement profiles along the DMC for the period December 24, 2007–July 26, 2010, indicate that the elevation of the canal experienced less than 15 mm of subsidence between Check Stations 1–6 (fig. 19). The California Aqueduct and the DMC are near each other in this area. Elevation data from GPS surveys along the California Aqueduct indicated 10–20 mm of subsidence during 2000–09 near DMC Checks 3 and 4; elevations at other locations along the Aqueduct in this area changed less than 10 mm (Forrest Smith, DWR, written commun., 2009).

Checks 7–9

The Checks 7–9 area includes Checks 7–9 and CGPS P259 (Area 2 in figure 13). Land-surface elevations within this area were either stable or had small net subsidence from December 2007 through July 2010 (fig. 15), but also underwent appreciable seasonal uplift and subsidence during this period (figs. 14 and 18*B*). InSAR-generated time series indicated that this area subsided about 10 mm over the 3-year period, but indicated as much as 30 mm of seasonal change, where the land surface uplifted during fall and winter and subsided during spring and summer (fig. 18*B*). For 2005 through 2010, CGPS data at P259 indicated seasonal uplift and subsidence ranging from about 10 to 30 mm superimposed on a longer-term subsidence trend of about 15 mm (fig. 14). Elevation data from GPS surveys along the California Aqueduct indicated stability during 2000–09 (Forrest Smith, DWR, written commun., 2009).

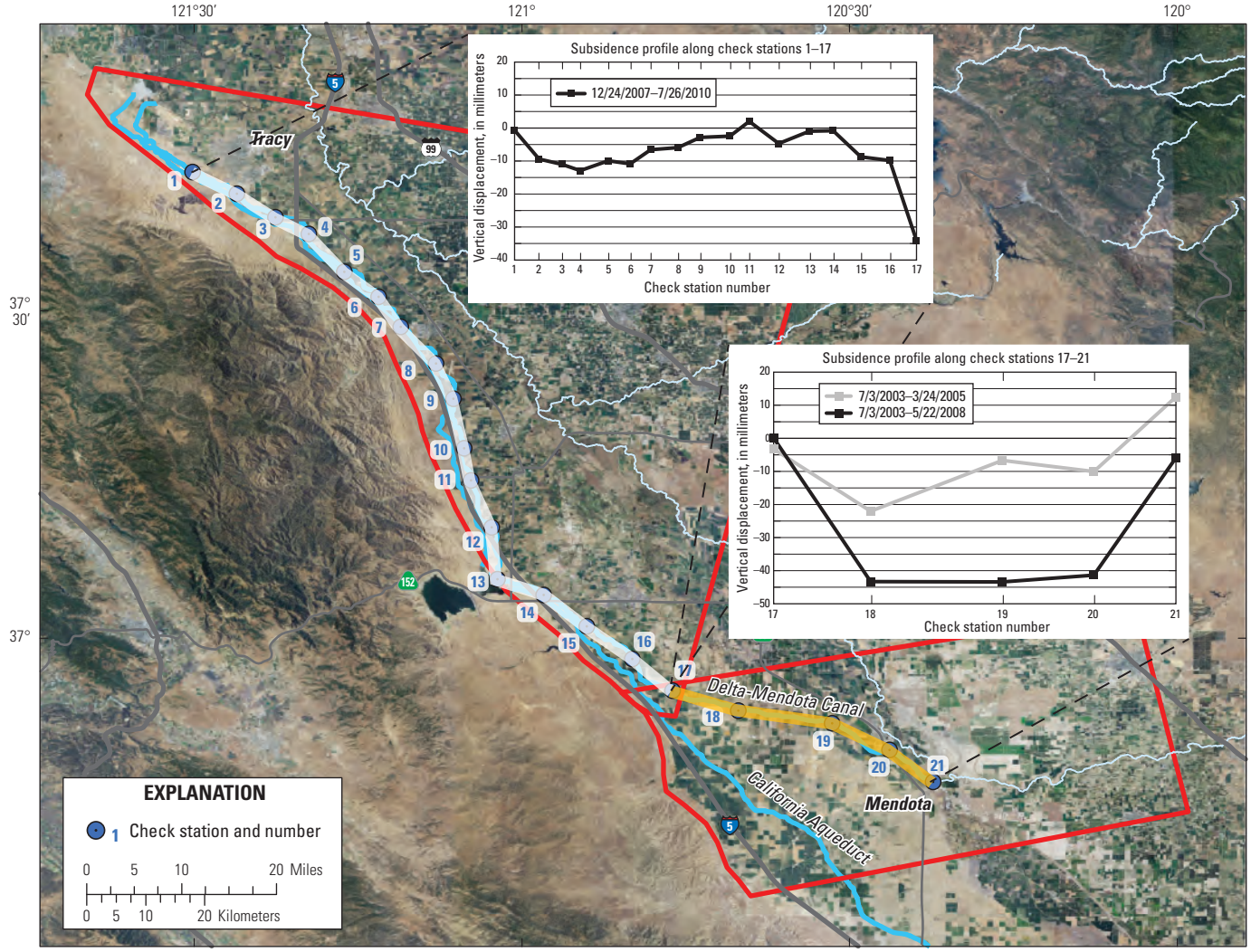

Figure 19. Persistent scatterer Interferometric Synthetic Aperture Radar (PS InSAR)-calculated vertical-displacement profiles for *A,* the northern reaches of the Delta-Mendota Canal, Checks 1–17, between December 24, 2007, and July 26, 2010, and *B,* the southern reaches of the Delta-Mendota Canal, Checks 17–21, between July 3, 2003, and May 22, 2008, San Joaquin Valley, California. See appendices A and B for the interferograms used to construct the vertical-displacement profiles.

Checks 10–14

The Checks 10–14 area includes Checks 10–14 and the area to the east (Area 3 in figure 13). The land-surface elevations within the area were fairly stable on longer and shorter-term scales from December 2007 through July 2010 (fig. 15). For this group of five check stations, elevation changed about 10 mm or less seasonally and was stable during 2007–10 (fig. 18*C*). Elevation data from GPS surveys along the California Aqueduct indicated stability during 2000–09 (Forrest Smith, DWR, written commun., 2009).

Check 15-P304 (El Nido)

The Check 15-P304 area includes Checks 15–21 and CGPS stations P303, P304, and P307 (Area 4 in figure 13). This area is part of a large subsidence feature centered south of the town of El Nido (figs. 15, 16, and 17) that is evident in interferograms for periods during 2003–04 and 2006–10 (appendices A–C). Land-surface elevation changes shown in the 2-year ALOS interferogram between January 8, 2008–January 13, 2010 show subsidence of 20 mm or more over 3,200 km^2 in the central part of the San Joaquin Valley, extending about 80 km west-east, from Check 17 to Madera, and 40 km north-south, from about Merced to about Mendota (fig. 17; Sneed and Phillips, 2012). For periods during 2003–10, the magnitude of subsidence derived from the ENVISAT and ALOS data was fairly consistent at Checks 18, 19, and 20, indicating that these check stations subsided similarly compared to Checks 16, 17, and 18, and Checks 20 and 21, where the subsidence magnitudes were fairly different, indicating differential subsidence at these two sets of adjacent check stations (figs. 16, 17, and 19). It is noted, however, that the magnitude of subsidence along the canal segments between the check stations varies in the individual interferograms shown in appendices A, B, and C. The maximum subsidence shown in the ALOS interferogram was more than 540 mm, or about 270 mm/yr, between the San Joaquin River and Eastside Bypass, about 10 km south of El Nido (fig. 17). The center of the subsidence maximum is obscured either by decorrelation from ground disturbance or an unresolvable steep subsidence gradient (large differences in subsidence magnitude within the small area).

ENVISAT data from InSAR track T435 did not cover the area of maximum subsidence shown by ALOS, but did capture the southern part of the subsidence bowl; a maximum of about 150 mm of subsidence occurred at Bypass Curve from July 3, 2003, to May 22, 2008, about 8 km southeast of the ALOS maximum (figs. 16 and 17). A time series was constructed for Bypass Curve (where the ENVISAT and ALOS data sets overlap) by combining ENVISAT interferograms shown in appendix B-1–B-6 (July 3, 2003–November 29, 2007), and the ALOS interferogram for January 8, 2008–January 13, 2010. Note that there are two gaps in this time series: March 24, 2005–March 9, 2006, and November 29, 2007–January 8, 2008. The total measured elevation change during the period July 3, 2003–January 13, 2010, was about 320 mm of subsidence—45 mm of subsidence during the period July 3, 2003–November 4, 2004, 0 mm of subsidence during the period November 4, 2004–March 24, 2005, 75 mm of subsidence during the period March 9, 2006–November 29, 2007, and 200 mm of subsidence during the period January 8, 2008–January 13, 2010 (fig. 18*D* and appendix B).The rate of subsidence in the Bypass Curve area was about 35 mm/yr during 2003–04, increased to about 45 mm/yr during 2006–07, and again increased to about 100 mm/yr during 2008–10 (fig. 18*D*). Subsidence calculations from GPS surveys done in 2008 and 2010 corroborated the high rate measured by InSAR during that period, and GPS surveys in 2012 by Reclamation indicated that the high rate of subsidence continued (Mark Morberg, Reclamation, written commun., 2012). Additional evidence of a subsidence-rate change in 2008 was given by comparing the longer-term elevation-change data at Check 17, where data from T299 and T435 overlap (figs. 15 and 16). The data for T435 indicated that Check 17 was fairly stable between July 3, 2003, and May 22, 2008 (figs. 16 and 19), whereas the data for T299 indicated about 35 mm of subsidence between December 24, 2007, and July 26, 2010 (figs. 15 and 19). Finally, individual interferograms (table 1) were used to calculate deformation rates for five selected locations in this subsidence area, which indicated that subsidence rates doubled about May 2008.

There are no CGPS sites near the area of maximum active subsidence, but three sites are situated along the edges of the subsidence bowl. CGPS data from P307, near Madera, and from P303 east of Los Banos on Highway 152, indicated subsidence of about 100 mm between August 2005 and 2010—a rate of about 20 mm/yr (fig. 14). CGPS P307 showed seasonally variable rates, including small amounts of uplift during winter seasons, but fairly stable long-term rates during 2005–10. P303 showed less seasonal variation, such that subsidence slowed or ceased (but did not uplift) during some shorter-term periods—mostly during fall and winter (fig. 14). P303 also showed a subsidence rate increase of greater than 50 percent after about May 1, 2008. CGPS data from P304, near Mendota, showed about 80 mm of subsidence between mid-2004 and 2010, with nearly all of it (70 mm) occurring after 2006, indicating a rate of nearly 20 mm/yr. P304 also showed seasonally variable rates, including small amounts of uplift during fall and winter seasons, which were most pronounced between 2007 and 2010 (fig. 14).

Comparison to Historical Land Subsidence

Subsidence contours for 1926–70 (Poland and others, 1975) showed the area of maximum active subsidence was southwest of Mendota (figs. 2 and 9*A*); whereas, data collected and compiled for this study for 2003–10 indicated that the area of maximum active subsidence had shifted northeast, to the area south of El Nido (figs. 9*C* and 17*A*). Historical subsidence exceeded 8.5 m in the Mendota area where rates exceeded 500 mm/yr during the mid-1950s and early 1960s (Ireland and others, 1984). Recent subsidence was about 0.54 m in the area south of El Nido (fig. 17*A*) where rates

were about 270 mm/yr during 2008–10. Historical subsidence rates along Highway 152, which bisects the 2003–10 area of active subsidence, calculated from leveling-survey data from 1972, 1988, and 2004 show that for the two 16-year periods (1972–88 and 1988–2004), maximum subsidence rates of about 50 mm/yr were found just south of El Nido (fig. 17*B*).

Geodetic surveys completed along the DMC in 1935, 1953, 1957, 1984, and annually during 1996–2001 indicated that subsidence rates were greatest between the 1953 and 1957 surveys, and that the maximum subsidence along the DMC (about 3 m) was just east of Check 18; a secondary maximum (nearly 2.7 m) was just east of Check 21 (fig. 17*C*). The surveys during 1997–2001 indicated that subsidence was minor along the DMC; maxima were near Checks 19 (about 40 mm) and 21 (about 45 mm) (fig. 17*C*). The InSAR time series constructed for the check stations for 2003–08 indicated subsidence maxima near Checks 18, 19, and 20 (about 40–45 mm) and subsidence of about 5 mm near Check 21 (fig. 19). The InSAR time series also indicated that most of the subsidence at checks 19 and 20 occurred after 2005. In the area south of where the California Aqueduct and the DMC diverge near Check 15, there were 10–50 mm of subsidence during 2006–09 and 20–80 mm of subsidence during 2000–09 along the part of the Aqueduct south of DMC Check 16 (Forrest Smith, DWR, written commun., 2009).

Groundwater Levels

Groundwater levels and groundwater-level changes in the study area were evaluated by using water-level hydrographs from 35 wells spread throughout the study area (figs. 13 and 20). Of particular importance was evaluating differences in groundwater levels and changes in wells screened above and below the Corcoran Clay. In this report a well is referred to as 'deep' if it was screened below the Corcoran Clay and referred to as 'shallow' if it was screened above the Corcoran Clay. In the case where the screened information is unknown for the particular well, but nearby wells were used to infer the screen in relation to the Corcoran Clay, the term 'inferred' is used to modify 'deep' or 'shallow.' If the screened information cannot be inferred, the terms 'deep' or 'shallow' are not used.

Clifton Court Forebay-Check 6-Turlock

Water levels near Checks 1–4, including Tracy and CGPS P257, were examined by using hydrographs from wells 2S/4E-15R2, cluster wells MW-1A and 1C, cluster wells MW-3A and 3C, 3S/6E-5R1, and 3S/6E-32E1 (fig. 20*A*). Cluster wells are monitor wells located adjacent to one another but screened at different depths; 'A' signifies the well is shallow and 'C' signifies the well is deep. Water levels in shallow well -15R2, located between the City of Tracy and Clifton Court Forebay, showed minor short-term variability superimposed on 3 m of water-level decline during 1958–2010. Cluster wells MW-1A/MW-1C and MW-3A/MW-3C have similar hydrographs, with water-level highs in the winter and lows in the summer. The shallow wells tended to have slightly smaller seasonal fluctuations than the deep wells. The wells at site MW-1 showed a slight recovery during 2007–09, whereas the wells at site MW-3 showed a slight decline over the same period. Water levels in deep well -5R1 indicated seasonal variability of as much as 15 m from the late 1950s through the mid-1990s, after which the seasonal variability decreased through 2010. These water levels showed some long-term variability, but water levels measured in the fall of 2009 were similar to those measured in the fall of 1960, when water levels recovered from record lows in the late 1950s. Water levels in shallow well -32E1 showed seasonal variability superimposed on periods of longer-term recovery and decline between 1960 and 2010, including a 1.5-m decline during 2003–10. The most notable feature in this hydrograph was the generally depressed (and lowest recorded) water levels beginning in the drought year of 1987 and continuing through 1996. The timing and increased seasonal variability associated with this feature indicated a period of increased local groundwater pumping. In summary, hydrographs in this area showed seasonal and climatic effects, and minor long-term variability with the lowest water levels measured in the late 1950s in the deep aquifer and in the 1980s and 1990s in the shallow aquifer.

Water levels near Checks 5 and 6 were examined by using hydrographs from wells 5S/7E-9J1, 4S/7E-27M1, 4S/6E-36C1 (fig. 20*B*). Groundwater levels in well 5S/7E-9J1 showed seasonal fluctuations as large as 6 m superimposed on periodic declines associated with drought periods, including 2007–10; water levels reached a record low in 2009 (fig. 20*B*). Water levels during 2003–10 were similar to those during the late- and post-drought period of 1991–96 and were generally lower than water levels prior to the 1987–92 drought. Groundwater levels in shallow well 4S/7E-27M1 and in deep well 4S/6E-36C1 showed shorter-term and longer-term fluctuations between the early 1960s and the late 1990s; there were no subsequent measurements (fig. 20*B*). Both wells show responses to drought conditions, although recovery in deep well -36C1 following the 1976–77 drought period was delayed until the late 1980s, indicating a prolonged period of increased groundwater pumping. After the 1987–92 drought, water levels in -36C1 continued to decline; water levels reached historical lows in 1997 (the end of the record). In summary, hydrographs in this area showed seasonal and climatic effects, and some long-term variability with the lowest water levels measured during and after the drought period 1987–92 in the deep and shallow aquifers; the lowest water level was measured in 2009 in a well with an unknown screened interval.

Water levels near Turlock were examined by using the hydrographs from shallow well 5S/11E-7P1 and deep well 6S/11E-6L1 (fig. 20*C*). Groundwater levels in well 5S/11E-7P1 showed seasonal fluctuations as large as about 5 m superimposed on periodic declines associated with drought periods (fig. 20*C*). Groundwater levels in deep well 6S/11E-6L1 showed seasonal fluctuations as large as about 18 m superimposed on periodic declines and recoveries; the lowest water level was measured in 1988; no additional measurements were made after 1994 (fig. 20*C*).

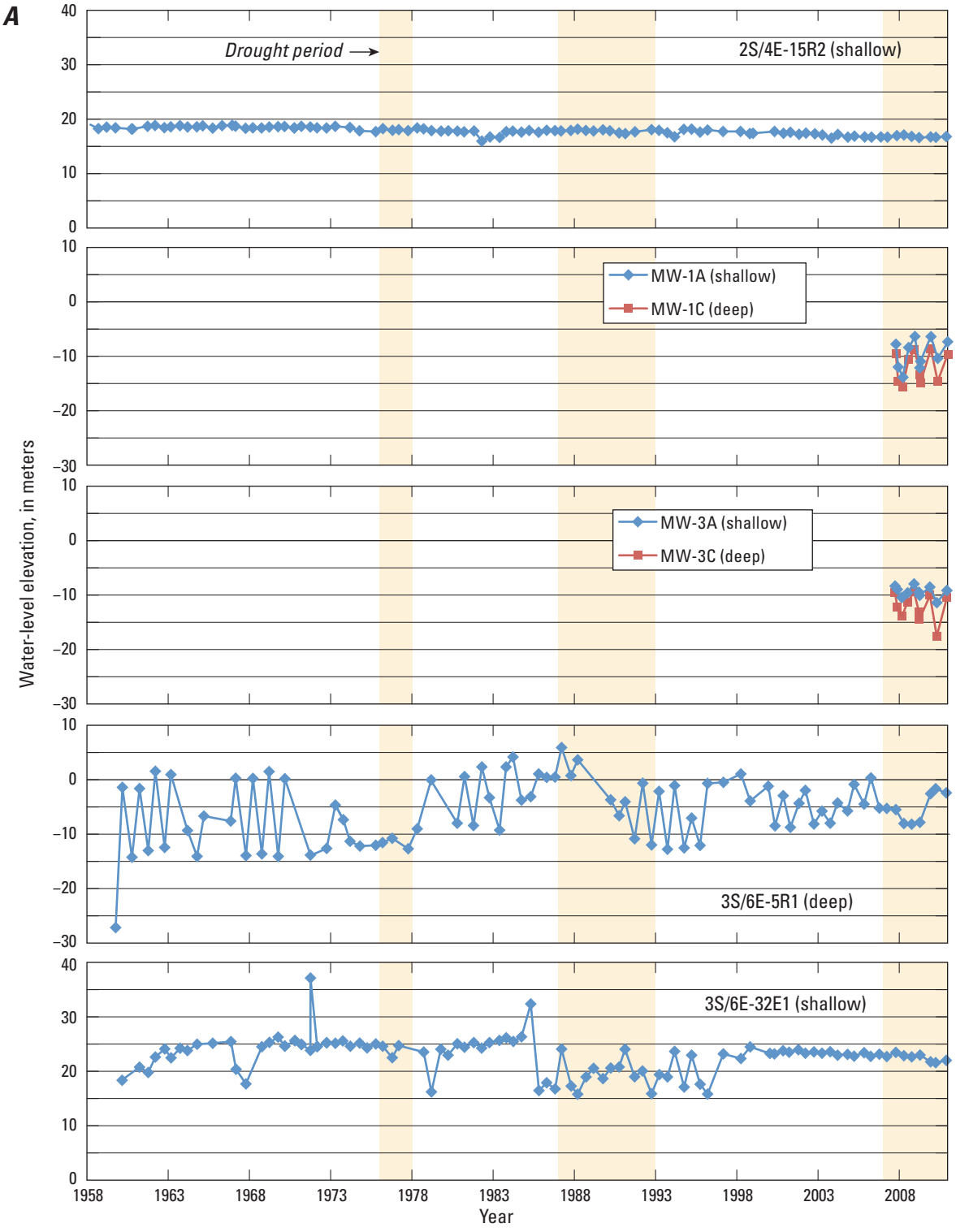

Figure 20. Discrete measurements for selected wells for areas in the San Joaquin Valley, California, near *A,* Checks 1–4 (data from wells MW-1A, MW-1C, MW-3A, and MW-3C were obtained from the City of Tracy); *B*, Checks 5–6 (data from wells -27M1 and -36C1 were from Department of Water Resources (DWR) and U.S. Geological Survey (USGS) databases); *C*, Turlock (data from well -6L1 were from DWR and USGS databases); *D*, Checks 7–9; *E*, Checks 10–14; *F*, CGPS P303; *G*, Checks 15–17; *H*, El Nido; *I*, Checks 18–20; and *J*, Check 21 and CGPS P304 (data before May 30, 2010, for wells -5J1 and -31J6 were from Glenn Browning, Luhdorff and Scalmanini Consulting Engineers; data after May 30, 2010, for wells -5J1 and -31J6 were from USGS). All water-level elevations were derived from California Department of Water Resources except where noted. Shaded areas indicate drought periods. A break in the hydrograph line indicates a data gap of at least 5 years. See figure 13 for well locations.

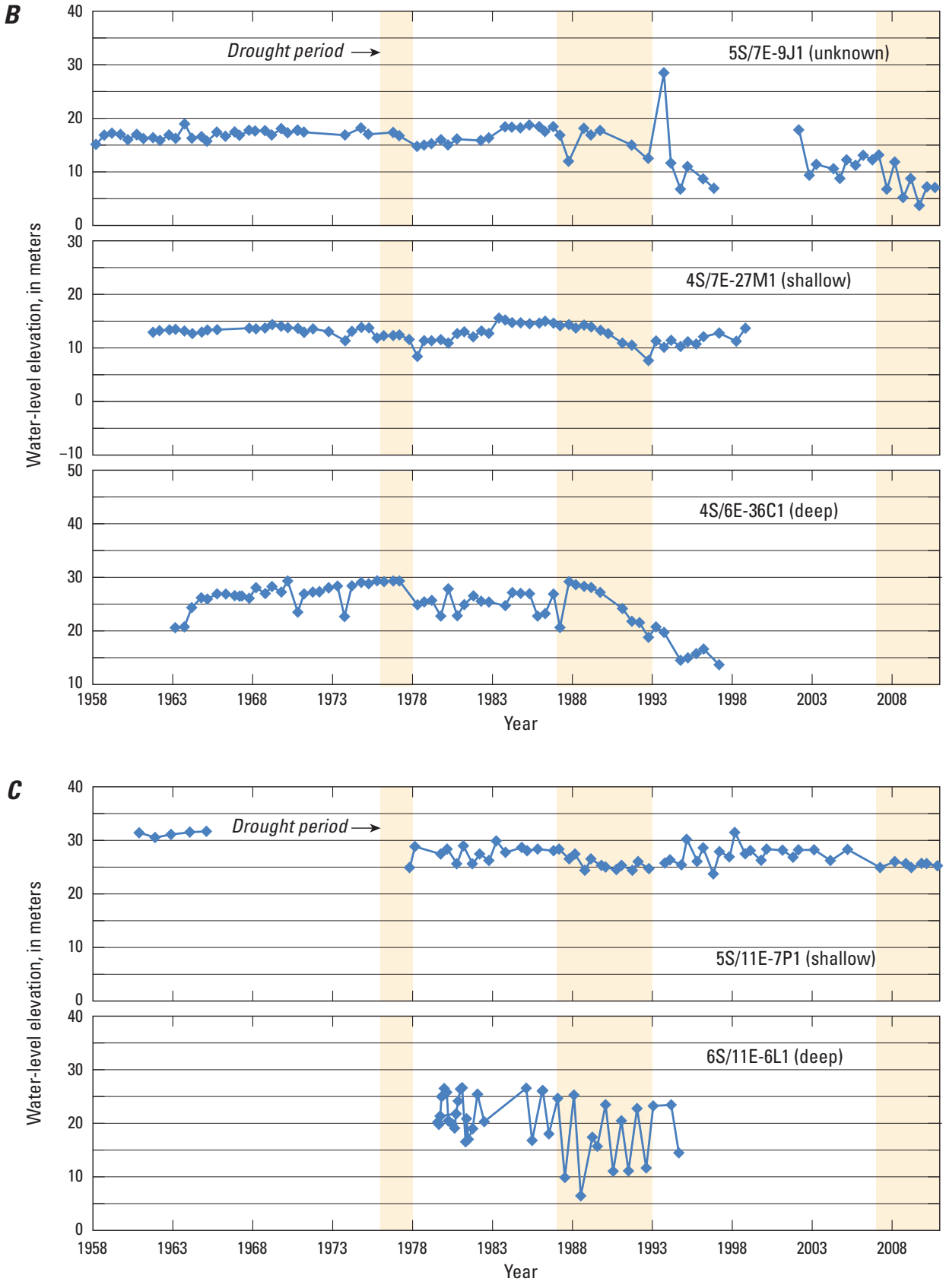

Figure 20. Continued.

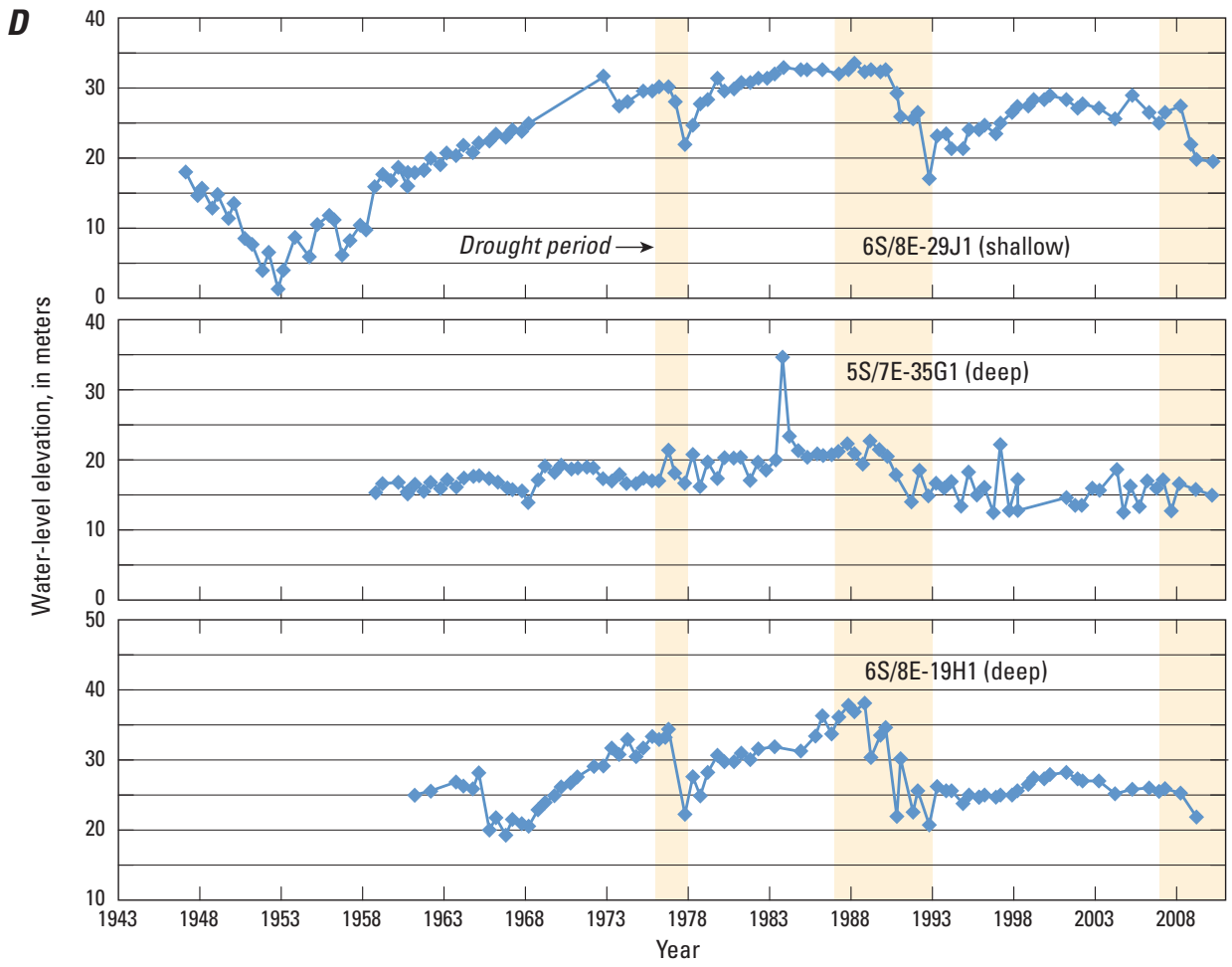

Figure 20. Continued.

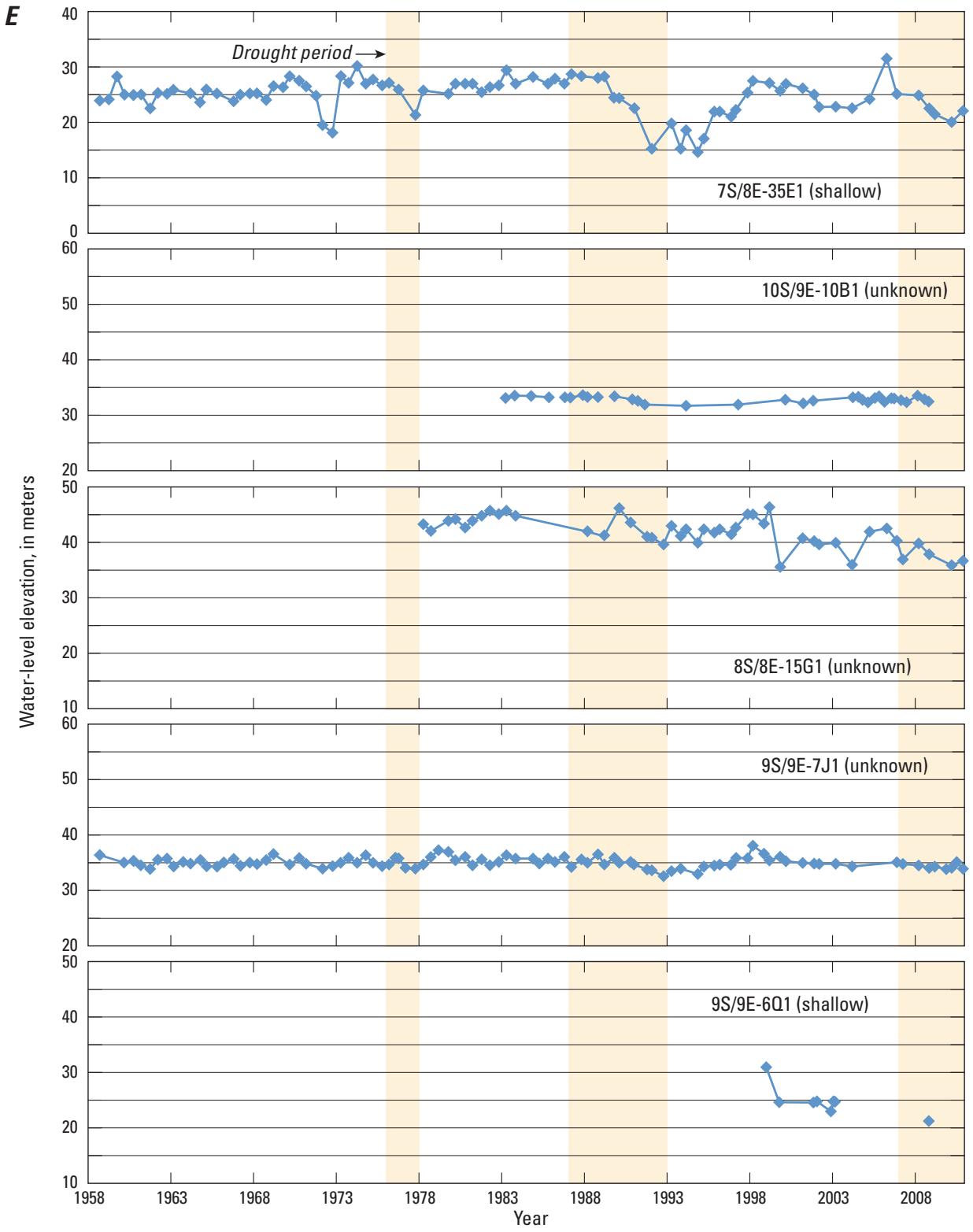

Figure 20. Continued.

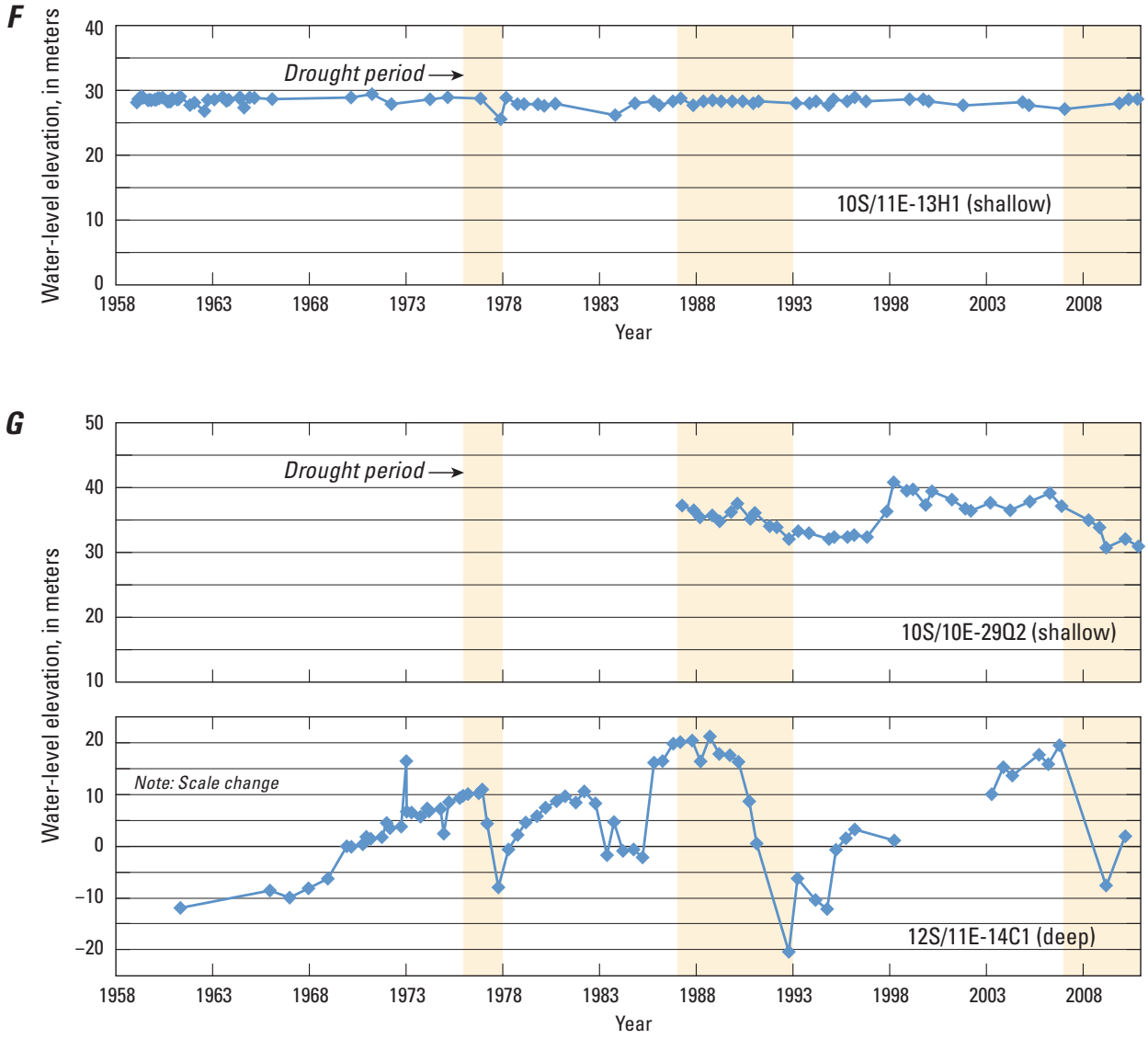

Figure 20. Continued.

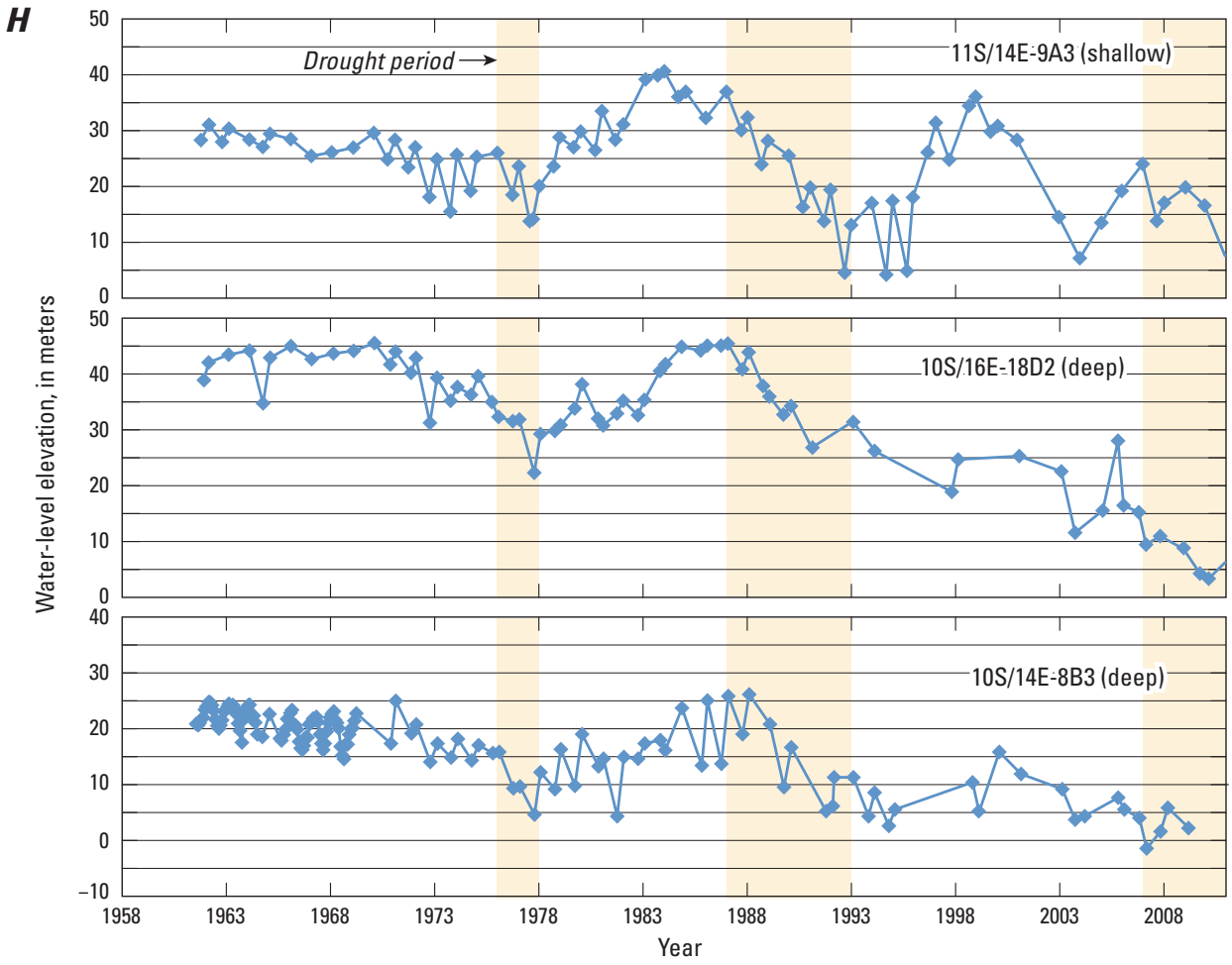

Figure 20. Continued.

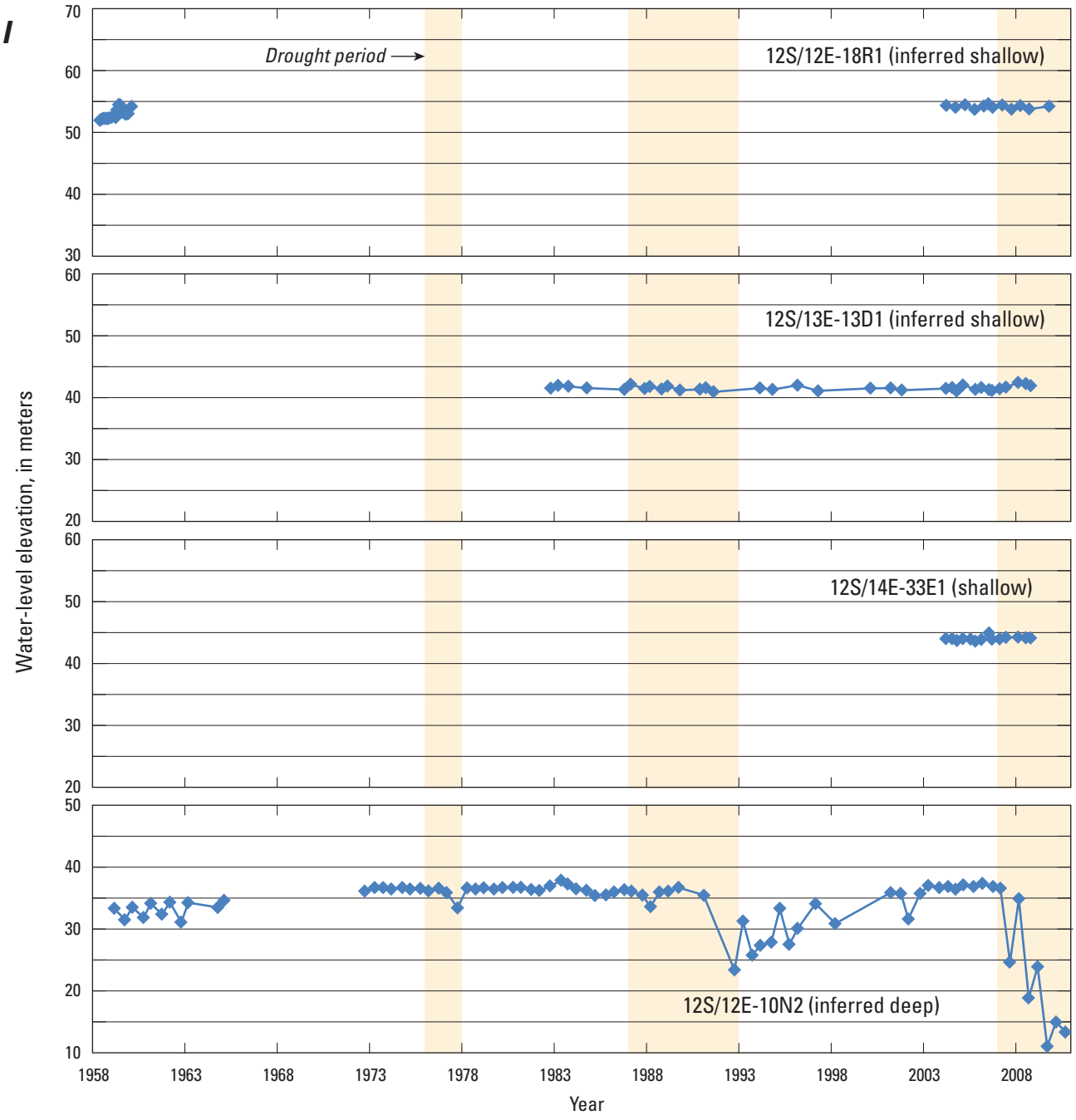

Figure 20. Continued.

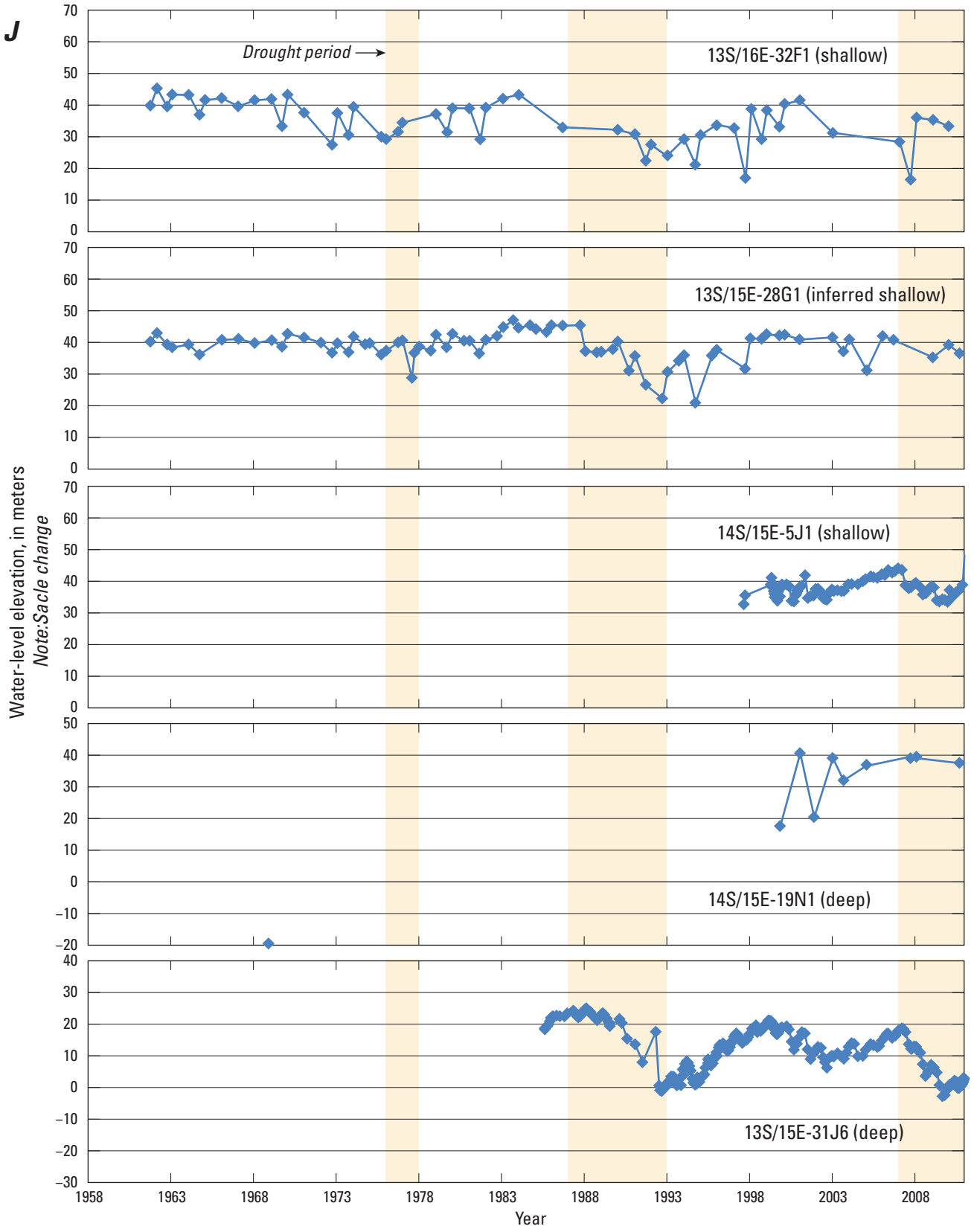

Figure 20. Continued.

Checks 7–9

Water levels near Checks 7–9 were examined by using the hydrographs from shallow well 6S/8E-29J1 and deep wells 5S/7E-35G1 and 6S/8E-19H1 (fig. 20*D*). Groundwater levels in these wells showed seasonal fluctuations superimposed on declines and recoveries that often are associated with climatic variations (fig. 20*D*). Water levels in shallow well -29J1 showed a declining water-level trend from the mid-1940s until reaching historical lows in the early 1950s, when a multi-decade recovery began, which was coincident with completion of the DMC. From 1953 to 1973, water levels rose by more than 30 m. Since this water-level recovery, water-levels have declined during the drought periods 1976–77, 1987–92, and 2007–10. The hydrograph for deep well -19H1 was similar to the hydrograph for shallow well -29J1, except water-level declines during the drought periods were larger in well -19H1. The historical low in -19H1 was measured in the mid-1960s, indicating a period of increased groundwater pumping from below the Corcoran Clay that did not affect water levels in the shallow aquifer system measured in -29J1. The hydrograph for deep well -35G1 showed short-term fluctuations, including a large water-level recovery during the historically wet year of 1983, superimposed on longer-term periods of recovery, stability, and declines during the late 1950s through 2010. The historical low was measured in 1996, several years after the end of the 1987–92 drought, indicating a prolonged period of increased groundwater pumping. In summary, hydrographs in this area showed seasonal, climatic, and longer-term variability, as well as the water-level recovery associated with the completion of the DMC. The lowest water levels were measured in the 1960s or in the mid-1990s in the deep aquifer and in the 1950s in the shallow aquifer.

Checks 10–14

Water levels near Checks 10–14 were examined by using the hydrographs from wells 7S/8E-35E1, 8S/8E-15G1, 10S/9E-10B1, 9S/9E-7J1, and 9S/9E-6Q1 (fig. 20*E*). Groundwater levels generally fluctuated seasonally and annually, with generally larger fluctuations in the northern portions of this area, and smaller fluctuations in the southern portions (fig. 20*E*). During the 1980s to 2010, water levels in shallow well 7S/8E-35E1 (near Check 10) and in well 8S/8E-15G1 (near Check 11) showed the most variability and greatest responses to drought periods, water levels in well 10S/9E-10B1 (near Check 14) showed the least variability, and water levels in wells 9S/9E-7J1 and 9S/9E-6Q1 (both near Check 12) showed relatively moderate variability. Water levels in -35E1, -15G1, and -6Q1 declined during the 2007–10 drought period, but only -6Q1 reached a historical low during this period. However, it is possible that this historical low does not represent a preconsolidation head because water levels are unknown prior to 1999, so historical drought periods were not represented. In summary, hydrographs in the northern portion of this area showed larger seasonal and climatic-related fluctuations than did hydrographs in the southern portion of this area.

Check 15-P304 (El Nido)

Water levels near CGPS P303 were examined by using the hydrograph from shallow well 10S/11E-13H1 (fig. 20*F*); data from deep wells were not available in this area. Groundwater levels in shallow wells like -13H1 showed fairly stable water levels on short-term and long-term scales during 1959–2010, generally deviating less than 3 m over the 50-year period (fig. 20*F*). The lowest water level was measured in 1977.

Water levels near Checks 15–17 were examined by using the hydrographs from wells 10S/10E-29Q2 and 12S/11E-14C1 (fig. 20G). Groundwater levels in shallow well 10S/10E-29Q2 showed small seasonal fluctuations superimposed on longer-term trends of decline, recovery, and stability between 1987 and 2010 (fig. 20*G*). Water levels generally declined during 1987–96, recovered in 1997, remained stable until 2006, and declined during 2006–10, a period during which historical low levels were measured. Groundwater levels in deep well 12S/11E-14C1 were variable, showing similar trends and features to water levels in well 6S/8E-19H1 (fig. 20*D*), which was about 70 km away, near Check 8; a longer-term groundwater-level recovery that began in the early 1960s was interrupted by declines during the drought periods of 1976–77, 1987–92, and 2007–10 (fig. 20*G*). In summary, hydrographs in this area showed seasonal and climatic effects, and more long-term variability in the deep aquifer than in the shallow aquifer. The lowest water levels were measured during the 1987–92 drought period in the deep aquifer and during the 2007–10 drought period in the shallow aquifer.

Water levels near El Nido were examined by using the hydrographs from wells 11S/14E-9A3, 10S/16E-18D2, and 10S/14E-8B3 (fig. 20*H*). Groundwater levels in shallow well -9A3 and deep wells -18D2 and -8B3 showed seasonal fluctuations as large as about 12 m superimposed on longer periods of declines and recoveries associated with climatic conditions (fig. 20*H*). Water levels in these three wells declined during the 1977–78, 1987–92, and 2007–10 drought periods, and had variable recoveries after the drought periods. Water levels in shallow well -9A3 recovered to levels near or above pre-drought levels after the 1977–78 and 1987–92 drought periods. Deep wells -8B3 and -18D2 recovered near or above pre-drought levels after 1977–78, but did not recover to pre-drought levels after the 1987–92 drought period. The historically lowest groundwater levels in the shallow aquifer were measured during the 1987–92 drought period, whereas the historically lowest groundwater levels in the deep aquifer were measured during the 2007–10 drought period.

Water levels near Checks 18–20 were examined by using the hydrographs from wells 12S/12E-18R1, 12S/13E-13D1, 12S/14E-33E1, and 12S/12E-10N2 (fig. 20*I*). Groundwater levels measured in inferred shallow wells -18R1 and -13D1, and shallow well -33E1, showed small seasonal fluctuations superimposed on stable water levels during their respective periods of record (fig. 20*I*). Groundwater levels in deep wells like inferred deep well -10N2 showed seasonal fluctuations that varied in magnitude between the late 1950s and 2010

(fig. 20*I*). There were longer-term trends of water-level stability throughout the record, except during and after the drought periods of 1976–77, 1987–92, and 2007–10, when water levels declined then subsequently recovered; the historically lowest water levels were measured during the 2007–10 drought period and were about 12 m lower than the previous historical low in 1992.

Water levels near Check 21 and CGPS P304 were examined by using the hydrographs from wells 13S/16E-32F1, 13S/15E-28G1, 14S/15E-5J1, 14S/15E-19N1, and 13S/15E-31J6 (fig. 20*J*). Hydrographs for shallow well -32F1 and inferred shallow well -28G1 were fairly similar to each other, but somewhat different from shallow well -5J1 (fig. 20*J*). Water levels in wells -32F1 and -28G1 showed seasonal fluctuations as large as about 21 m and 15 m, respectively, which were superimposed on longer term trends associated with climatic conditions. The lowest water level in well -32F1 was measured in 2007, whereas the lowest water level in well -28G1 was measured in 1994. No water level measurements were made in -28G1 in 2007. Water levels in well -5J1 showed short-term fluctuations superimposed on variable annual levels during 1997–2010, which repeatedly approached, but did fall below, the historical low measured in 1997. The hydrographs for deep wells 14S/15E-19N1 and 13S/15E-31J6 were fairly different from each other. The hydrograph for deep well 14S/15E-19N1 showed biennial fluctuations as large as 23 m superimposed on overall recovery during 1999–2010; furthermore, water levels in 1999 were about 37 m higher than the single measurement made in 1968 (fig. 20*J*). The hydrograph for deep well 13S/15E-31J6 showed seasonal fluctuations superimposed on periods of decline associated with the drought periods of 1987–92 and 2007–10, and periods of recovery that followed the droughts (fig. 20*J*). The water levels in well -31J6 reached historical lows in 2009. In summary, hydrographs in this area showed seasonal and climatic effects, and some long-term variability with the lowest water levels measured at various periods during the respective records.

Groundwater Levels and Land Subsidence

Groundwater levels were compared to land-subsidence patterns and timing to help determine the relationship of land-surface deformation to changes in groundwater levels. Groundwater-level data are useful in the interpretation of subsidence data; however, groundwater levels generally represent a discrete location within the aquifer system, whereas subsidence data generally represent a large aggregate thickness of the aquifer system. Available groundwater-level and elevation measurements did not generally coincide in space, time, or both, so a detailed analysis comparing particular water-level changes (stresses) and associated elevation changes (strains) was not possible. Instead, the paired data were analyzed in a broader context to determine if the preconsolidation stress threshold was surpassed during 2003–10 and, by extension, if measured deformation was elastic or inelastic during this period.

Clifton Court Forebay-Check 6-Turlock

For the northernmost extent of the study area in and near the city of Tracy and Checks 1–4, recent (2003–10) water levels in shallow and deep wells were higher than historical lows, indicating that water levels were above the preconsolidation head. The coincident location and timing of seasonally fluctuating groundwater levels and deformation indicated that groundwater levels caused elastic deformation of the aquifer system in this area (figs. 15, 18*A*, and 20*A*).

Near Checks 5 and 6, water levels during 2003–10 in well 5S/7E -9J1 (unknown screened interval) showed seasonal fluctuations and longer-term declines reaching historical lowest levels in 2009; no other water-level records were available for 2003–10 (fig. 20*B*). The seasonally compacting and expanding aquifer system had stable longer-term trends (fig. 15). The lack of subsidence associated with a historically low groundwater level could be due to one or more of the following: (1) the local geology is not conducive to aquifer-system compaction; (2) the water-level changes in this well did not represent the stresses responsible for (potential) aquifer-system deformation; (3) the low water level measured in 2009 did not represent the preconsolidation head; (4) the water levels recovered quickly enough that compactable units did not have sufficient time to drain and compact (time constant); or (5) the InSAR measurements did not capture the subsidence because of precision, timing, or other factors.

In Turlock, the hydrographs from shallow and deep wells showed similarities in shorter- and longer-term trends, but the seasonal variability in the deep well was significantly greater, probably owing to the relatively small storativity typical of confined aquifers (fig. 20*C*). Available records indicated groundwater levels reached historical lows in the late 1980s or mid-1990s, but there were no measurements during the recent drought period in deep well 6S/11E-6L1, where water levels did decline during the 1987–92 drought. However, the available data indicated that the small amounts of subsidence and uplift measured in this area during 2003–10 were elastic (fig. 18*A*).

Checks 7–9

Near Checks 7–9, the water levels in deep wells (fig. 20*D*) and the deformation shown by InSAR time series (fig. 18*B*) and CGPS P259 (fig. 14) indicated seasonal variability and some longer-term water-level declines and land subsidence, respectively. CGPS and InSAR measurements at P259 indicated longer-term subsidence during 2007–09; the CGPS data indicated this area was fairly stable during 2005–07 and during 2009–10. Water levels in deep well 6S/8E-19H1 during 2005–10 were generally stable except for a 3.4-m decline during March 2008–March 2009 (fig. 20*D*). The hydrograph for shallow well 6S/8E-29J1 showed 6.7 m of water-level decline during 2007–09. Because water-levels declined above and below the Corcoran Clay, it is unclear if compaction took place in one or both zones. The deformation

measured in this area, however, was probably mostly elastic, since the historically low water levels in wells -19H1 and -29J1 were measured in the mid-1960s and early 1950s, respectively.

Checks 10–14

Near Checks 10–14, the land surface was stable during 2007–10 (fig. 15), and groundwater levels declined in wells in the northern parts of this area, but generally were stable in the southern parts (fig. 20*E*). The lack of deformation in the northern parts of the area could be due to one or more of the following: (1) the local geology is not conducive to aquifer-system deformation; (2) the water-level changes in wells 7S/8E-35E1, 8S/8E-15G1, and 9S/9E-6Q1 did not represent the stresses responsible for (potential) aquifer-system deformation; (3) the water levels subsequently recovered quickly enough that compactable units did not have sufficient time to drain and compact (time constant); or (4) the InSAR measurements did not capture the subsidence because of precision, timing, or other factors.

Check 15-P304 (El Nido)

The area that includes Checks 15–21, P303, and P304 is near the edge of the previously discussed large subsidence bowl centered south of El Nido that covers 3,200 km^2 (fig. 17). More than 100 mm of subsidence during mid-2005–10 was calculated from the CGPS measurements at P303 (fig. 14). Water levels in nearby shallow wells were stable without exception, (for example, fig. 20*F*); deep wells were not found near P303. The concurrency of water-level stability in shallow wells and significant subsidence indicated that the subsidence was not caused by groundwater-level-induced stresses in the shallow system. Although water-level data from deep wells near P303 were not available, it is likely that the stresses causing the subsidence originate below the Corcoran Clay. The lack of water-level data from deep wells precludes determining the nature—elastic or inelastic—of the subsidence. However, this site's proximity to the larger, rapidly subsiding bowl indicates that at least some of the aquifer-system compaction could be permanent

In the area near Checks 15–17, about 10 mm and 35 mm of subsidence was measured at Check 15 and 17, respectively, during 2007–10 (figs. 15 and 19). Water levels in shallow well 10S/10E-29Q2 near Check 15 showed about 6 m of decline, reaching the historical low in 2009, and the water levels in deep well 12S/11E-14C1 near Check 17 showed nearly 28 m of decline between late 2006 and 2009, but did not surpass the historical low measured in 1992 (fig. 20*G*). The water-level measurements in well -14C1 during 2007–09 were made during the spring, however, when water-level elevations are expected to generally be near seasonal highs. No water-level measurements were available for late summer or early fall, during expected seasonal lows. It is likely that the lowest water-level elevations were not captured in this area. Although the small amounts of subsidence measured could be elastic, this area's proximity to the larger, rapidly subsiding bowl indicates that at least some of the aquifer-system compaction could be permanent.

In the area south of El Nido, the center of the large subsidence bowl previously discussed (fig. 17), and near Bypass Curve, the hydrographs from deep and shallow wells were somewhat similar (fig. 20*H*). An important distinction in the hydrographs is that water levels in deep wells (10S/16E-18D2 and 10S/14E-8B3) reached historical lows during the 2007–10 drought period, which is consistent and concurrent with the nearly doubling of subsidence rates measured near this region (fig. 18*D*). The spatial and temporal coincidence of historically lowest groundwater levels and the increased subsidence rate indicated that the preconsolidation stress was surpassed during this period and that the resulting subsidence could be largely permanent. Although water levels in shallow wells did not surpass the historical lows that were measured in the 1990s, water levels did decline as much as about 12 m during this period (fig. 20*H*), such that compaction of sediments in the shallow system could have contributed to some of the subsidence measured during this period; this component could be largely recoverable.

In the area near Checks 18–20, near the edge of the large El Nido subsidence bowl, where as much as about 45 mm of subsidence was measured during 2003–08 (figs. 16 and 19), the hydrographs from deep and shallow wells were markedly different, indicating a relatively poor hydraulic connection through the Corcoran Clay (fig. 20*I*). Water levels in shallow wells were stable over shorter and longer periods, but water levels in deep wells showed a decline of about 26 m during 2006–09, surpassing the historical low measured in 1992 by more than 12 m (fig. 20*I*). The concurrent measurements of subsidence and historically lowest groundwater levels indicated that the preconsolidation stress was surpassed during this period and that the resulting subsidence could be largely permanent.

Near Check 21 and CGPS P304, about 5 mm of subsidence occurred during 2003–08 (figs. 16 and 19), and CGPS data indicated about 70 mm of subsidence at P304 during 2007–10 (fig. 14). The hydrographs for this area indicated some differences between the shallow and deeper zones and within each zone. The three hydrographs for shallow wells indicated that 13S/16E-32F1 reached a historical low in 2007, whereas 13S/15E-28G1 and 14S/15E-5J1 did not (fig. 20*J*). Similarly, the hydrograph for deep well 13S/15E-31J6 reached a historical low in 2009, whereas 14S/15E-19N1 did not—in fact, water levels rose in this deep well (fig. 20*J*). The spatial and temporal coincidence of historically lowest groundwater levels in some shallow and deep wells and subsidence, however, indicated that the preconsolidation stress was surpassed in parts of the aquifer system during this period and that the resulting subsidence could be largely permanent.

Summary

Generally, in areas where water levels fluctuated seasonally, but were fairly stable on longer-term scales (such as near Tracy during 2003–10), deformation also fluctuated seasonally and was similarly stable long-term (figs. 15, 18*A*, and 20*A*). In areas where water levels below the Corcoran Clay sometimes showed seasonal fluctuations but declined during 2003–10, such as near Check 18, subsidence was measured (figs. 16, 17, and 20*I*). In areas where water levels in shallow and deep wells declined at a high rate, such as near El Nido and Bypass Curve, large magnitudes of subsidence were measured (figs. 16, 17, 18*D*, and 20*H*).

Depth Intervals of Aquifer-System Compaction

The compacting depth intervals within an aquifer system can be delimited at locations where two or more extensometers at different depths are co-located, or at locations where one or more extensometers are co-located with repeat land-surface elevation measurements, such as those derived from repeat leveling surveys, GPS observations (including continuous), and InSAR. Land-subsidence calculations are based on measurements from land surface (or in the case of continuous GPS, the depth of the GPS antenna mount) and integrate the deformation from the entire subsurface geologic column. Because extensometers are anchored at a specific depth, the aquifer-system compaction measurement is specific to a depth-interval. Where the measurements of land subsidence and aquifer-system compaction are co-located, then depths at which compaction occurs can be deduced for that location. The determination of compacting depth intervals determined from multi-depth measurements at a few specific locations, however, cannot presently be extended to other locations in the valley because of variability in groundwater use, depth of extraction, and aquifer-system structure and composition (heterogeneity), and because numerous wells screened across the Corcoran Clay have created preferential flow through the unit, further altering the hydraulic head distribution in the aquifer system.

Previous investigations in the San Joaquin Valley (Lofgren, 1961; Ireland and others, 1984) analyzed leveling surveys and extensometer data to conclude that most compaction was occurring below the bottom of the Corcoran Clay and that even the deepest extensometers were measuring only a portion of the total land subsidence. These results indicate that some compaction was occurring below the depths of the extensometers. More recently, comparison of data from the Fordel (13S/15E-31J-) extensometer (anchored near the top of the Corcoran Clay) and CGPS P304 indicated that most of the aquifer-system compaction is occurring below the top of the Corcoran Clay (fig. 21). One-dimensional modeling of the stress (water level)-strain (compaction) relationship at the multi-piezometer and multi-extensometer Oro Loma site (12S/12E-16H) supported this conclusion and further indicated that nearly all of the compaction at that site was occurring below the bottom of the Corcoran Clay as previous investigators had concluded (Sneed and others, 2011).

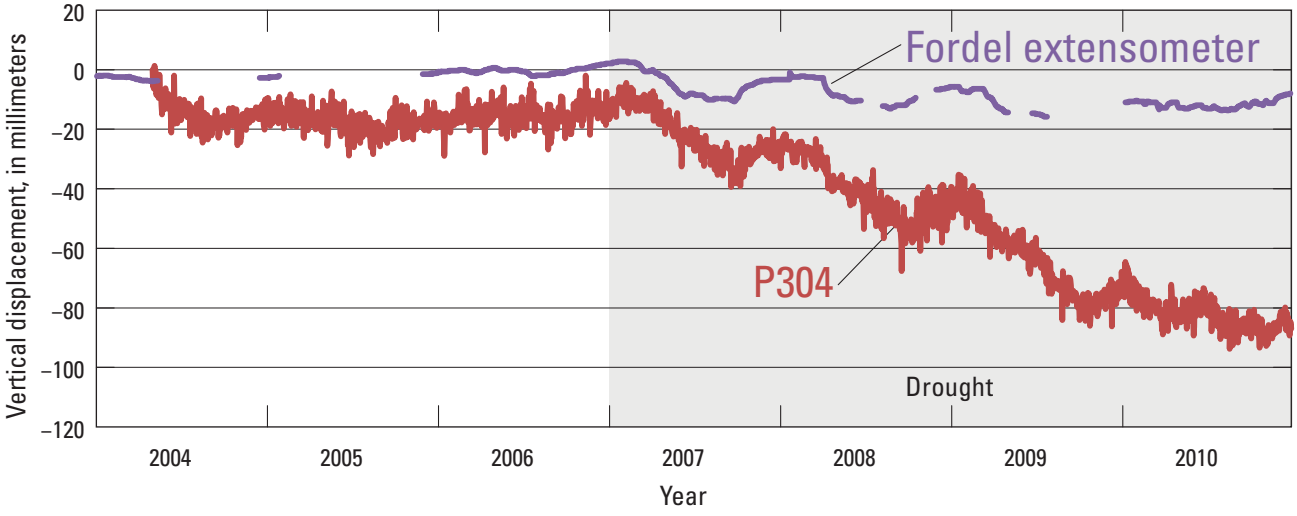

Figure 21. Aquifer-system compaction measured by the Fordel (13S/15E-31J-) extensometer (anchored near the top of the Corcoran Clay) and land subsidence at continuous Global Positioning System station P304 near Mendota, California, 2004–10. Fordel data were obtained from Glenn Browning, Luhdorff and Scalmanini Consulting Engineers. P304 data were obtained from the University NAVSTAR Consortium.

Effects of Land Subsidence on Infrastructure

Significant resources have been applied to mitigate subsidence-induced infrastructure damage on segments of the DMC and canals near Checks 18 and 21, and continued maintenance and repairs are expected (Bob Martin, SLDMWA and Chris White, CCID, oral commun., 2011; Swanson, 1998). Near Check 18, flow capacity in the DMC has been maintained by extending the height of infrastructure, including check structures, raising embankments and bridges, and tolerating reduced freeboard (Seth Harris, SLDMWA, oral commun., 2012). Despite some similar mitigation efforts on other nearby canals, design flow capacity has been reduced as much as 50 percent (Chris White, CCID, oral commun., 2011). Near Check 21, at least one irrigation district has had difficulty maintaining adequate diversions from the south end of Mendota Pool behind the Mendota Dam, even though water levels were raised to nearly the top of the dam embankment (Swanson, 1998). The repair or replacement of Mendota Dam is being considered (Swanson, 1998; Reclamation EIS/EIR, *http://www.usbr.gov/mp/nepa/nepa_projdetails.cfm?Project_ID=9086*, accessed October 2, 2012).

Significant resources also have been applied to mitigate subsidence along the Eastside Bypass, the primary flood-control channel for the region. By 1995, there had been about 1.2 m of subsidence since its construction in 1965, requiring the raising of levees on the west bank. The levee district calculated a 27-percent reduction in flow capacity, and erosion and deposition were occurring in this unlined channel (Swanson, 1998). In 2012, resources were being applied to characterize the subsidence magnitudes and rates in order to mitigate subsidence-related design problems of the Arroyo Canal Fish Screen and Sack Dam Fish Passage Project, which is part of the multi-agency San Joaquin River Restoration Program.

Future Monitoring

Continued groundwater-level and land-subsidence monitoring in the San Joaquin Valley is important because (1) regulatory- and drought-related reductions in surface-water deliveries since 1976 have resulted in increased groundwater pumping and associated land subsidence and (2) land use and associated groundwater pumping continue to change throughout the valley. The combination of both of these factors resulted in the historical subsidence shift about 40 km to the northeast; however, because of insufficient monitoring, this shift was unforeseen until this study was undertaken. The availability of surface water remains uncertain; even during precipitation record-setting years, such as 2010–11, water deliveries have fallen short of requests. Future subsidence, therefore, is likely. Spatially detailed InSAR-derived maps of ground displacements could be processed annually or more frequently depending on data availability. Extensometers can continue to be monitored continuously by using the potentiometer and data logger, intermittently using the dial gauge, or both. Continuous GPS stations can be monitored depending on data availability. The continuous data from extensometers and CGPS, and spatially detailed InSAR data, could be used to indicate when and where additional monitoring effort should be made, such as GPS or leveling surveys to measure and map land subsidence, or establishing new CGPS or extensometer stations for continuous monitoring. Because InSAR-detected areas of subsidence spatially overlap the CGPS network, future monitoring of the CGPS network could provide ground truth for the more spatially detailed InSAR measurements, as was done during this study. Extensometers also could be used in conjunction with InSAR or other measurements of land-surface change to delineate the depths at which compaction is occurring.

Generally, the frequency of water-level measurements in monitoring wells has been too low to permit meaningful interpretations of shorter-term aquifer-system responses to water-level changes. As a part of the recent work in the study area by the USGS, Reclamation, and SLDMWA, however, five multi-piezometer well sites were constructed and instrumented to collect continuous water-level data above and below the Corcoran Clay, including one nearby CGPS P259. In addition, four extensometer sites were instrumented to collect continuous water levels (appendix E). Paired continuous deformation and water-level data permit (1) detection of changes in the relationship between water-level change and aquifer-system deformation, and (2) estimation of key hydraulic parameters that govern groundwater flow and the timing and rate of land subsidence, including the preconsolidation head—the critical head at which elastic (recoverable) deformation converts to inelastic (permanent) subsidence. This information can be used to improve numerical model simulations of groundwater flow and aquifer-system compaction, allowing for consideration of land subsidence in the evaluation of water resource management alternatives.

Summary and Conclusions

The extensive withdrawal of groundwater from the unconsolidated deposits of the San Joaquin Valley has caused widespread land subsidence—locally exceeding 8.5 meters (m) by 1970 and reaching 9 m by 1981. Land subsidence from groundwater pumping began in the mid-1920s, and by 1970, there had been more than 0.3 m of land subsidence over an area of about 13,500 square kilometers (km^2). The importation of surface water after completion of the Central Valley Project's Delta-Mendota Canal (DMC) in the early 1950s and the State Water Project's California Aqueduct in the early 1970s, and the associated decrease in groundwater

pumping in some parts of the valley, was accompanied by a steady recovery of water levels and a reduced rate of compaction in some areas. During the drought periods of 1976–77, 1987–92, and 2007–10, diminished deliveries of imported water prompted pumping of groundwater to meet irrigation demands. This increased groundwater pumping resulted in water-level declines and periods of renewed compaction. Subsidence has reduced the flow capacity and freeboard of several channels that deliver irrigation water to farmers and transport floodwater out of the valley.

The location, magnitude, and stress regime of land-surface deformation during 2003–10 in parts of the San Joaquin Valley traversed by the DMC were determined by using Interferometric Synthetic Aperture Radar (InSAR), Global Positioning System (GPS), spirit leveling, extensometer, and groundwater-level data. The data and images processed for the InSAR measurements described in this report span the length of the DMC from about Tracy to Mendota. InSAR measurements were useful for detailed mapping of areas affected by subsidence over multiple time periods. Continuous Global Positioning System (CGPS) measurements were useful for constructing continuous time series at a few locations and also for constraining the InSAR measurements. Campaign GPS and leveling data were useful for identifying areas near highways and canals affected by subsidence and for computing longer-term rates of subsidence, which were compared to longer-term rates computed with InSAR data. Extensometer data were useful in determining the depth of aquifer-system compaction and comparing to InSAR data. Water-level data were useful in determining whether the aquifer-matrix deformation was elastic or inelastic in some areas.

Land-surface deformation measurements indicated that much of the northern portion of the DMC (Clifton Court Forebay to Check 14) was fairly stable or was minimally subsiding on an annual basis; some areas showed seasonal periods of subsidence and of uplift, which resulted in either no longer-term elevation change or a slight loss in elevation. The minor subsidence measured was probably mostly elastic because water levels in many wells in this area did not reach historical lows during 2003–10.

Although the northern portion of the DMC was relatively stable, land-surface deformation measurements indicated the southern portion of the DMC (Checks 15–21) subsided as part of a large subsidence feature centered south of the town of El Nido, which is about 15 kilometers (km) northeast of the DMC. The area affected by 20 millimeters (mm) or more of subsidence extended about 80 km west-east, from Check 17 to the town of Madera, and 40 km north-south, from near Merced to near Mendota, and the maximum subsidence was at least 540 mm during 2008–10.

There is some evidence of seasonal variations in elevations given by CGPS stations on the fringes of the subsidence area, but these variations were small compared to the large and longer-term subsidence magnitudes measured in this area. Water levels in many deep wells in the subsiding area reached historical lows during 2007–10, indicating that at least some of the subsidence measured in this area probably was inelastic. Calculations of subsidence rates indicated that the subsidence rate doubled in 2008 in some areas. GPS survey data from 2008 and 2010 corroborated the high subsidence rate measured by InSAR during that period, and GPS survey data collected in 2012 by Reclamation indicated that the high rate of subsidence continued into 2012. Comparison of data from the Fordel extensometer (anchored near the top of the Corcoran Clay) and CGPS P304, and the historically low water levels in deep wells during the years 2007–10 indicated that most of the aquifer-system compaction was below the top of the Corcoran Clay. Results of a one-dimensional groundwater-flow and compaction model, completed for a previous investigation at the Oro Loma site, indicate that the most of the compaction occurred below the bottom of the Corcoran Clay, which supports the conclusions of previous investigators.

Continued groundwater-level and land-subsidence monitoring in the San Joaquin Valley is important because (1) regulatory- and drought-related reductions in surface-water deliveries since 1976 have resulted in increased groundwater pumping and associated land subsidence and (2) land use and associated groundwater pumping continue to change throughout the valley. The availability of surface water remains uncertain; even during precipitation record-setting years, such as 2010–11, water deliveries fell short of requests and groundwater pumping was required to meet the irrigation demand. Due to the expected continued demand for irrigation supply water and the limitations and uncertainty of surface-water supplies, groundwater pumping and associated land subsidence is likely to continue in the future. Spatially detailed information on land subsidence is needed to minimize future subsidence-related damages to the DMC and other infrastructure in the San Joaquin Valley. InSAR-derived maps of ground displacements could be processed annually, or more frequently (depending on data availability). Data from the four refurbished extensometers could be collected continuously with the recently installed potentiometers and data loggers, discretely with the associated dial gauges, or both. Data from CGPS stations could be collected and analyzed regularly depending on data availability. The CGPS and extensometer data, paired with continuous water-level data, could improve analysis of aquifer-system response, could be useful in detecting changes in the relationship between aquifer-system compaction and water-levels, and could be used to identify or calculate aquifer-system properties controlling subsidence. This information could also be used to improve numerical model simulations of groundwater flow and aquifer-system compaction, thereby refining the estimates of the governing parameters that predict potential aquifer-system compaction. Such predictions could be useful to the Bureau of Reclamation and other agencies that manage water resources while considering land subsidence.

References Cited

Bawden, G.W., Sneed, Michelle, Stork, S.V., and Galloway, D.L., 2003, Measuring human-induced land subsidence from space: U.S. Geological Survey Fact Sheet 069–03, 4 p.

Belitz, Kenneth, and Heimes, F.J., 1990, Character and evolution of the ground-water flow system in the central part of the western San Joaquin Valley, California: U.S. Geological Survey Water-Supply Paper 2348, 28 p.

Bertoldi, G.L., 1989, Ground-water resources of the Central Valley of California: U.S. Geological Survey Open-File Report 89–251, 2 p.

Bertoldi, G.L., Johnston, R.H., and Evenson, K.D., 1991, Ground water in the Central Valley, California—A summary report: U.S. Geological Survey Professional Paper 1401-A, 44 p.

Brandt, J.T., Bawden, G., and Sneed, Michelle, 2005, Evaluating subsidence in the San Joaquin Valley, California using InSAR: (abstract) EOS Transactions, American Geophysical Union, v. 86, no. 52, Fall Meeting Supplement, Abstract G51C-0851.

Bull, W.B., 1964, Alluvial fans and near-surface subsidence in western Fresno County, California: U.S. Geological Survey Professional Paper 437-A, 78 p.

Bull, W.B., 1972, Prehistoric near-surface subsidence cracks in western Fresno County, California: U.S. Geological Survey Professional Paper 437-C, 85 p.

Bull, W.B., 1975, Land subsidence due to ground-water withdrawal in the Los Banos-Kettleman City area, California; Part 2. Subsidence and compaction of deposits: U.S. Geological Survey Professional Paper 437-F, 90 p.

Bull, W.B., and Miller, R.E., 1975, Land subsidence due to ground-water withdrawal in the Los Banos-Kettleman City area, California; Part 1. Changes in the hydrologic environment conducive to subsidence: U.S. Geological Survey Professional Paper 437-E, 70 p.

Bull, W.B., and Poland, J.F., 1975, Land subsidence due to ground-water withdrawal in the Los Banos-Kettleman City area, California; Part 3. Interrelations of water-level change, change in aquifer-system thickness, and subsidence: U.S. Geological Survey Professional Paper 437-G, 62 p.

California Department of Water Resources, 2003, California's ground water, update 2003: California Department of Water Resources Bulletin 118, 246 p.

Climate Source, 2006, Precipitation data from PRISM data: accessed November 14, 2012, at *http://www.climatesource.com/*.

Davis, G.H., Green, J.H., Olmsted, F.H., and Brown, D.W., 1959, Ground-water conditions and storage capacity in the San Joaquin Valley, California: U.S. Geological Survey Water-Supply Paper 1469, 287 p.

Farrar, C.D., and Bertoldi, G.L., 1988, Region 4, Central Valley and Pacific Coast Ranges, *in* Back, William, Rosenshein, J.S., and Seaber, P.R., eds., Hydrogeology: Boulder, Colorado, Geological Society of America, Geology of North America, v. O-2, p. 59–67.

Faunt, C.C., ed., 2009, Groundwater availability of California's Central Valley: U.S. Geological Survey Professional Paper 1766, 225 p.

Freeman, L.A., 1996, Time-series ground-water-level and aquifer-system compaction data, Edwards Air Force Base, Antelope Valley, California, January 1991 through September 1993: U.S. Geological Survey Open-File Report 96–186, 32 p.

Galloway, D.L., Jones, D.R., and Ingebritsen, S.E., 1999, Land subsidence in the United States: U.S. Geological Survey Circular 1182, 175 p.

Galloway, D.L., and Riley, F.S., 1999, San Joaquin Valley, California—Largest human alteration of the Earth's surface: *in* Galloway, D.L., Jones, D.R., and Ingebritsen, S.E., eds., Land Subsidence in the United States: U.S. Geological Survey Circular 1182, p. 23–34, *http://pubs.usgs.gov/circ/circ1182/*, accessed February 2, 2008.

Hanson, R.T., 1989, Aquifer-System Compaction, Tucson Basin and Avra Valley, Arizona: U.S. Geological Survey Water-Resources Investigations Report 88–4172, 69 p.

Helm, D.C., 1978, Field verification of a one-dimensional mathematical model for transient compaction and expansion of a confined aquifer system, Verification of Mathematical and Physical Models in Hydraulic Engineering, *in* Proceedings 26th Hydraulic Division Specialty Conference: American Society of Civil Engineers, p. 189–196.

Holzer, T.L., 1998, The history of the aquifer-drainage model, *in* Borchers, J., ed., Land Subsidence—Case Studies and Current Research, Proceedings of the Dr. Joseph F. Poland Symposium: Association of Engineering Geologists Special Publication 8, p. 7–12.

Ireland, R.L., 1986, Land subsidence in the San Joaquin Valley, California, as of 1983: U.S. Geological Survey Water-Resources Investigations Report 85–4196, 50 p.

Ireland R.L., Poland, J.F., and Riley, F.S., 1984, Land subsidence in the San Joaquin Valley, California, as of 1980: U.S. Geological Survey Professional Paper 437-I, 93 p., accessed August 18, 2008, at *http://pubs.er.usgs.gov/publication/pp437I*

Johnson, A.I., Moston, R.P., and Morris D.A., 1968, Physical and hydrologic properties of water-bearing deposits in subsiding areas in central California: U.S. Geological Survey Professional Paper 497-A, 71 p., 14 pls.

Langbein, John, 2008, Noise in GPS displacement measurements from Southern California and Southern Nevada: Journal of Geophysical Research, v. 113, B05405, 12 p.

Leake, S.A., and Prudic, D.E., 1991, Documentation of a computer program to simulate aquifer-system compaction using the modular finite-difference groundwater flow model: U.S. Geological Survey Techniques of Water-Resources Investigations, book 6, chap. A2, 68 p.

Lofgren, B.E., 1961, Measurement of compaction of aquifer systems in areas of land subsidence, *in* Short Papers in the Geologic and Hydrologic Sciences, Articles 1–146: U.S. Geological Survey Professional Paper 424-B, p. B49–B52.

Lofgren, B.E., 1975, Land subsidence due to ground-water withdrawal, Arvin-Maricopa area, California: U.S. Geological Survey Professional Paper 437-D, 55 p.

Lofgren, B.E., 1976, Hydrogeologic effects of subsidence, San Joaquin Valley, California: International Symposium on Land Subsidence, 2nd, Anaheim, California, December 13–17, program and abstracts, no. 12, unnumbered pages.

Lofgren, B.E., and Klausing, R.L., 1969, Land subsidence due to ground-water withdrawal, Tulare-Wasco area, California: U.S. Geological Survey Professional Paper 437-B, 103 p.

Meade, R.H., 1964, Removal of water and rearrangement of particles during the compaction of clayey sediments—review: U.S. Geological Survey Professional Paper 497-B, 23 p.

Meade, R.H., 1967, Petrology of sediments underlying areas of land subsidence in central California: U.S. Geological Survey Professional Paper 497-C, 83 p.

Meade, R.H., 1968, Compaction of sediments underlying areas of land subsidence in central California: U.S. Geological Survey Professional Paper 497-D, 39 p.

Meinzer, O.E., 1928, Compressibility and elasticity of artesian aquifers: Economic Geology, v. 23, no. 3, p. 263–291.

Miller, R.E., Green, J.H., and Davis, G.H., 1971, Geology of the compacting deposits in the Los Banos-Kettleman City subsidence area, California: U.S. Geological Survey Professional Paper 497-E, 46 p.

Moore, S.B., Winckel, J., Detwiler, S.J., Klasing, S.A., and Gaul, P.A., 1990, Fish and wildlife resources and agricultural drainage in the San Joaquin Valley, California: Sacramento, California, San Joaquin Valley Drainage Program, 974 p.

National Geodetic Survey, various dates, archives, Silver Spring, Maryland.

Page, R.W., 1986, Geology of the fresh ground-water basin of the Central Valley, California, with texture maps and sections: U.S. Geological Survey Professional Paper 1401-C, 54 p.

Page, R.W., and Bertoldi, G.L., 1983, A Pleistocene diatomaceous clay and a pumiceous ash: California Geology, v. 36, no. 1, p. 14–20.

Phillips, S.P., Carlson, C.S., Metzger, L.F., Howle, J.F., Galloway, D.L., Sneed, Michelle, Ikehara, M.E., Hudnut, K.W., and King, N.E., 2003, Analysis of tests of subsurface injection, storage, and recovery of freshwater in Lancaster, Antelope Valley, California: U.S. Geological Survey Water-Resources Investigations Report 03–4061, 122 p.

Planert, Michael, and Williams, J.S., 1995, Ground water atlas of the United States: Segment 1, California, Nevada: U.S. Geological Survey Hydrologic Atlas 730-B, 1 atlas, 28 p.

Poland, J.F., 1984, Guidebook to studies of land subsidence due to ground-water withdrawal: Studies and Reports in Hydrology 40, prepared for the International Hydrological Programme, Working Group 8.4, United Nations Educational, Scientific, and Cultural Organization (UNESCO), Paris, France, 305 p., 5 appendixes.

Poland, J.F., Lofgren, B.E., Ireland, R.L., and Pugh, A.G., 1975, Land subsidence in the San Joaquin Valley, California, as of 1972: U.S. Geological Survey Professional Paper 437-H, 78 p.

Quinn N.W.T., and Faghih, J.A., 2008, WESTSIM: Groundwater conjunctive use, agricultural drainage and wetland return flow simulation on the west-side of the San Joaquin Basin, *in* Brush C.F., Miller N.L., eds., Proceedings of the California Central Valley Groundwater Modeling Workshop, July 10–11, 2008, Lawrence Berkeley National Laboratory, Berkeley, Calif., Sacramento, Calif.: California Water and Environmental Modeling Forum. p. 26–32.

The R Foundation for Statistical Computing., 2008, R version 2.8.1, December 22, 2008.

Riley, F.S., 1969, Analysis of borehole extensometer data from central California, *in* Tison, L.J., Land Subsidence: International Association of Hydrological Sciences Publication 89, v. 2, p. 423–431.

Riley, F.S., 1970, Land-surface tilting near Wheeler Ridge, southern San Joaquin Valley, California: U.S. Geological Survey Professional Paper 497-G, 29 p.

Riley, F.S., 1986, Developments in borehole extensometry, *in* Johnson, I.A., Carborgnin, Laura, and Ubertini, L., eds., Land subsidence: International Association of Scientific Hydrology Publication 151, p. 169–186.

Riley, F.S., 1998, Mechanics of aquifer systems—The scientific legacy of Joseph F. Poland, *in* Borchers, J., ed., Land Subsidence—Case Studies and Current Research: Proceedings of the Dr. Joseph F. Poland Symposium on Land Subsidence, Association of Engineering Geologists Special Publication 8, p. 13–27.

Sandwell, D.T., Myer, D., Mellors, R., Shimada, M., Brooks, B., and Foster, J., 2008, Accuracy and resolution of ALOS interferometry: Vector deformation maps of the Father's Day Intrusion at Kilauea, Geoscience and Remote Sensing, IEEE Transactions, v. 46, no. 11, p. 3524–3534, doi: 10.1109/TGRS.2008.2000634

Sneed, Michelle, 2001, Hydraulic and mechanical properties affecting ground-water flow and aquifer-system compaction, San Joaquin Valley, California: U.S. Geological Survey Open-File Report 01–35, 26 p.

Sneed, Michelle, and Galloway, D.L., 2000, Aquifer-system compaction and land subsidence: Measurements, analyses, and simulations—the Holly site, Edwards Air Force Base, Antelope Valley, California: U.S. Geological Survey Water-Resources Investigations Report 00–4015, 65 p.

Sneed, Michelle, and Brandt, J.T., 2013, Detection and measurement of land subsidence using global positioning system and interferometric synthetic aperture radar, Coachella Valley, California, 1996–2005—Ver. 2.0: U.S. Geological Survey Scientific Investigations Report 2007–5251, 31 p.

Sneed, Michelle, Brandt, Justin, and Solt, Mike, 2011, Integration of remotely-sensed and ground-based measurements to constrain simulations of groundwater flow and land subsidence, San Joaquin Valley, Calif., abstract H43D-1248 presented at 2011 Fall Meeting, American Geophysical Union, San Francisco, Calif., 5–9 Dec.

Sneed, Michelle, and Phillips, S.P., 2012, Recently measured rapid land subsidence in Eastern San Joaquin Valley, California: Proceedings from the 2012 National Ground Water Association Summit, May 7–9, 2012, Anaheim, Calif. (abstract).

Strozzi, Tazio, Wegmüller, Urs, Werner, Charles, Teatini, Pietro, and Tosi, Luigi, 2005, SAR interferometric point target analysis and application to the monitoring of land subsidence in the Venice lagoon: Proceedings of the Seventh International Symposium on Land Subsidence, p. 417.

Swanson, A.A., 1998, Land subsidence in the San Joaquin Valley, updated to 1995, *in* Borchers, J.W., ed., Land subsidence case studies and current research: Proceedings of the Dr. Joseph F. Poland Symposium on Land Subsidence, Sacramento, Calif., October 4–5, 1995, Association of Engineering Geologists, Special Publication no. 8, p. 75–79.

Terzaghi, Karl, 1925, Principles of soil mechanics: IV; settlement and consolidation of clay: Erdbaummechanic, v. 95, no. 3, p. 874–878.

Thomas, H.E., and Phoenix, D.A., 1976, Summary appraisal of the Nation's ground-water resources—California region: U.S. Geological Survey Professional Paper 813-E, 51 p.

Werner, C., Wegmüller, U., Strozzi, T., and Wiesmann, A., 2003, Interferometric point target analysis for deformation mapping: in IGARSS 2003, Institute of Electrical and Electronics Engineering, v. VII, p. 4362–4364.

Williams, S.D.P., Bock, Yehuda, Fang, Peng, Jamason, Paul, Nikolaidis, R.M., Prawirodirdjo, Linette, Miller, Meghan, and Johnson, D.J., 2004, Error analysis of continuous GPS position time series: Journal of Geophysical Research, v. 109, B03412, 19 p.

Williamson, A.K., Prudic, D.E., and Swain, L.A., 1989, Ground-water flow in the Central Valley, California: U.S. Geological Survey Professional Paper 1401-D, 127 p.

Zebker, H.A., Rosen, P.A., and Hensley, S., 1997, Atmospheric effects in interferometric synthetic aperture radar surface deformation and topographic maps: Journal of Geophysical Research, v. 102, p. 7547–7563.

Zerbini, Susanna, Richter, Bernd, Negusisi, Monia, Romagnoli, Claudia, Simon, Dietrich, Domenichini, Francesco, and Schwahn, Wolfgang, 2001, Height and gravity variations by continuous GPS, gravity and environmental parameter observations in the southern Po Plain, near Bologna, Italy: Earth and Planetary Science Letters, v. 192, no. 3, p. 267–279.

Appendix

Appendix A. Persistent Scatterer Interferometric Synthetic Aperture Radar (PS InSAR) Interferograms for the Northern Reaches of the Delta-Mendota Canal, ENVIronmental SATellite (ENVISAT) Track 299, December 24, 2007–March 3, 2008; March 3–May 12, 2008; May 12–July 21, 2008; July 21–August 25, 2008; August 25, 2008–April 27, 2009; April 27–June 1, 2009; June 1–December 28, 2009; December 28, 2009–June 21, 2010; and June 21–July 26, 2010, San Joaquin Valley, California

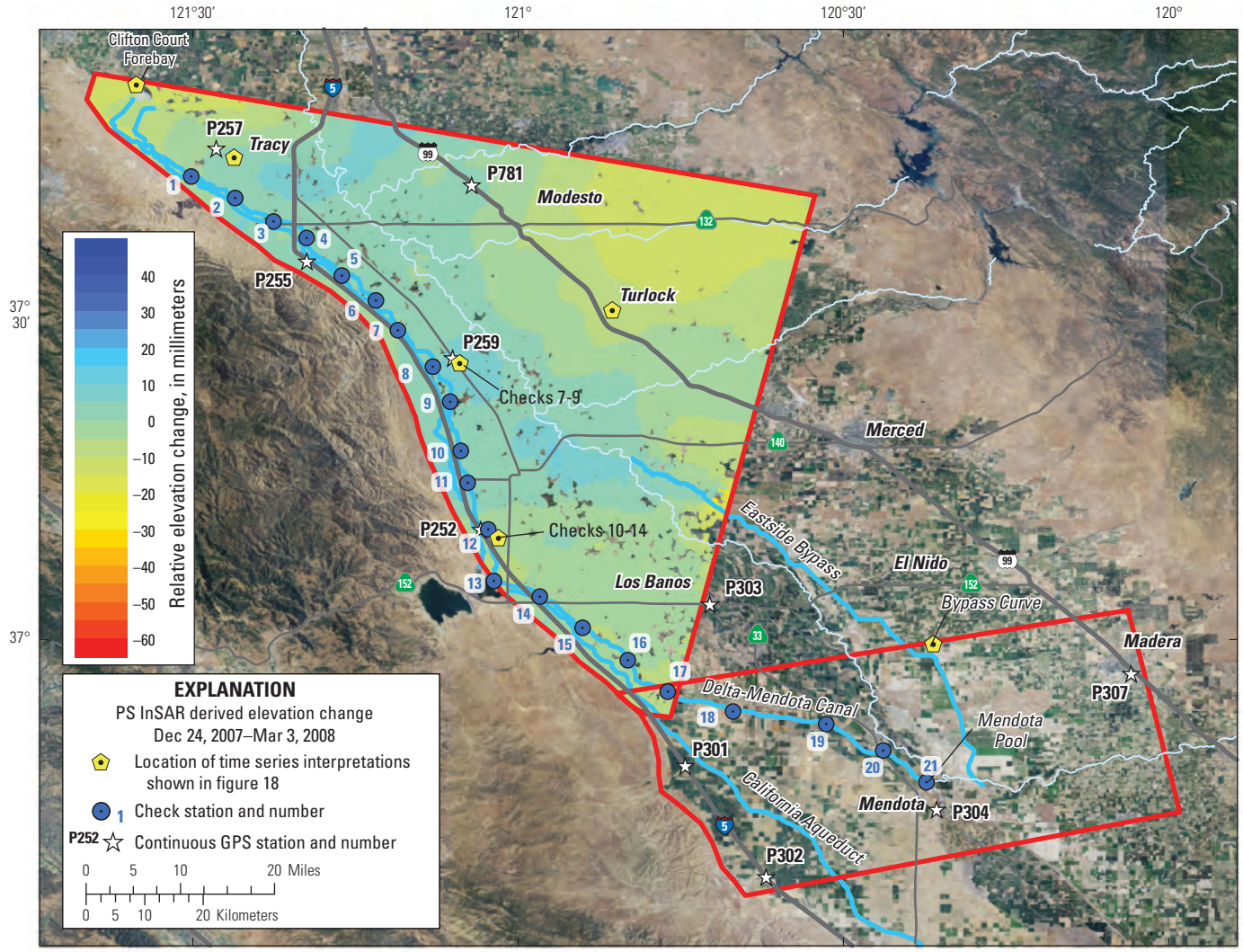

Figure A-1. Persistent Scatterer Interferometric Synthetic Aperture Radar (PS InSAR) Interferogram for the Northern Reaches of the Delta-Mendota Canal, ENVIronmental SATellite (ENVISAT) Track 299, December 24, 2007–March 3, 2008, San Joaquin Valley, California. Negative values indicate subsidence, and positive values indicate uplift.

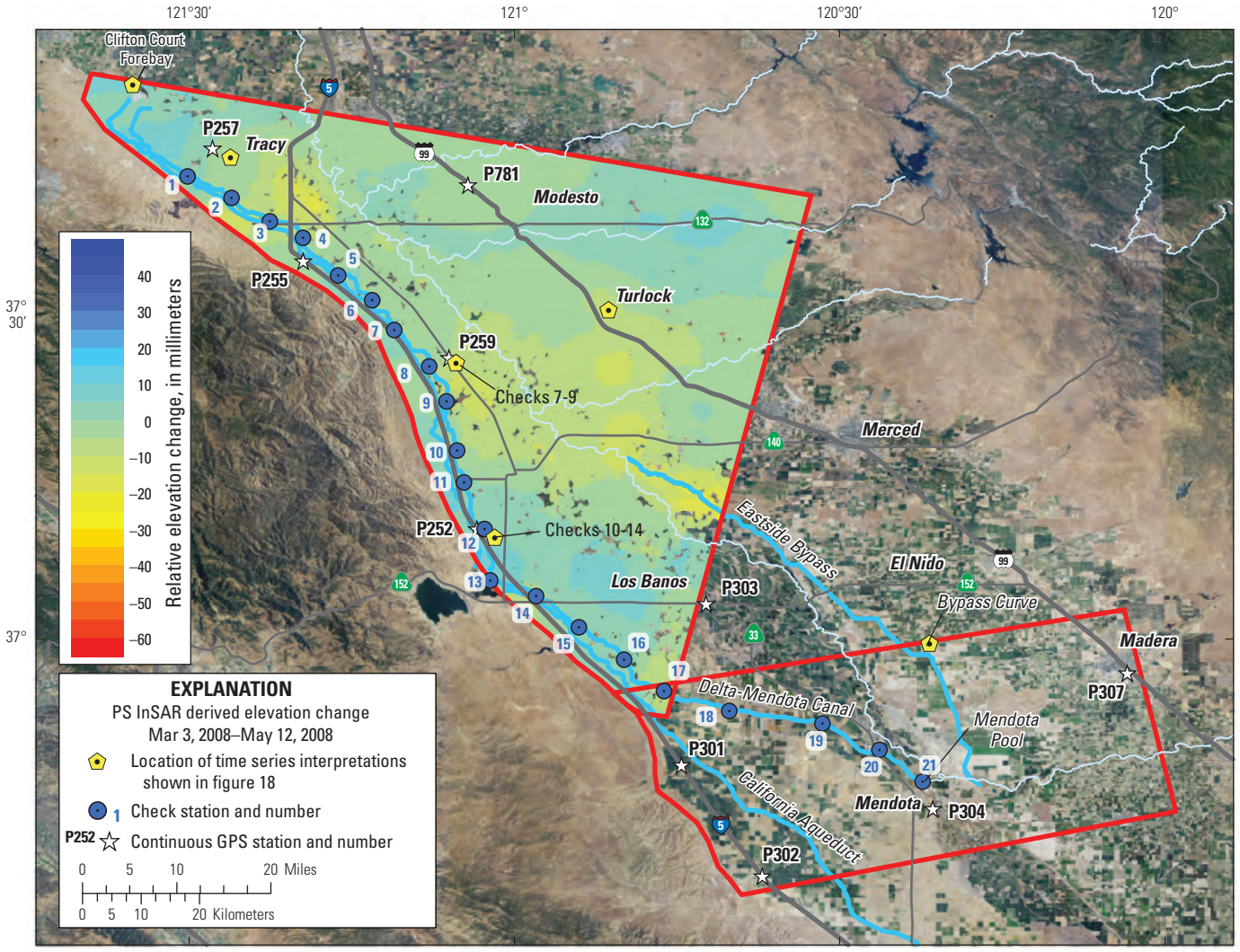

Figure A-2. Persistent Scatterer Interferometric Synthetic Aperture Radar (PS InSAR) Interferogram for the Northern Reaches of the Delta-Mendota Canal, ENVIronmental SATellite (ENVISAT) Track 299, March 3–May 12, 2008, San Joaquin Valley, California. Negative values indicate subsidence, and positive values indicate uplift.

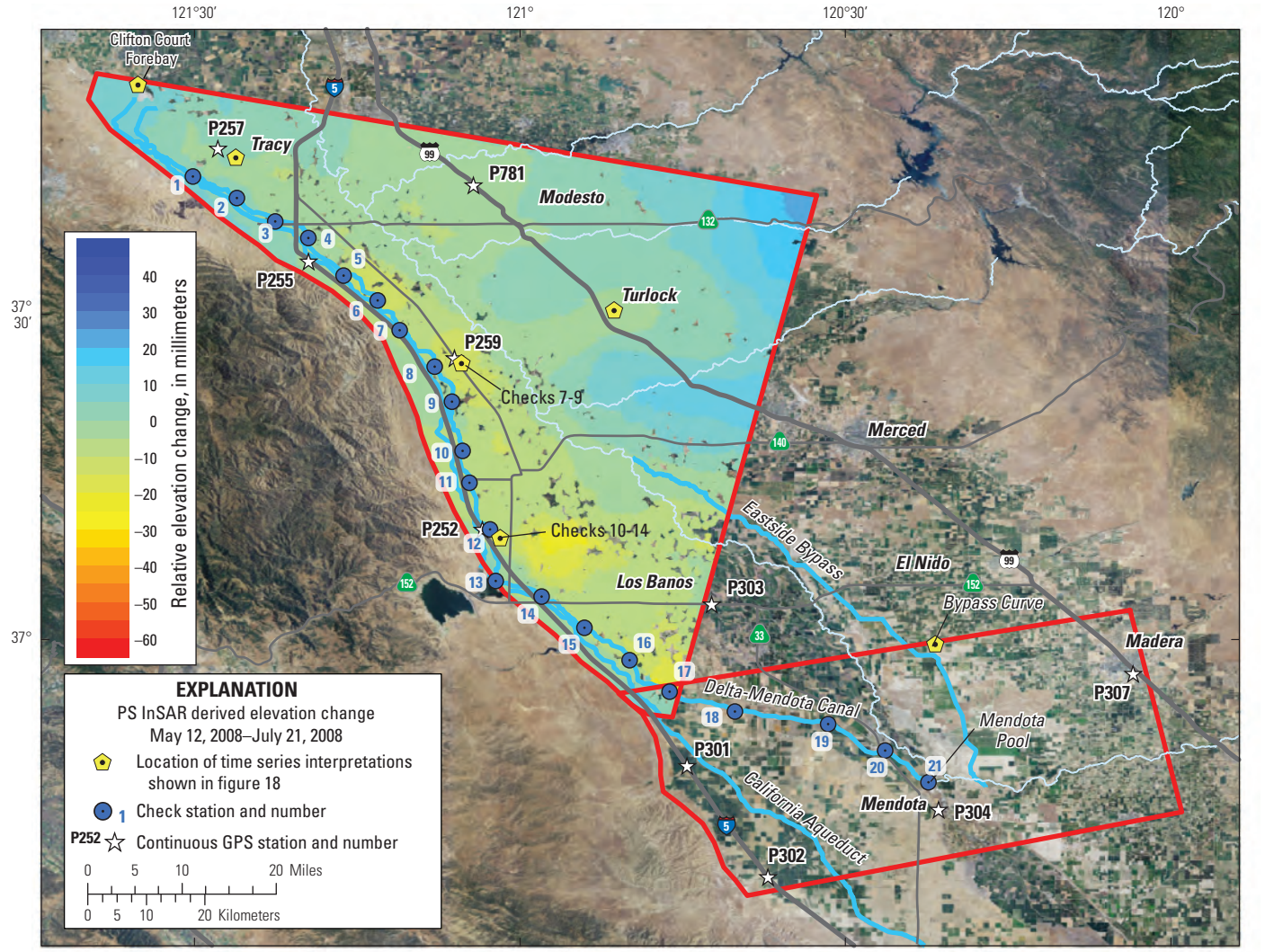

Figure A-3. Persistent Scatterer Interferometric Synthetic Aperture Radar (PS InSAR) Interferogram for the Northern Reaches of the Delta-Mendota Canal, ENVIronmental SATellite (ENVISAT) Track 299, May 12–July 21, 2008, San Joaquin Valley, California. Negative values indicate subsidence, and positive values indicate uplift.

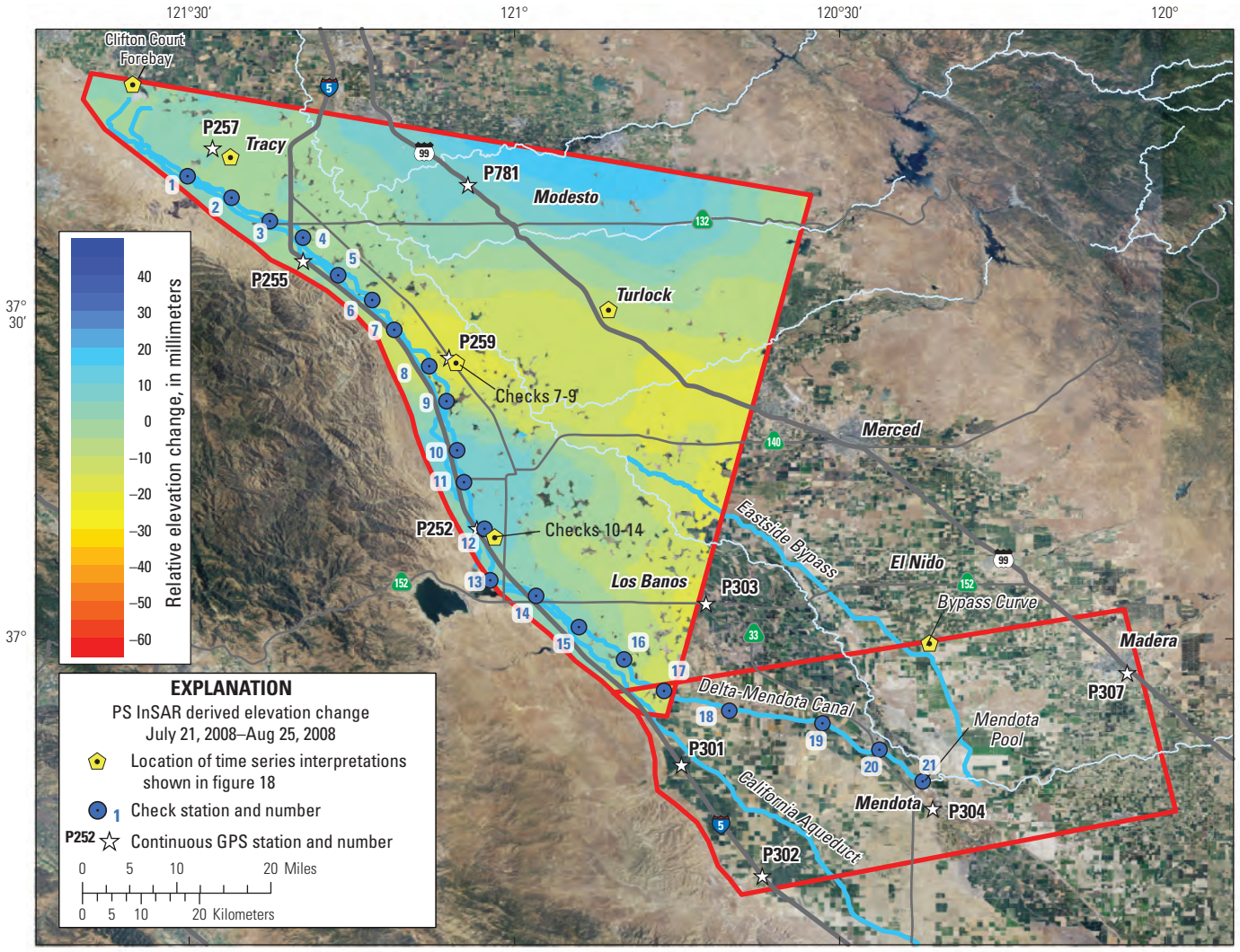

Figure A-4. Persistent Scatterer Interferometric Synthetic Aperture Radar (PS InSAR) Interferogram for the Northern Reaches of the Delta-Mendota Canal, ENVIronmental SATellite (ENVISAT) Track 299, July 21–August 25, 2008, San Joaquin Valley, California. Negative values indicate subsidence, and positive values indicate uplift.

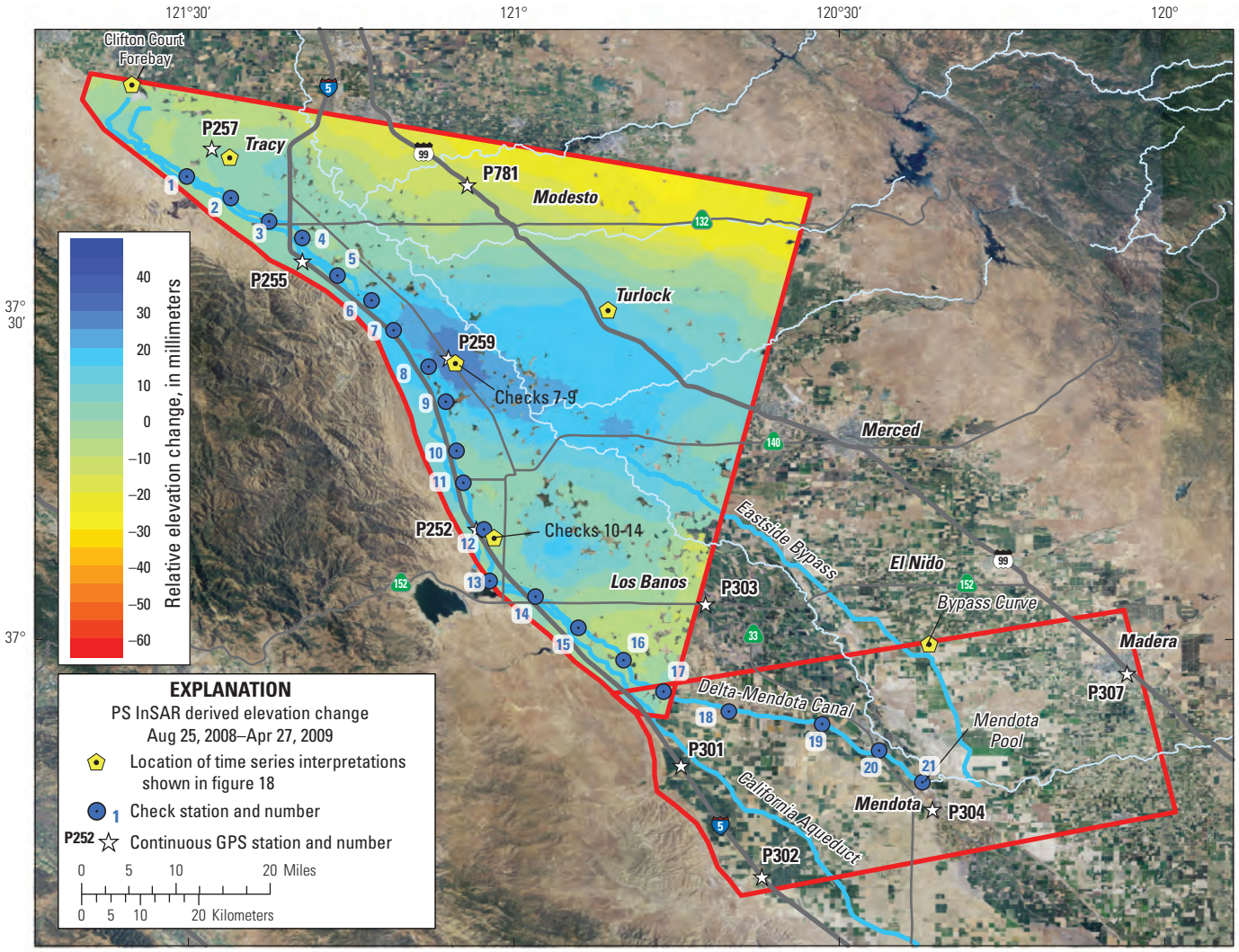

Figure A-5. Persistent Scatterer Interferometric Synthetic Aperture Radar (PS InSAR) Interferogram for the Northern Reaches of the Delta-Mendota Canal, ENVIronmental SATellite (ENVISAT) Track 299, August 25, 2008–April 27, 2009, San Joaquin Valley, California. Negative values indicate subsidence, and positive values indicate uplift.

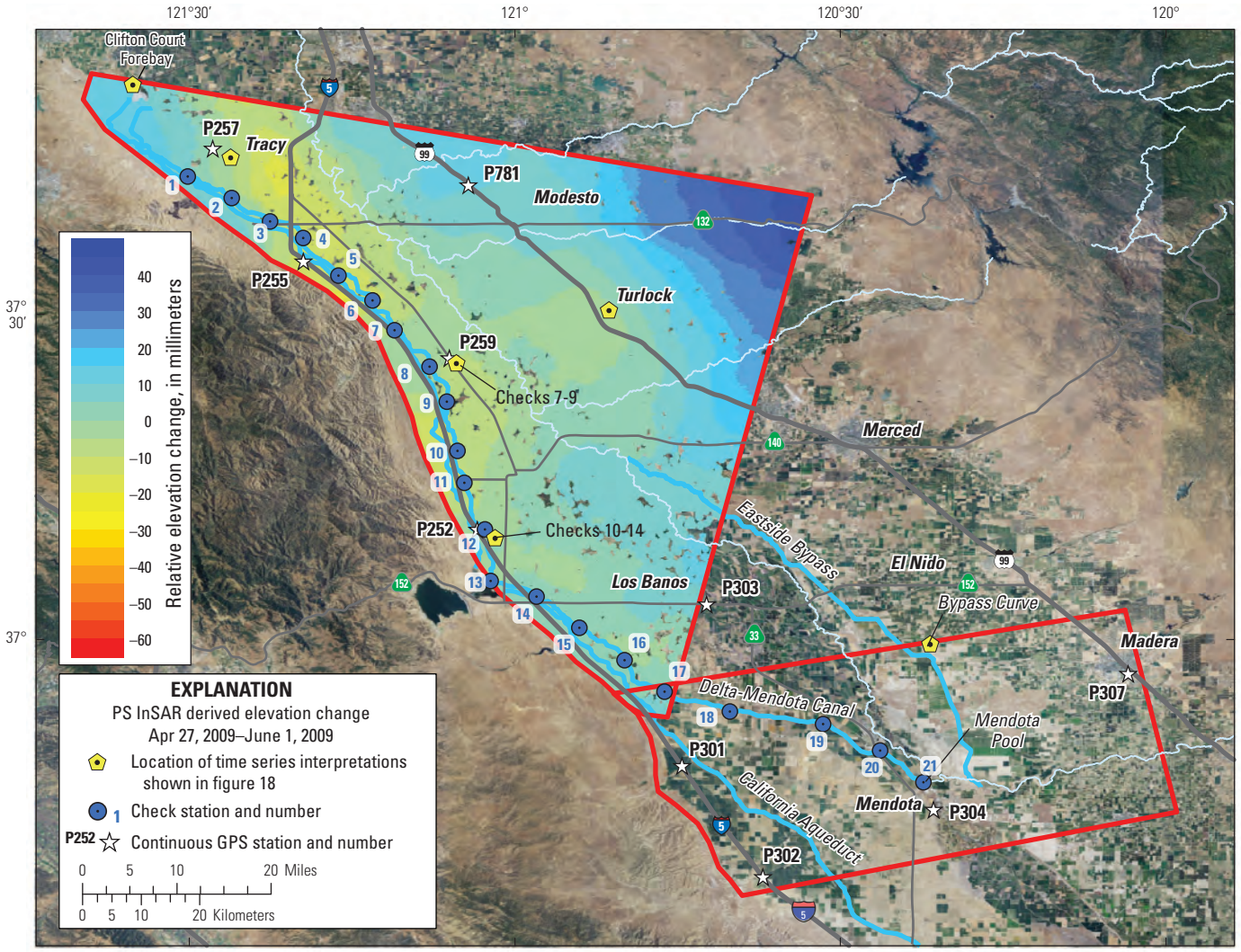

Figure A-6. Persistent Scatterer Interferometric Synthetic Aperture Radar (PS InSAR) Interferogram for the Northern Reaches of the Delta-Mendota Canal, ENVIronmental SATellite (ENVISAT) Track 299, April 27–June 1, 2009, San Joaquin Valley, California. Negative values indicate subsidence, and positive values indicate uplift.

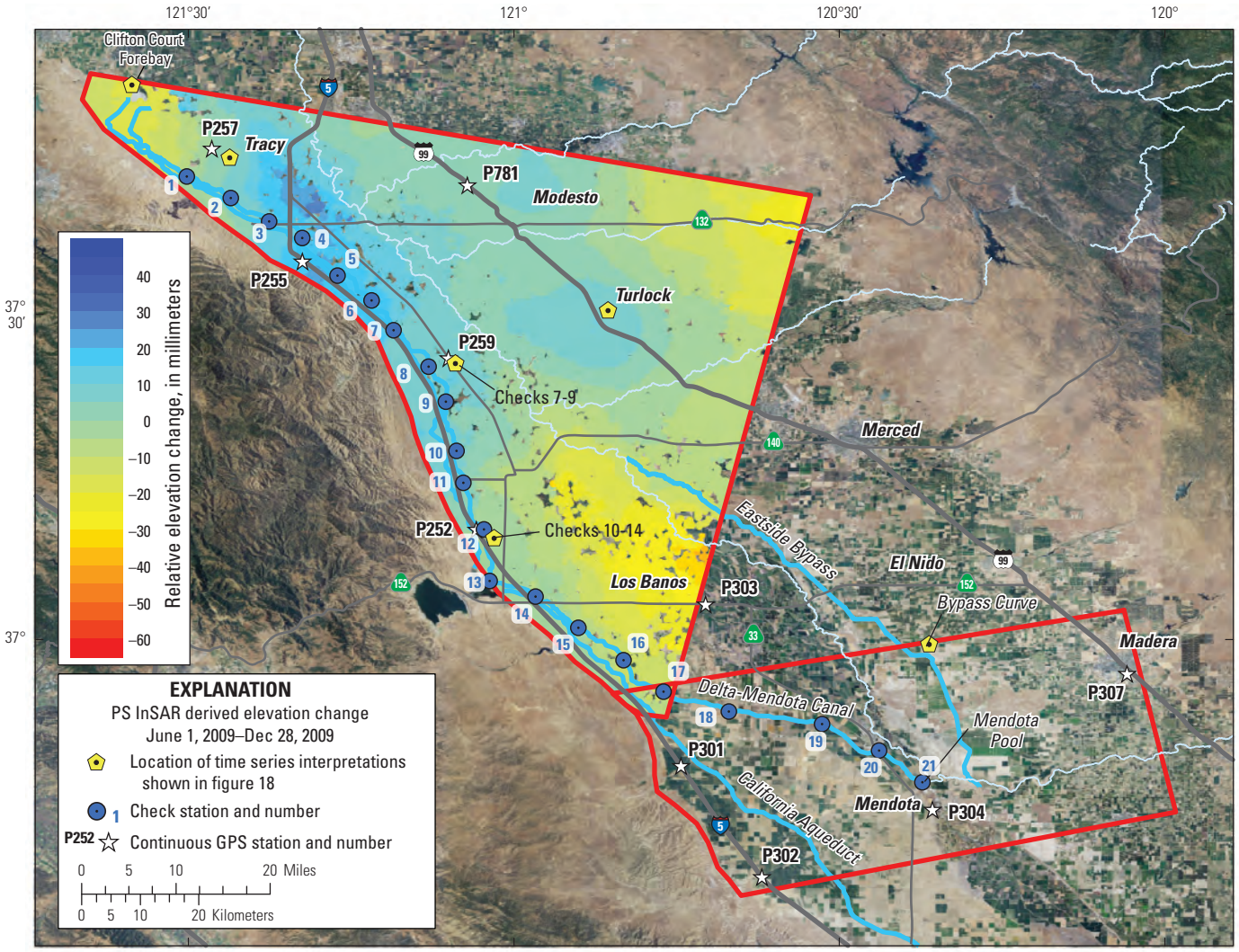

Figure A-7. Persistent Scatterer Interferometric Synthetic Aperture Radar (PS InSAR) Interferogram for the Northern Reaches of the Delta-Mendota Canal, ENVIronmental SATellite (ENVISAT) Track 299, June 1–December 28, 2009, San Joaquin Valley, California. Negative values indicate subsidence, and positive values indicate uplift.

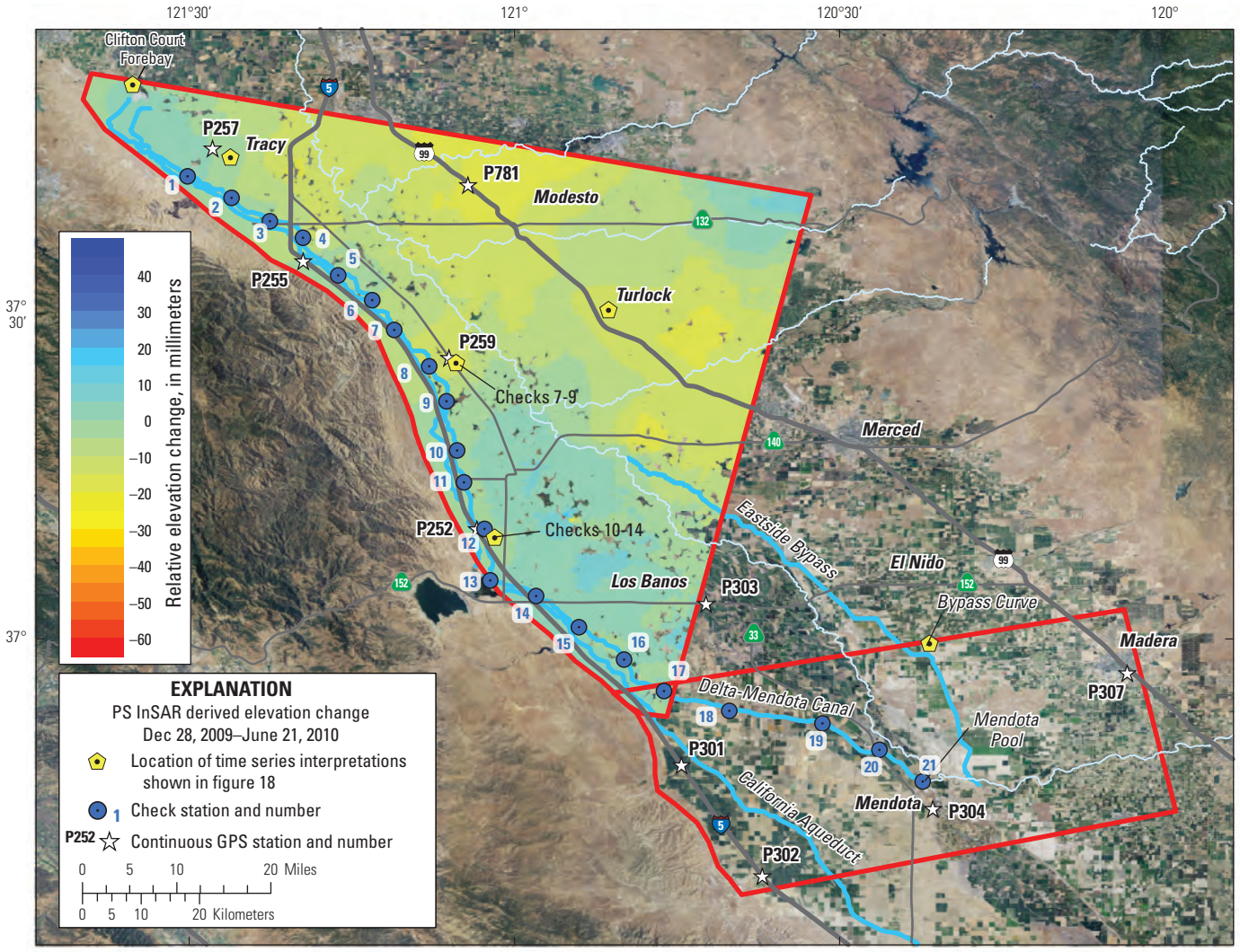

Figure A-8. Persistent Scatterer Interferometric Synthetic Aperture Radar (PS InSAR) Interferogram for the Northern Reaches of the Delta-Mendota Canal, ENVIronmental SATellite (ENVISAT) Track 299, December 28, 2009–June 21, 2010, San Joaquin Valley, California. Negative values indicate subsidence, and positive values indicate uplift.

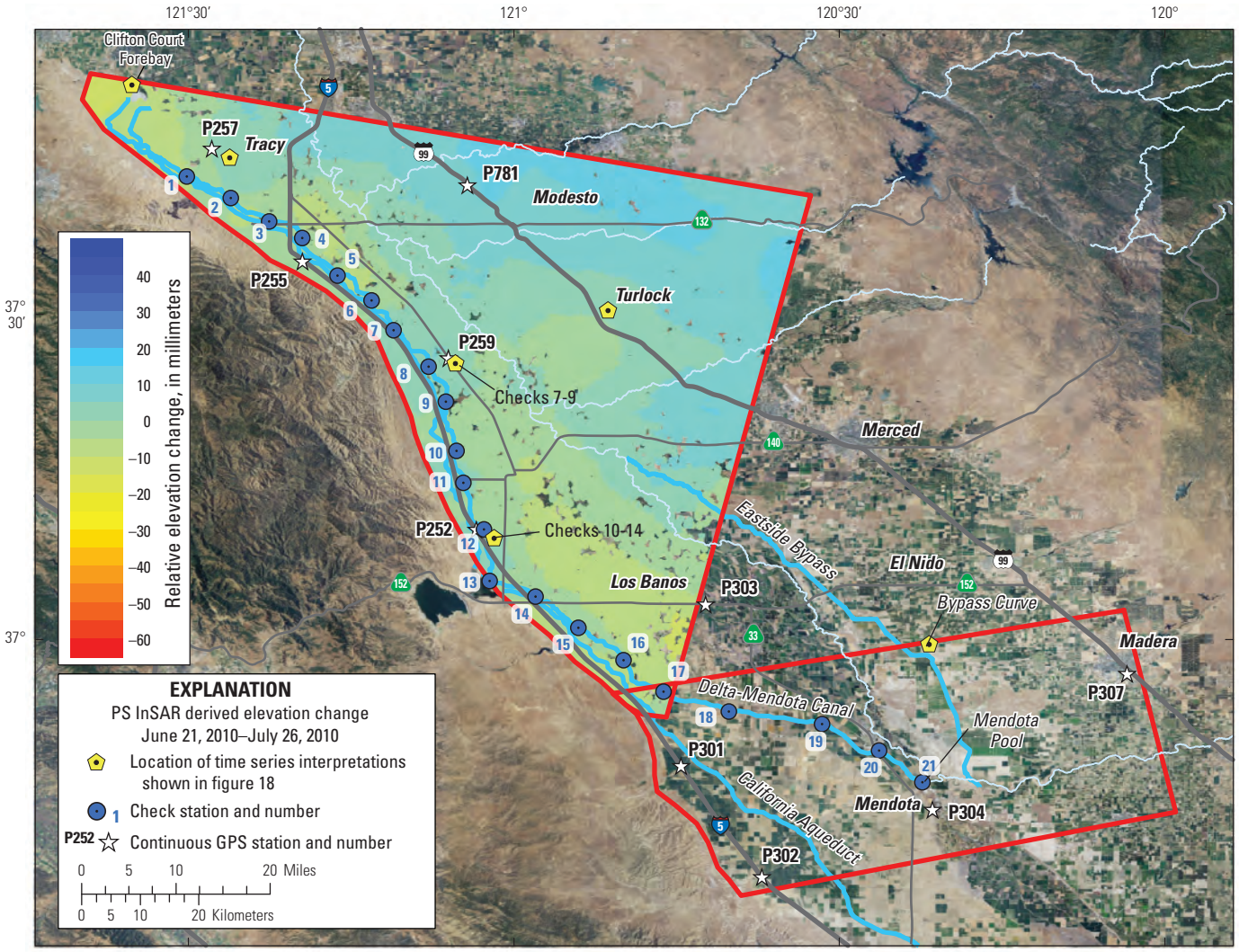

Figure A-9. Persistent Scatterer Interferometric Synthetic Aperture Radar (PS InSAR) Interferogram for the Northern Reaches of the Delta-Mendota Canal, ENVIronmental SATellite (ENVISAT) Track 299, June 21–July 26, 2010, San Joaquin Valley, California. Negative values indicate subsidence, and positive values indicate uplift.

Appendix B. Persistent Scatterer Interferometric Synthetic Aperture Radar (PS InSAR) Interferograms for the Southern Reaches of the Delta-Mendota Canal, ENVIronmental SATellite (ENVISAT) Track 435, July 3, 2003–May 13, 2004; May 13–November 4, 2004; November 4, 2004–January 13, 2005; January 13–March 24, 2005; March 9, 2006–January 18, 2007; January 18–November 29, 2007; November 29, 2007–April 17, 2008; and April 17–May 22, 2008, San Joaquin Valley, California.

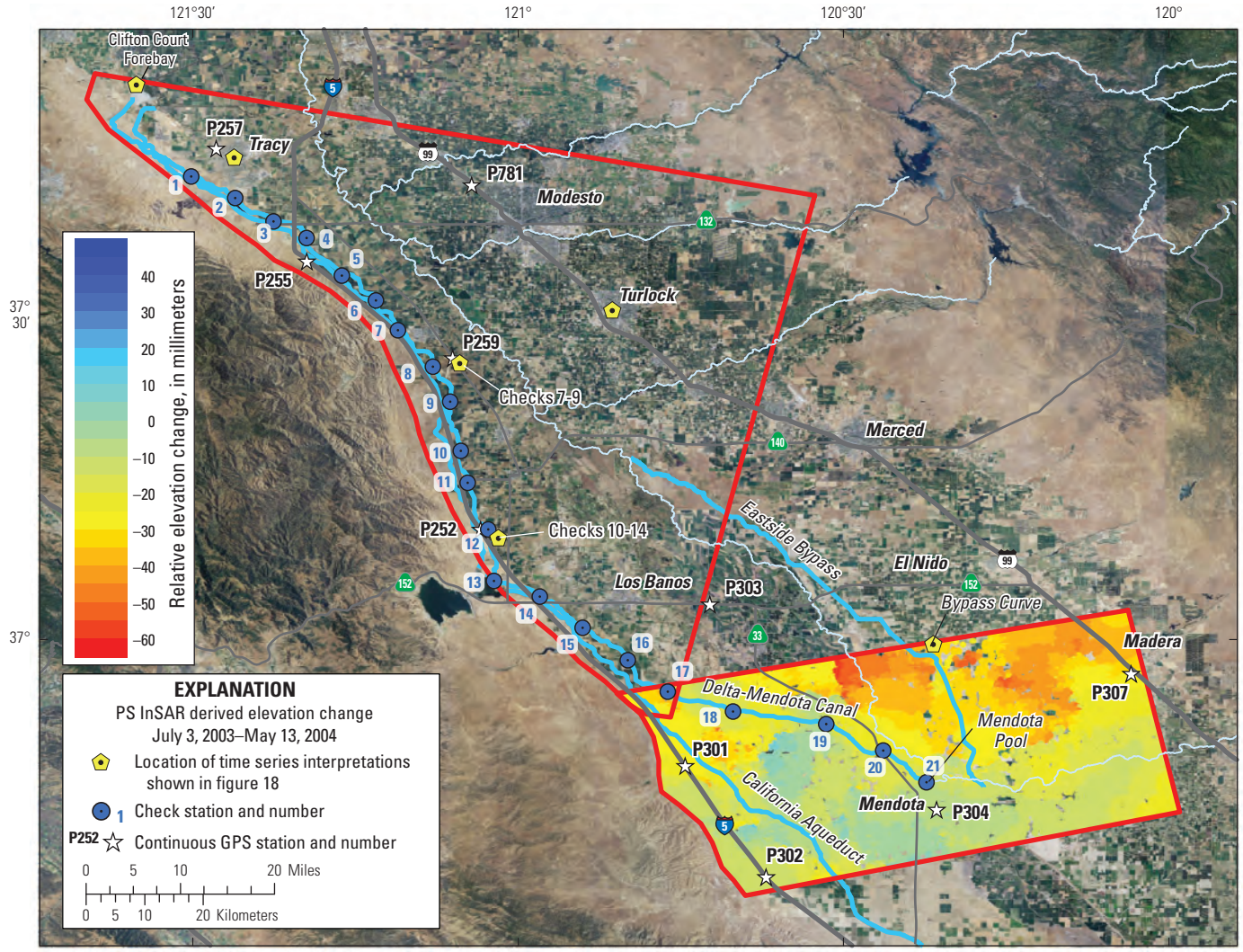

Figure B-1. Persistent Scatterer Interferometric Synthetic Aperture Radar (PS InSAR) Interferogram for the Southern Reaches of the Delta-Mendota Canal, ENVIronmental SATellite (ENVISAT) Track 435, July 3, 2003–May 13, 2004, San Joaquin Valley, California. Negative values indicate subsidence, and positive values indicate uplift.

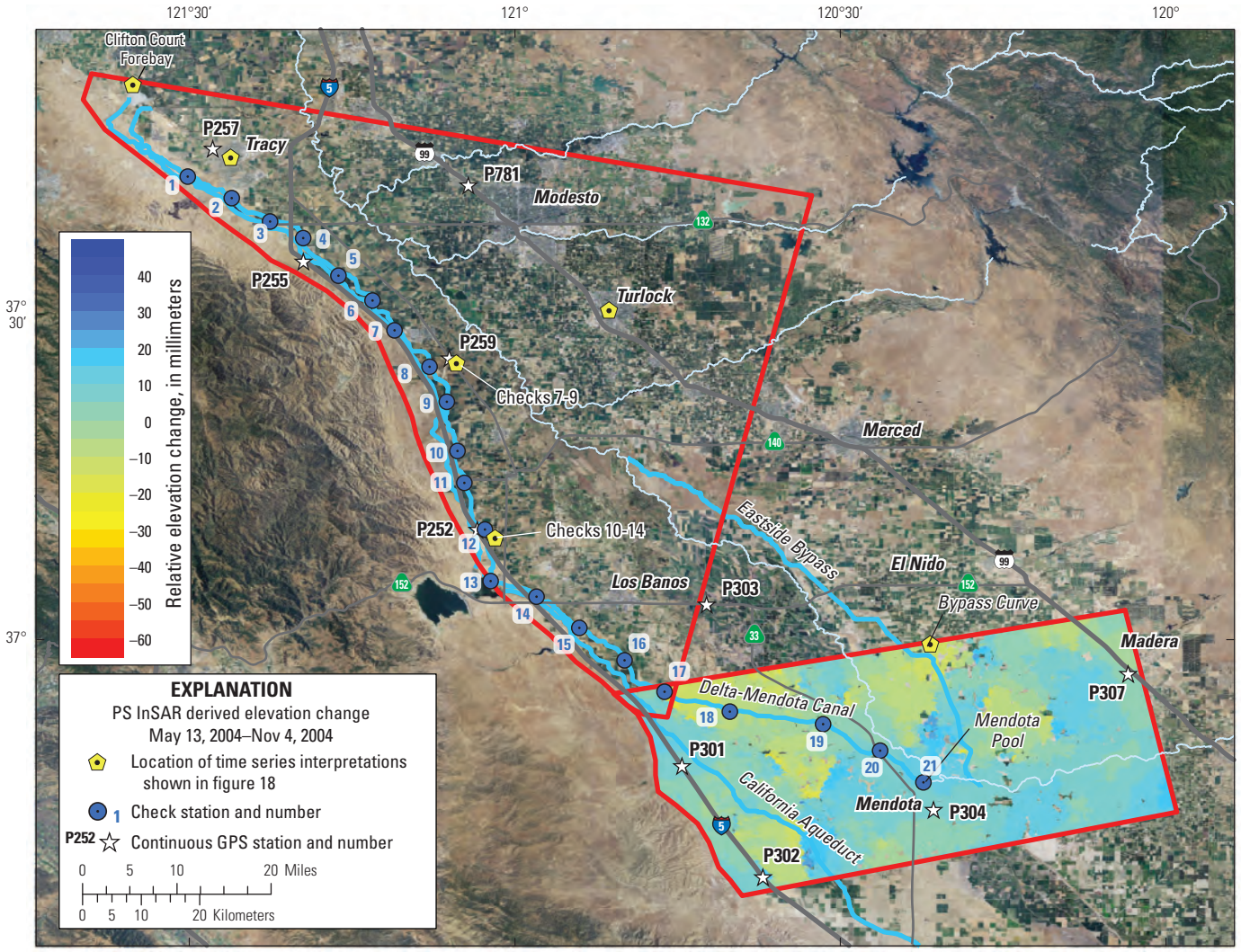

Figure B-2. Persistent Scatterer Interferometric Synthetic Aperture Radar (PS InSAR) Interferogram for the Southern Reaches of the Delta-Mendota Canal, ENVIronmental SATellite (ENVISAT) Track 435, May 13–November 4, 2004, San Joaquin Valley, California. Negative values indicate subsidence, and positive values indicate uplift.

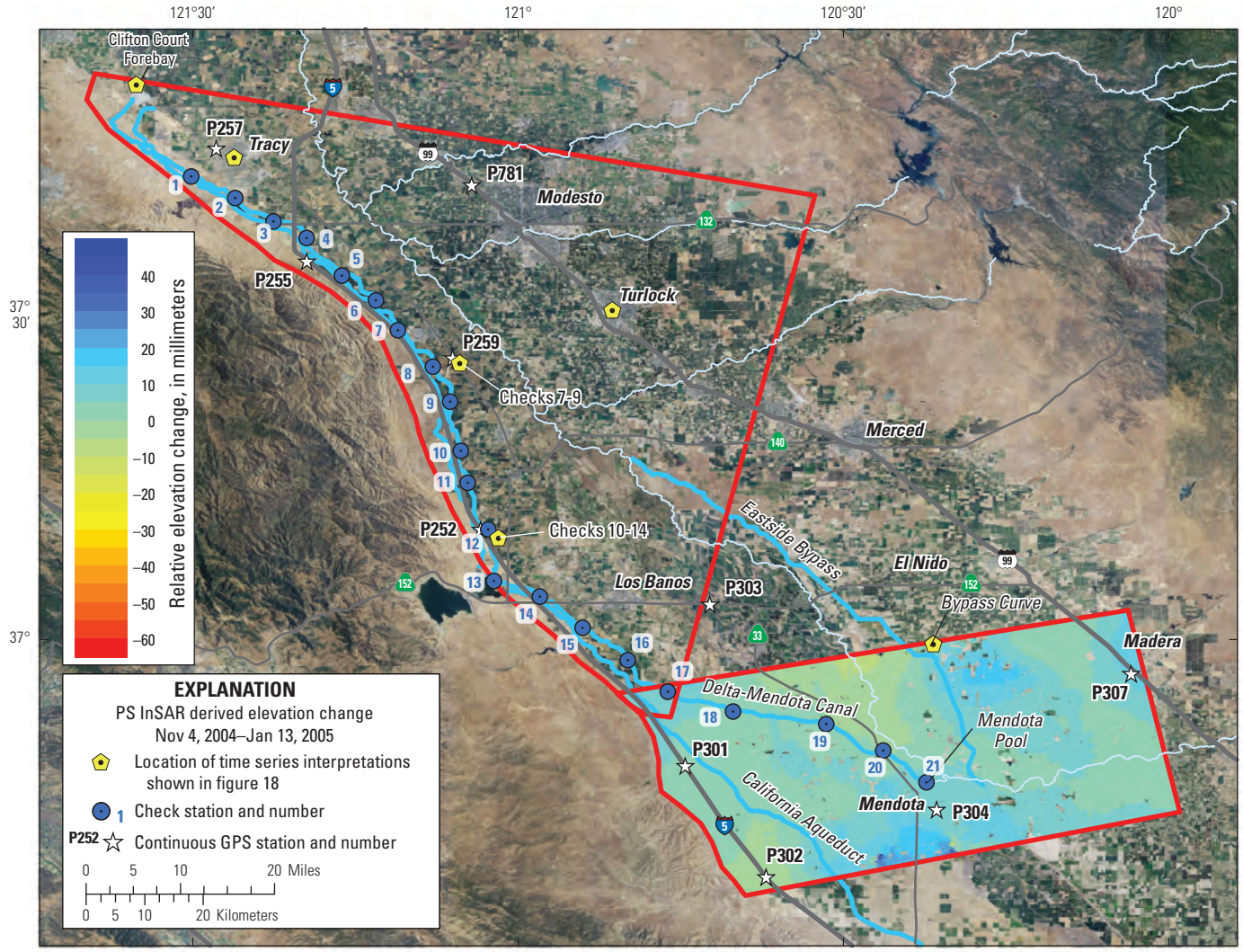

Figure B-3. Persistent Scatterer Interferometric Synthetic Aperture Radar (PS InSAR) Interferogram for the Southern Reaches of the Delta-Mendota Canal, ENVIronmental SATellite (ENVISAT) Track 435, November 4, 2004–January 13, 2005, San Joaquin Valley, California. Negative values indicate subsidence, and positive values indicate uplift.

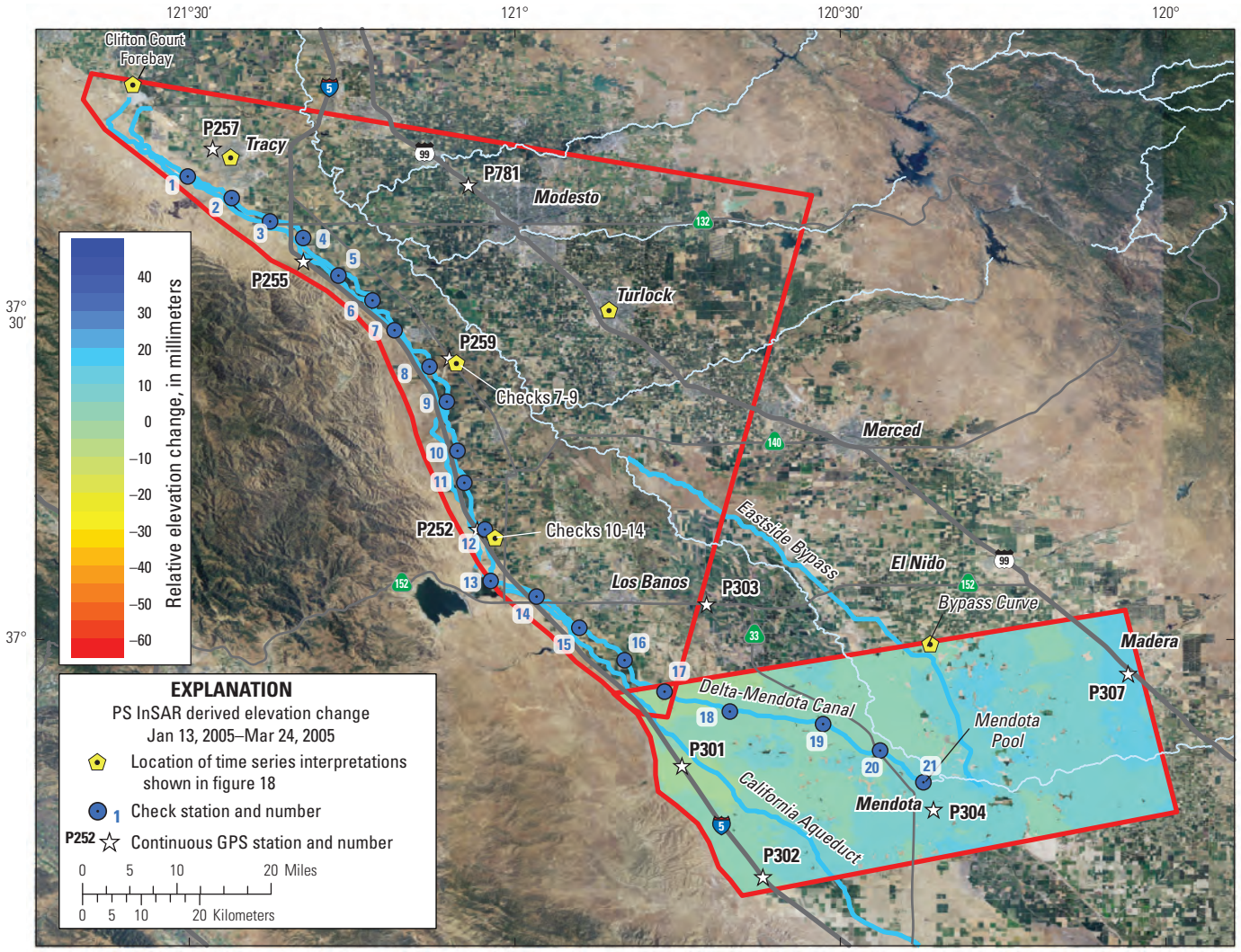

Figure B-4. Persistent Scatterer Interferometric Synthetic Aperture Radar (PS InSAR) Interferogram for the Southern Reaches of the Delta-Mendota Canal, ENVIronmental SATellite (ENVISAT) Track 435, January 13–March 24, 2005, San Joaquin Valley, California. Negative values indicate subsidence, and positive values indicate uplift.

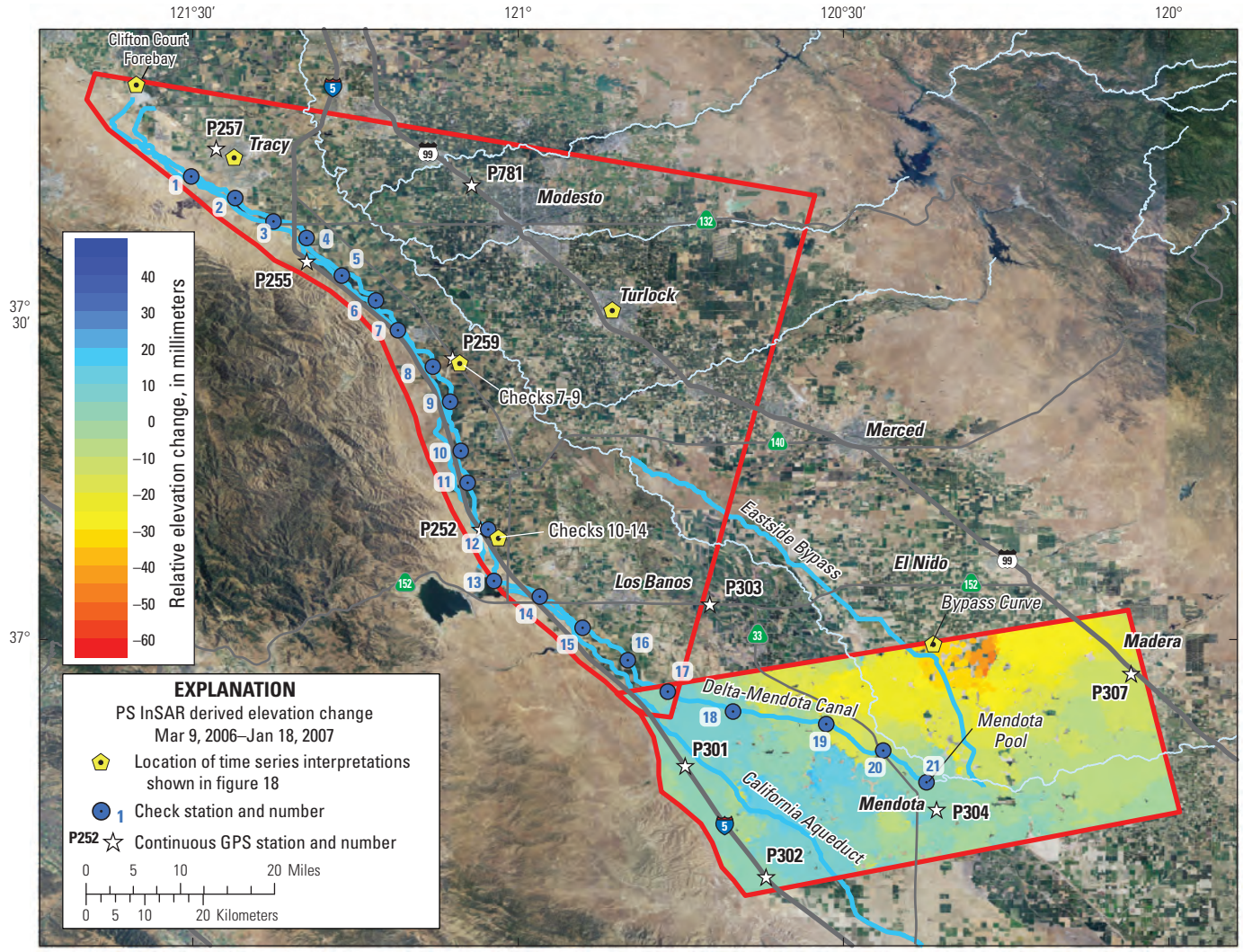

Figure B-5. Persistent Scatterer Interferometric Synthetic Aperture Radar (PS InSAR) Interferogram for the Southern Reaches of the Delta-Mendota Canal, ENVIronmental SATellite (ENVISAT) Track 435, March 9, 2006–January 18, 2007, San Joaquin Valley, California. Negative values indicate subsidence, and positive values indicate uplift.

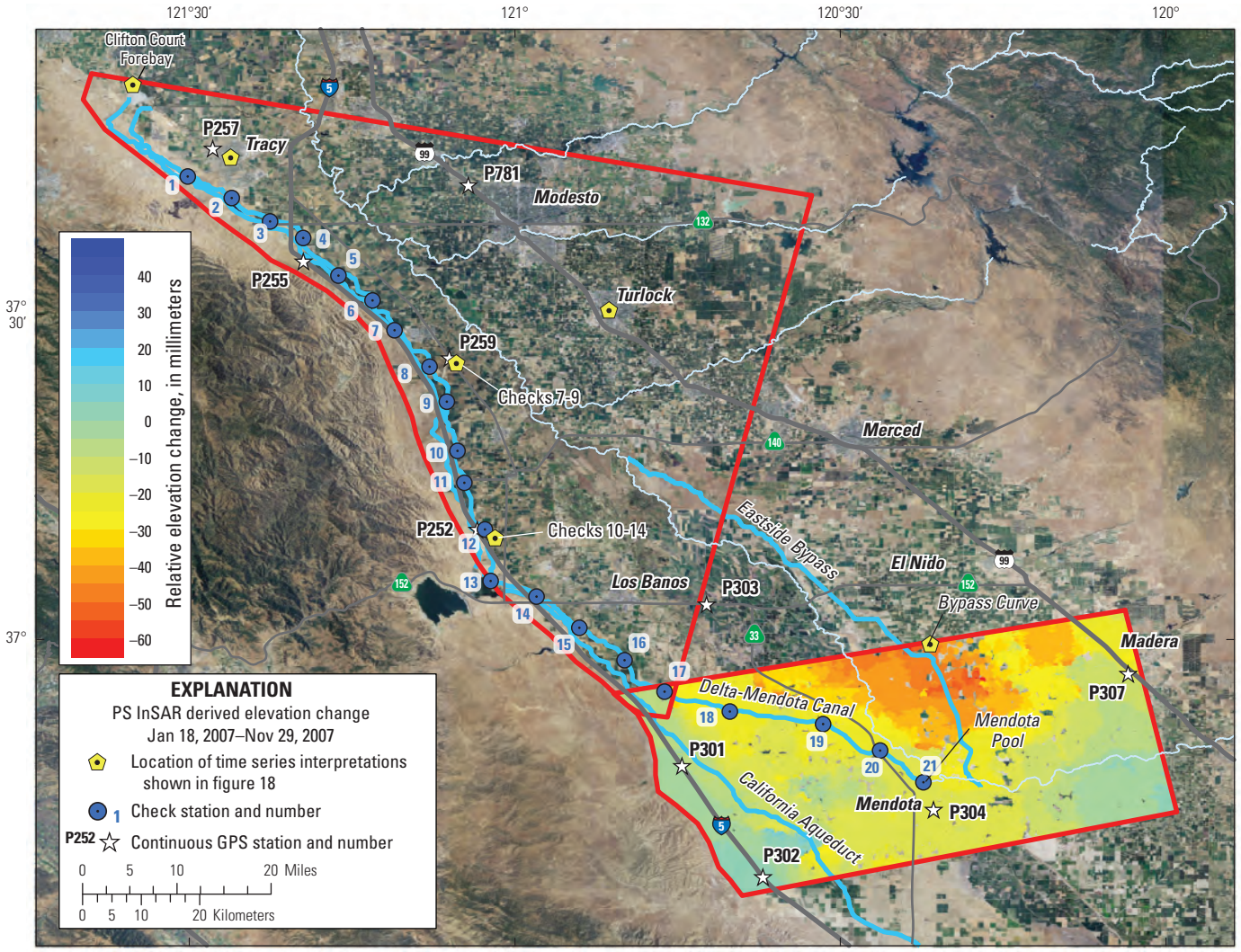

Figure B-6. Persistent Scatterer Interferometric Synthetic Aperture Radar (PS InSAR) Interferogram for the Southern Reaches of the Delta-Mendota Canal, ENVIronmental SATellite (ENVISAT) Track 435, January 18–November 29, 2007, San Joaquin Valley, California. Negative values indicate subsidence, and positive values indicate uplift.

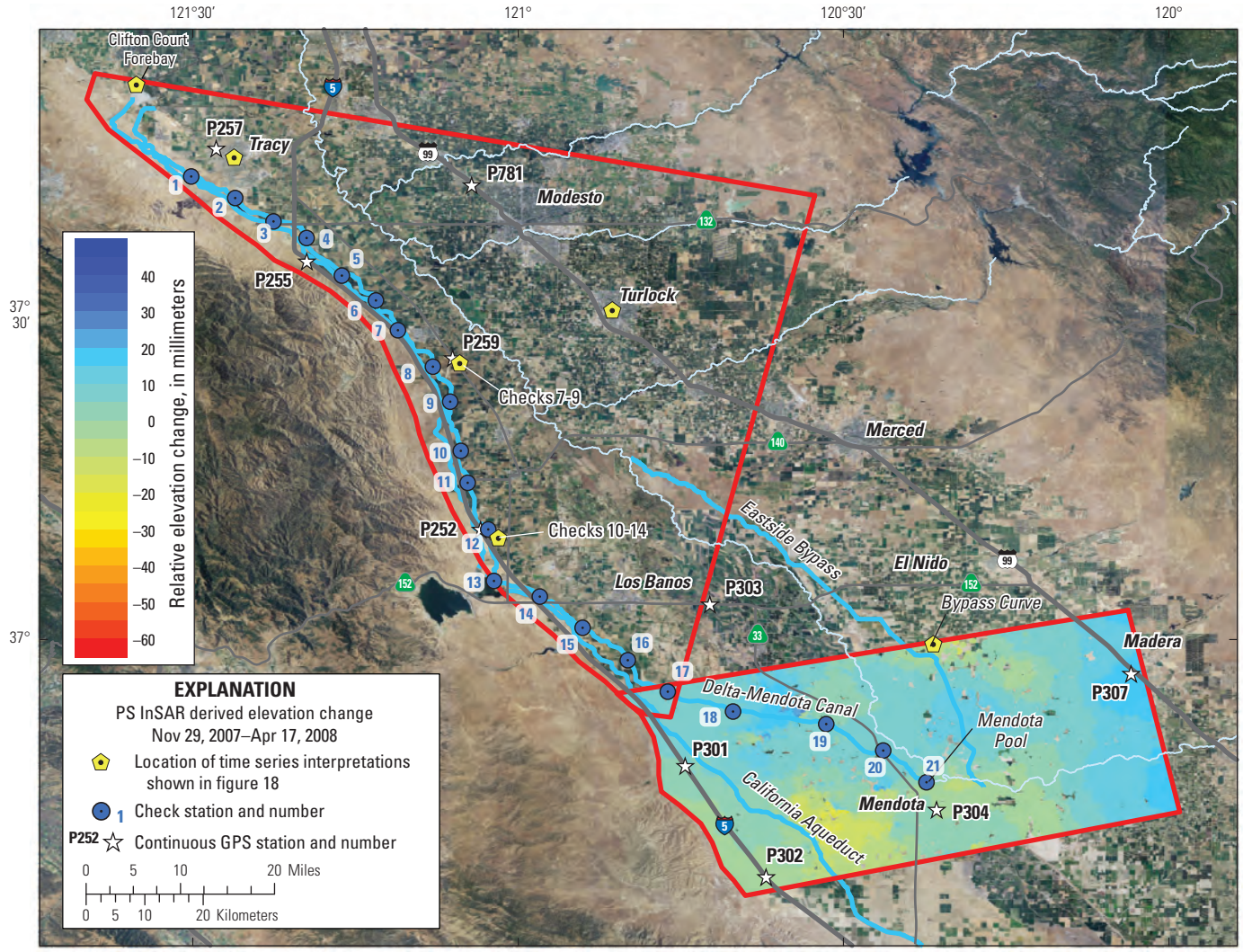

Figure B-7. Persistent Scatterer Interferometric Synthetic Aperture Radar (PS InSAR) Interferogram for the Southern Reaches of the Delta-Mendota Canal, ENVIronmental SATellite (ENVISAT) Track 435, November 29, 2007–April 17, 2008, San Joaquin Valley, California. Negative values indicate subsidence, and positive values indicate uplift.

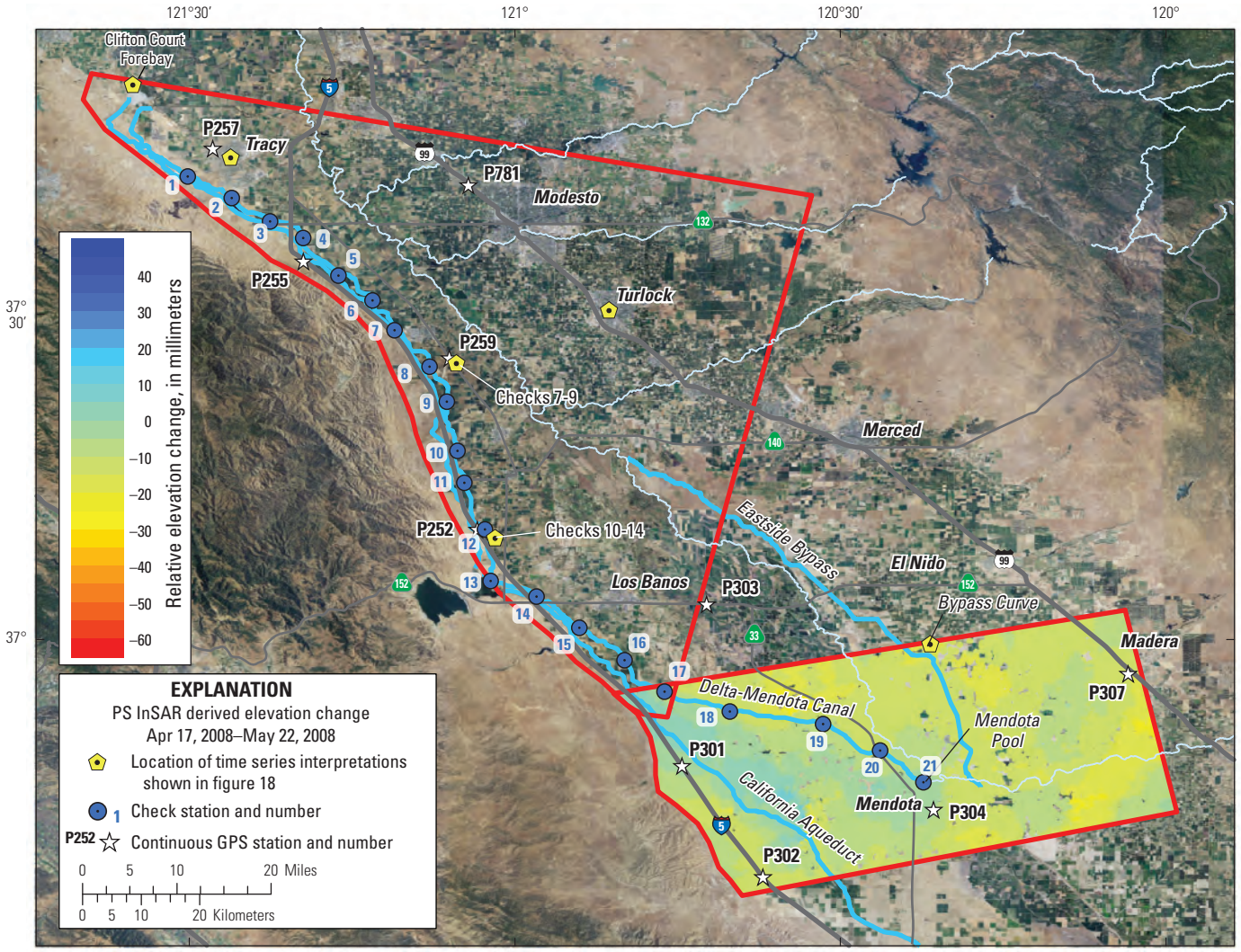

Figure B-8. Persistent Scatterer Interferometric Synthetic Aperture Radar (PS InSAR) Interferogram for the Southern Reaches of the Delta-Mendota Canal, ENVIronmental SATellite (ENVISAT) Track 435, April 17–May 22, 2008, San Joaquin Valley, California. Negative values indicate subsidence, and positive values indicate uplift.

Appendix C. Persistent Scatterer Interferometric Synthetic Aperture Radar (PS InSAR) Interferograms for the Northern Reaches of the Delta-Mendota Canal, ENVIronmental SATellite (ENVISAT) Track 299, December 24, 2007–September 29, 2008; September 29, 2008–February 16, 2009; February 16–July 6, 2009; July 6–November 23, 2009; November 23, 2009–February 1, 2010; February 1–June 21, 2010; and June 21–July 26, 2010, San Joaquin Valley, California.

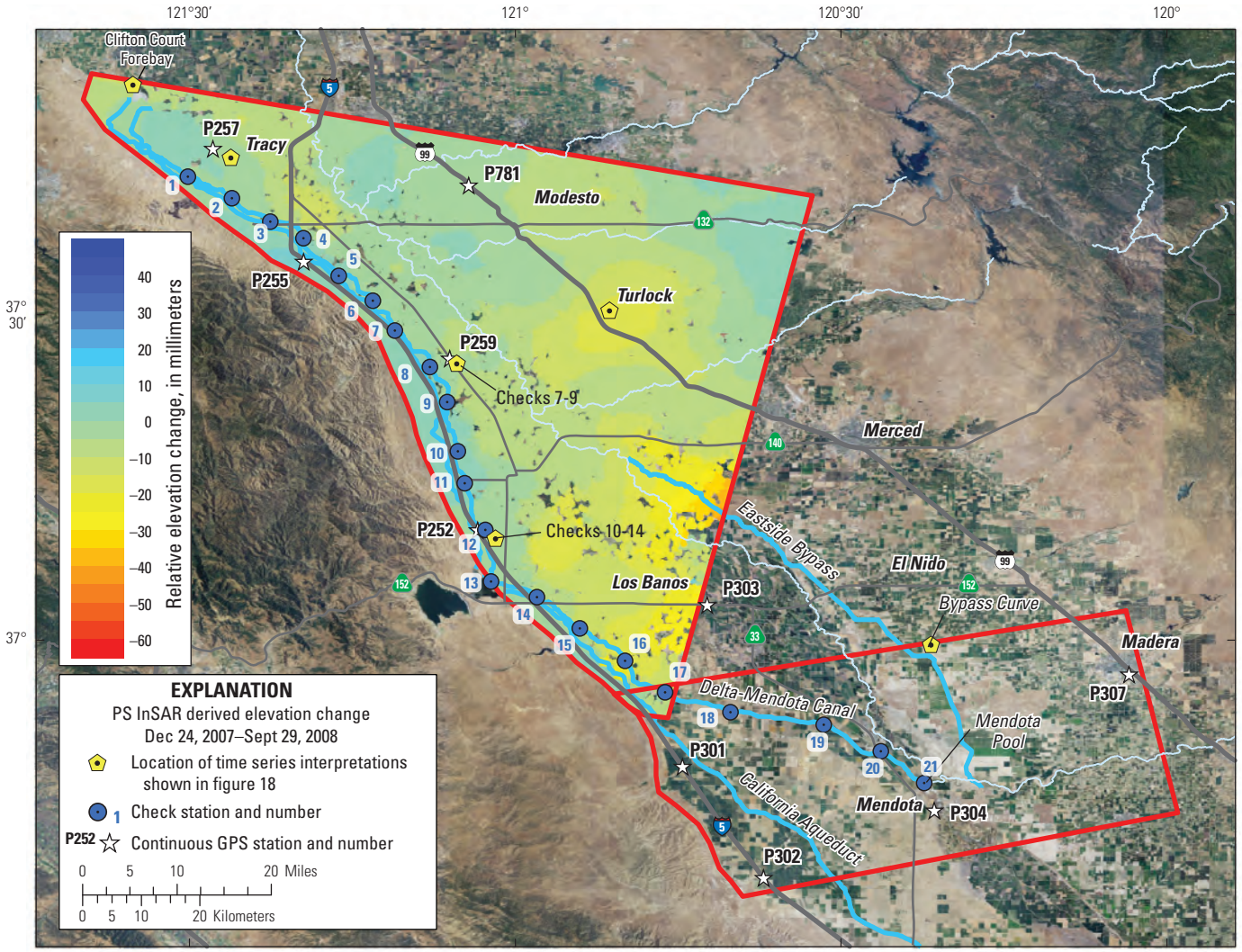

Figure C-1. Persistent Scatterer Interferometric Synthetic Aperture Radar (PS InSAR) Interferogram for the Northern Reaches of the Delta-Mendota Canal, ENVIronmental SATellite (ENVISAT) Track 299, December 24, 2007–September 29, 2008, San Joaquin Valley, California. Negative values indicate subsidence, and positive values indicate uplift.

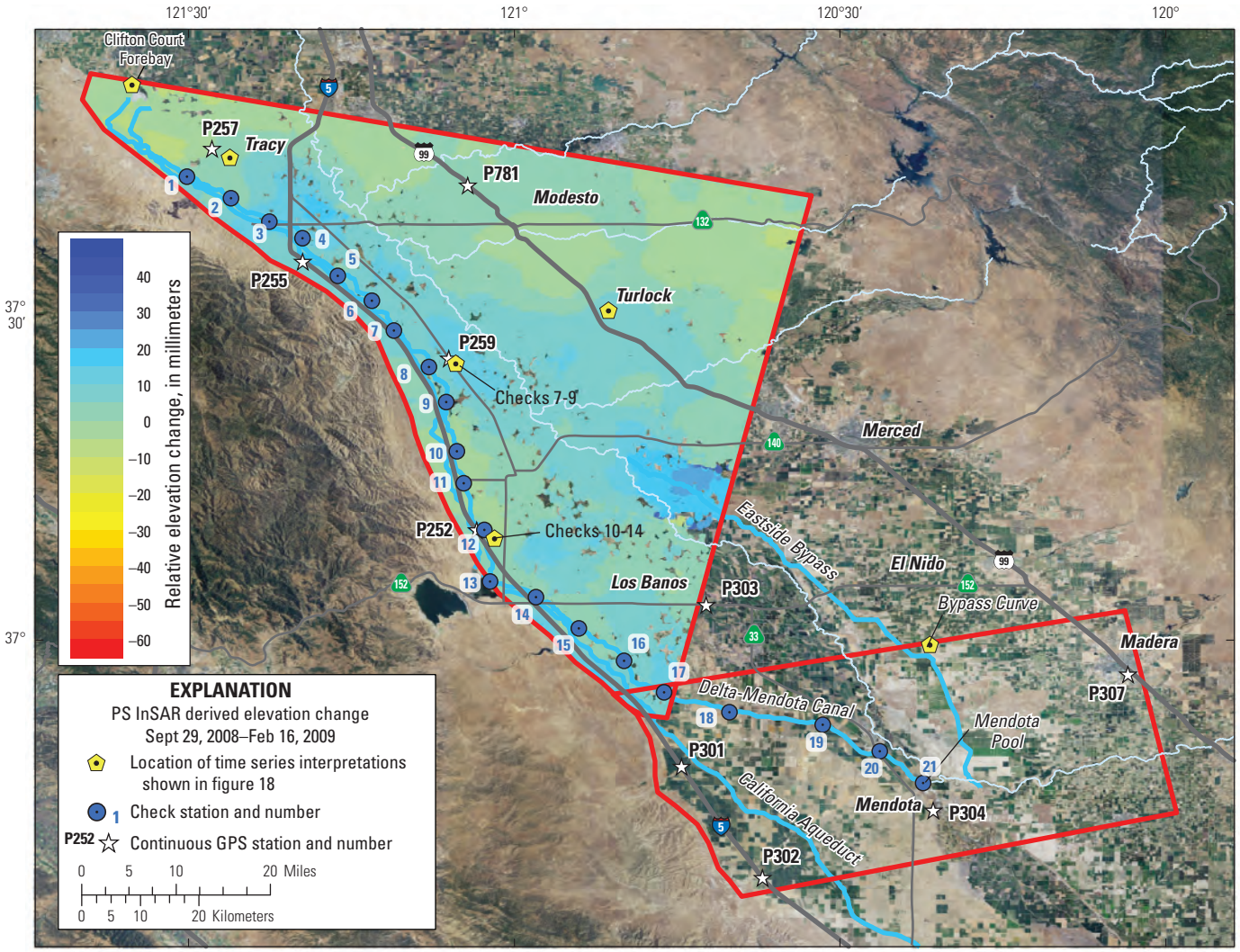

Figure C-2. Persistent Scatterer Interferometric Synthetic Aperture Radar (PS InSAR) Interferogram for the Northern Reaches of the Delta-Mendota Canal, ENVIronmental SATellite (ENVISAT) Track 299, September 29, 2008–February 16, 2009, San Joaquin Valley, California. Negative values indicate subsidence, and positive values indicate uplift.

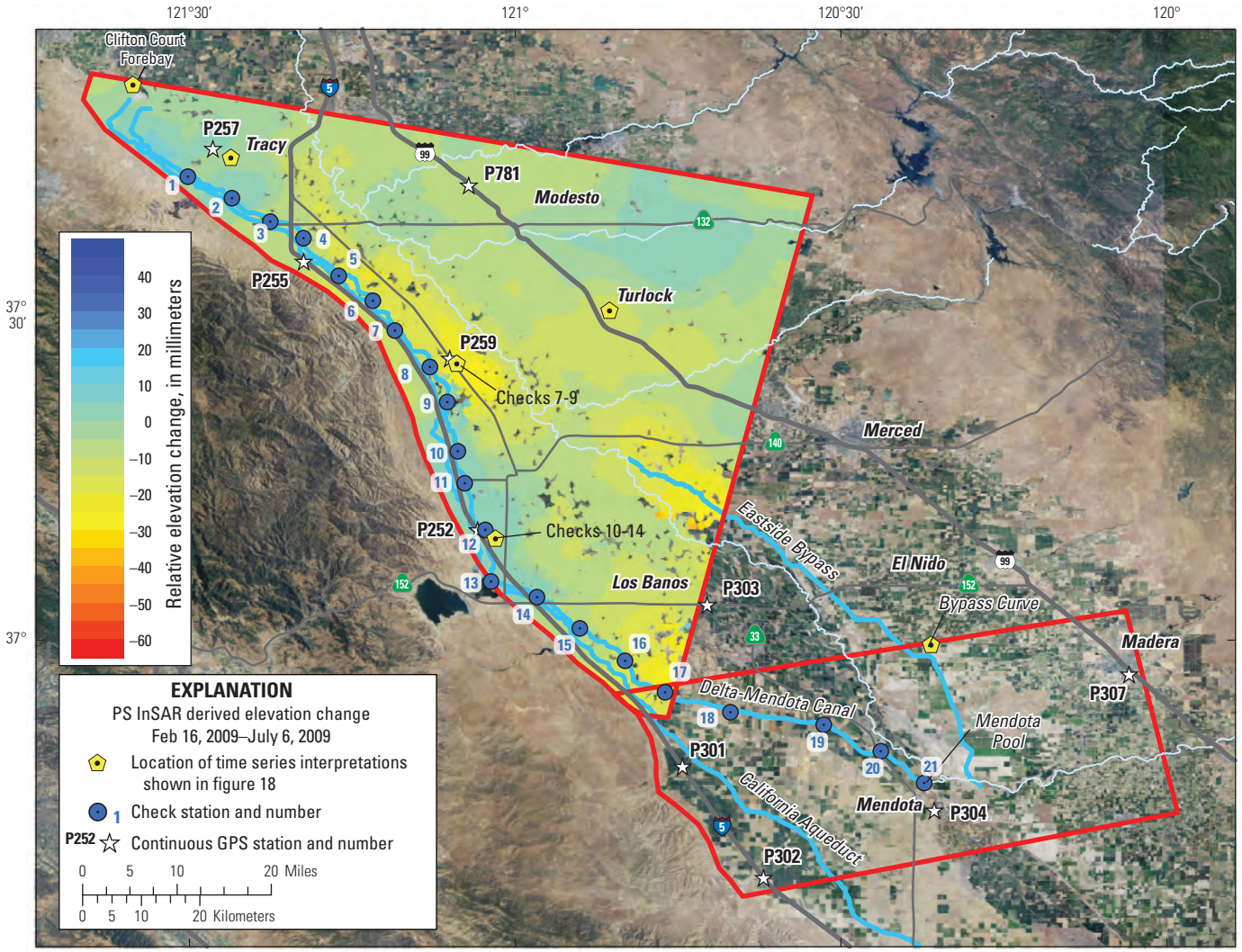

Figure C-3. Persistent Scatterer Interferometric Synthetic Aperture Radar (PS InSAR) Interferogram for the Northern Reaches of the Delta-Mendota Canal, ENVIronmental SATellite (ENVISAT) Track 299, February 16–July 6, 2009, San Joaquin Valley, California. Negative values indicate subsidence, and positive values indicate uplift.

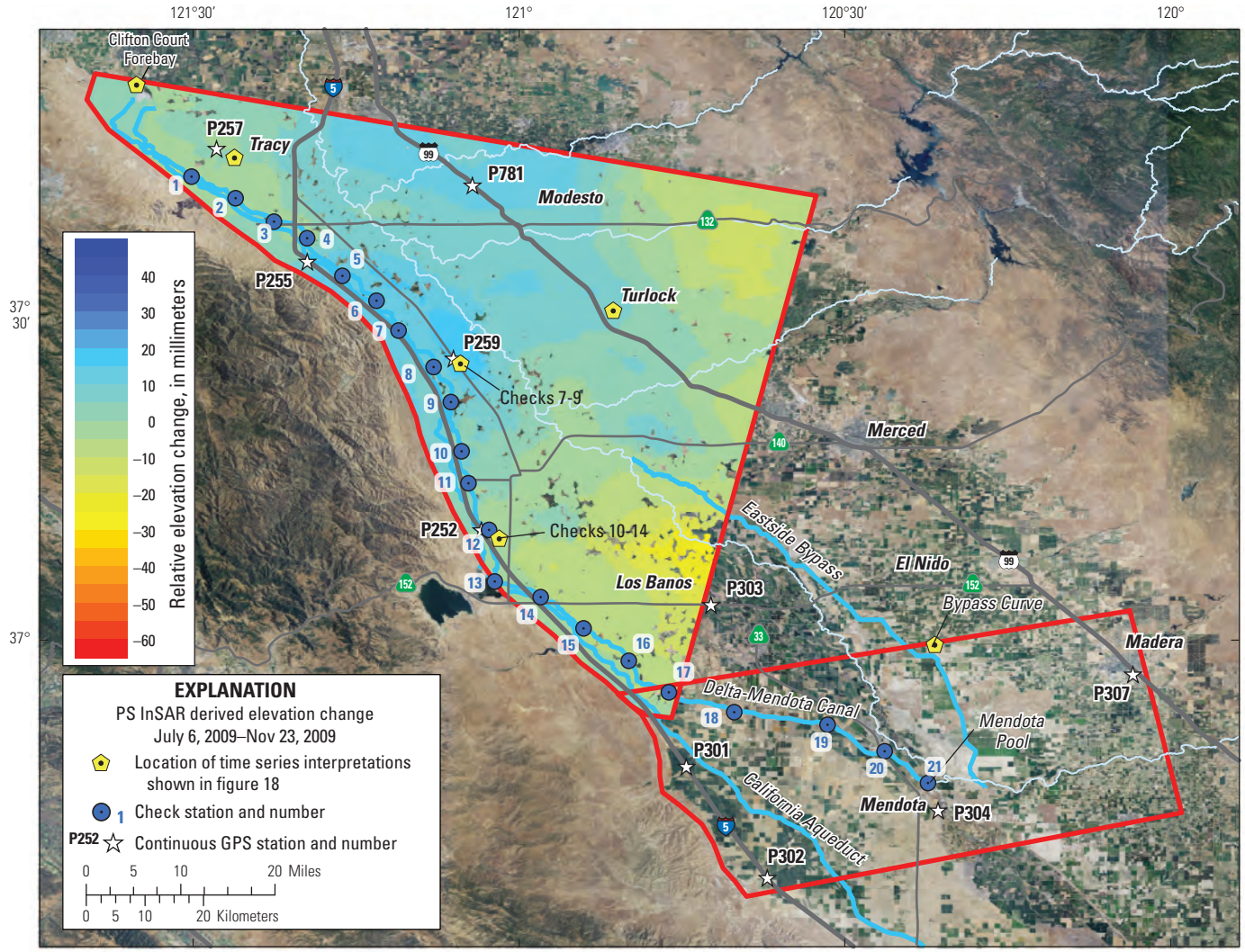

Figure C-4. Persistent Scatterer Interferometric Synthetic Aperture Radar (PS InSAR) Interferogram for the Northern Reaches of the Delta-Mendota Canal, ENVIronmental SATellite (ENVISAT) Track 299, July 6–November 23, 2009, San Joaquin Valley, California. Negative values indicate subsidence, and positive values indicate uplift.

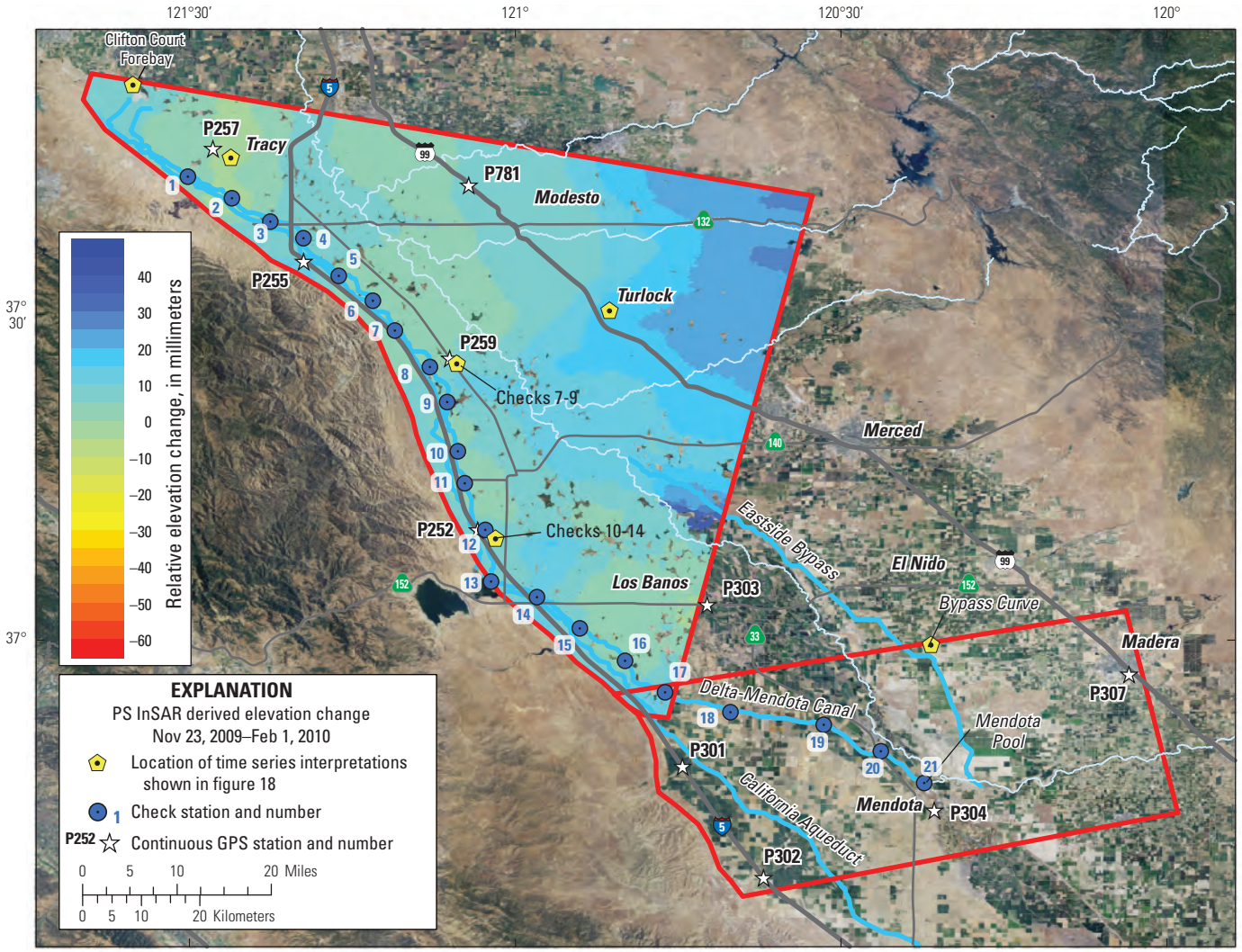

Figure C-5. Persistent Scatterer Interferometric Synthetic Aperture Radar (PS InSAR) Interferogram for the Northern Reaches of the Delta-Mendota Canal, ENVIronmental SATellite (ENVISAT) Track 299, November 23, 2009–February 1, 2010, San Joaquin Valley, California. Negative values indicate subsidence, and positive values indicate uplift.

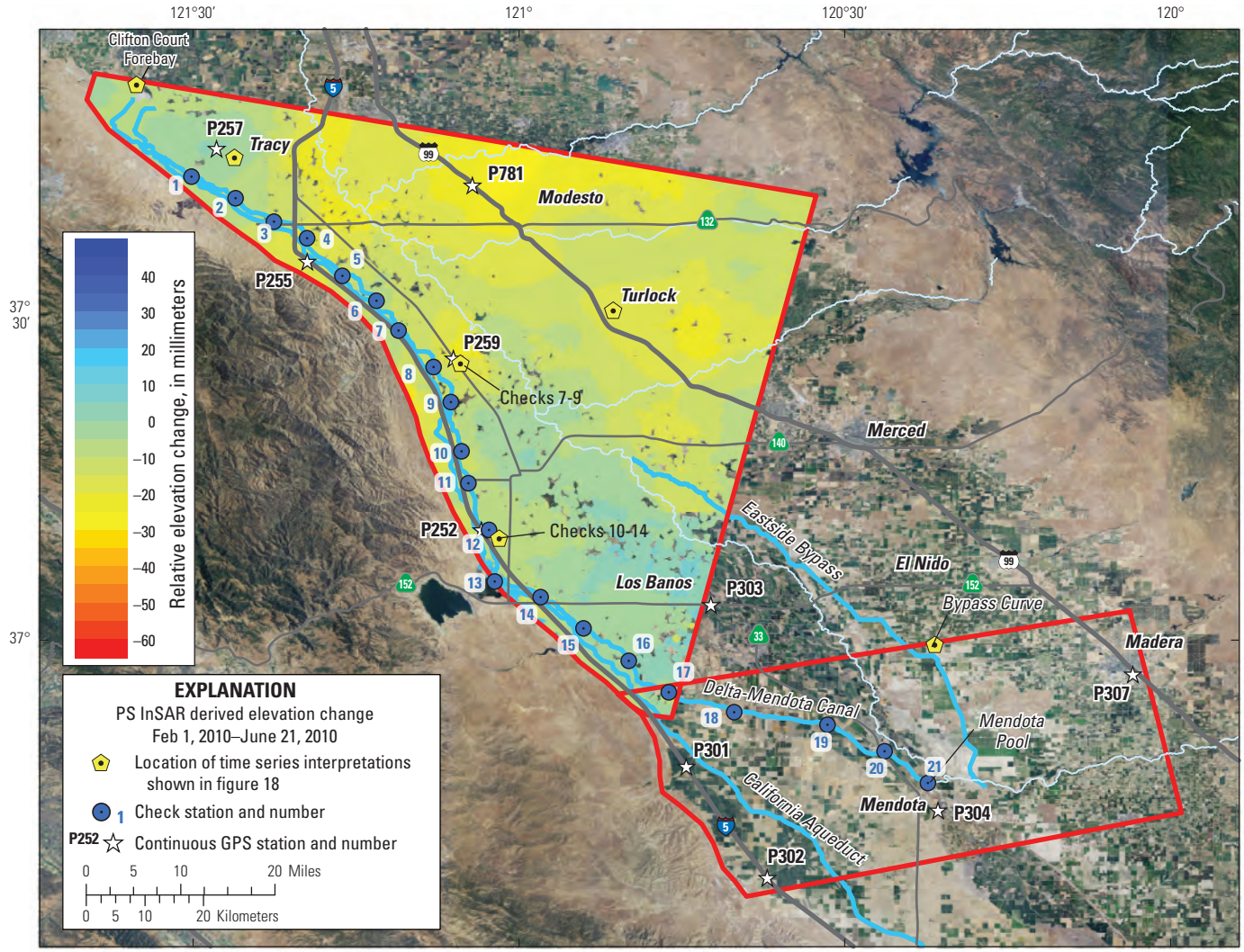

Figure C-6. Persistent Scatterer Interferometric Synthetic Aperture Radar (PS InSAR) Interferogram for the Northern Reaches of the Delta-Mendota Canal, ENVIronmental SATellite (ENVISAT) Track 299, February 1–June 21, 2010, San Joaquin Valley, California. Negative values indicate subsidence, and positive values indicate uplift.

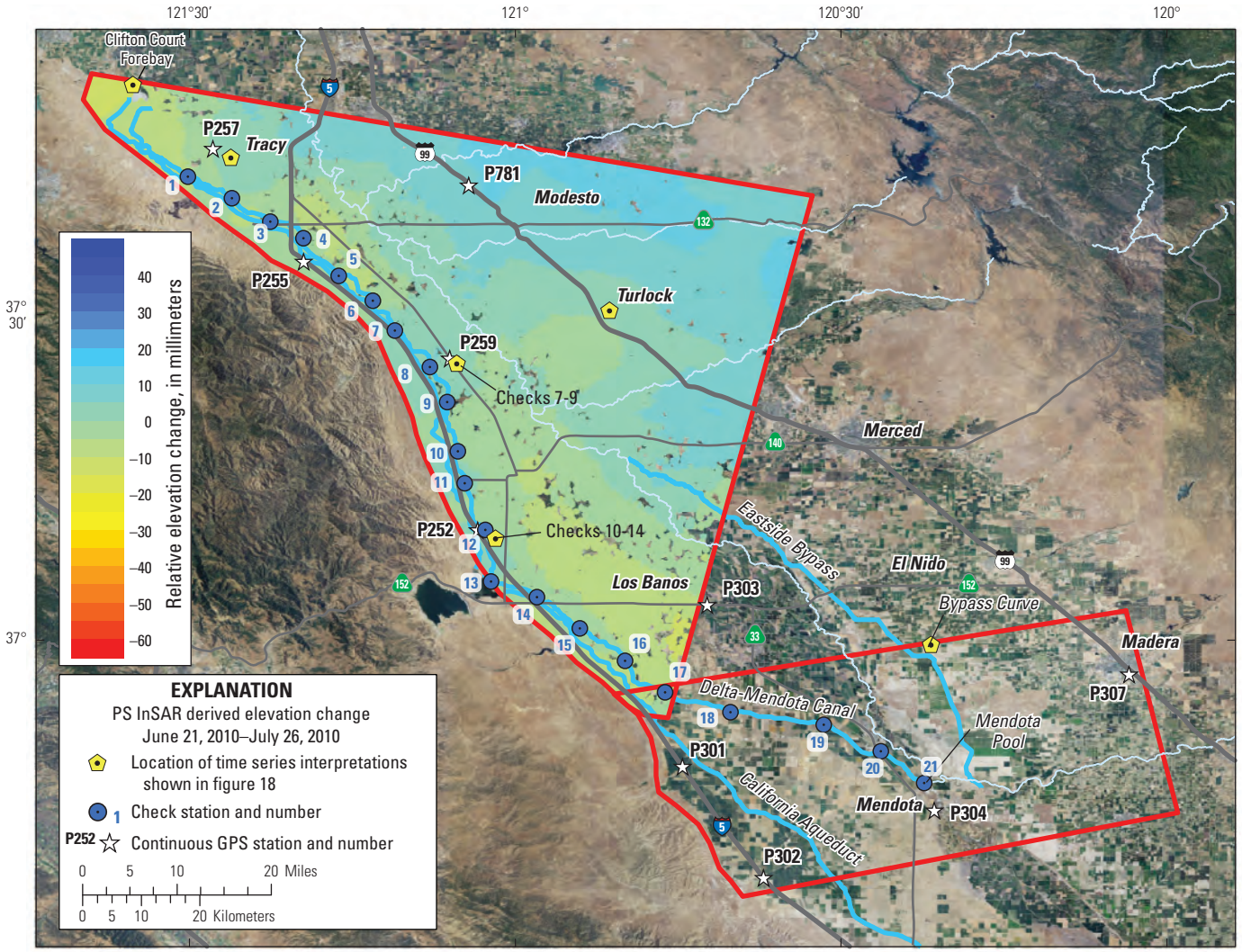

Figure C-7. Persistent Scatterer Interferometric Synthetic Aperture Radar (PS InSAR) Interferogram for the Northern Reaches of the Delta-Mendota Canal, ENVIronmental SATellite (ENVISAT) Track 299, June 21–July 26, 2010, San Joaquin Valley, California. Negative values indicate subsidence, and positive values indicate uplift.

Appendix D. Kriging Theory

Kriging is a method of interpolating the value of a random field (such as elevation) at an unobserved location based on a weighted average of observed values at nearby locations. Ordinary kriging was used to predict ENVIronmental SATellite (ENVISAT) Synthetic Aperture Radar (SAR) range changes where Persistent Scatterer (PS) Interferometric Synthetic Aperture Radar (InSAR) processing was unable to identify a stable point. If data are collected at spatial locations x_1, x_2,…, x_n, and the data are denoted $V(x_1)$, $V(x_2)$,…, $V(x_n)$, then the predicted value at an unobserved location x_0 is as follows:

$$\hat{V}(x_o) = \sum_{i=1}^{n} w_i \cdot V(x_i) \quad (1)$$

where

w_i are weights that sum to one, which are calculated so that the resulting prediction has desirable statistical properties (Isaaks and Srivastava, 1989).

A random function model underlies kriging and enables one to obtain estimated margins of error for interpolated values. In addition, ordinary kriging produces the best linear, unbiased estimator by minimizing the variance of modeled errors. The weights, w_i, are selected to minimize the kriging error:

$$w = C^{-1} \bullet D \quad (2)$$

where

C^{-1} is the inverse of the correlation matrix and

D represents the ordinary kriging system (Isaaks and Srivastava, 1989).

Kriging uses the spatial correlation of the data to improve interpolation. In kriging applications, spatially correlated data refer to data in which data values resemble values of nearby data. The data must exhibit spatial correlation for kriging to result in an improved interpolation over other interpolation techniques, such as inverse distance weighting. An empirical semivariogram can be used to quantify the spatial correlation as a function of distance between points and to calculate the weights in equations 1 and 2. The empirical semivariogram values are computed for each distance, *h*. First, all points separated by a distance *h* are identified. Second, for each such pair of points, the squared difference in observed values at the two locations is calculated. Third, the semivariogram value at *h* is one-half the average of the values computed in the second step. More succinctly, it is expressed:

$$\lambda(h) = \frac{1}{2N(h)} \sum_{i=1}^{N(h)} (x_i - y_i)^2 \quad (3)$$

where

$N(h)$ is the number of pairs separated by distance *h* (Isaaks and Srivastava, 1989).

This distance, *h*, is called the lag distance. Because few pairs of sites will be exactly *h* units apart, each lag distance, *h*, includes a tolerance so that the semivariogram estimate for *h* includes the distances that are near *h*.

Terminology related to the semivariogram includes the range, sill, and nugget effect. The range describes the distance at which the maximum variation among spatially correlated samples is achieved. The sill describes the maximum variation, which occurs at the range. A nugget effect accounts for the jump of values associated with the discontinuity at the origin. Typically, a mathematical model is fit to the semivariogram estimated from the data. Commonly used mathematical models include spherical, Gaussian, and linear functions. This mathematical function is plotted with the empirical semivariogram calculated from the observation data. This permits the analyst to determine how well the model fits the data. Once the semivariogram model is fit, the kriging weights and interpolated values can be calculated. A complete discussion on kriging methods can be found in Isaaks and Srivastava, 1989.

References Cited

Isaaks, E.H., and Srivastava, R.M., 1989, An introduction to applied geostatistics: New York, Oxford University Press.

Appendix E. Aquifer-System Compaction and Water Levels at Refurbished Extensometer Sites

Hourly aquifer-system compaction and water-level data have been recorded from the four refurbished extensometer sites (Oro Loma, Panoche, DWR Yard, and Rasta sites) since early 2012 (fig. 9C; table E-1*A*–*D*). Only the Oro Loma site is in the Delta-Mendota Canal study area. Although only a few months of data were available when this report was prepared, preliminary observations were made regarding the data collected from these sites and the performance of the extensometers. Small diurnal fluctuations correlated with shelter and equipment temperatures, and larger changes could be associated with water-level changes (table E-1; figs. E-1, E-2, E-3, and E-4). The digital extensometer record was not filtered to remove fluctuations associated with temperature variability because a longer dataset (covering a larger range in temperature variation) is needed to effectively filter the data and because this signal is significantly smaller than the signal that responds to water-level changes. Note that metric and English units are given in this section because table E-1 and the websites referenced show the data in English units.

Table E-1. Summary of preliminary data collected at the *A*, Oro Loma, *B*, Panoche, *C*, California Department of Water Resources (DWR) Yard, and *D*, Rasta refurbished extensometer sites from early 2012 through mid-June 2012. [Table E-1 is available in a Microsoft® Excel spreadsheet or an Adobe® Portable Document File (PDF) that can be accessed and downloaded from *http://pubs.usgs.gov/sir/2013/5142*].

Oro Loma Site

At the Oro Loma site, hourly data collection of water levels in 12S/12E-16H5 and -16H6, both screened below the Corcoran Clay, began February 3, 2012 (*http://waterdata.usgs.gov/ca/nwis/inventory/?site_no=365325120391504&agency_cd=USGS&amp*; and *http://waterdata.usgs.gov/ca/nwis/inventory/?site_no=365325120391505&agency_cd=USGS&amp*, respectively), and hourly data collection of aquifer-system compaction in Oro Loma Deep (-16H2) began February 27, 2012 (*http://waterdata.usgs.gov/ca/nwis/inventory/?site_no=365325120391501&agency_cd=USGS&amp*; table E-1*A*). The Oro Loma Deep extensometer measures aquifer-system compaction above 305 m (1,000 ft). Hourly records of water levels from February through mid-June 2012 in well-16H5 showed small fluctuations superimposed on an overall rise of less than 0.5 m (1.5 ft); those in well-16H6 showed small fluctuations superimposed on overall decline of about 2 m (6.5 ft; fig. E-1*A*). Hourly records of aquifer-system compaction from the Oro Loma Deep extensometer showed small diurnal fluctuations (fig. E-1*B*) superimposed on overall compaction of 3 mm (0.01 ft), mostly between late-May and mid-June, that could be associated with water-level changes in the deeper piezometer, -16H6; responses to water-level recovery in -16H5 were not readily discernible in the extensometer record. Beginning May 23, 2012, the effects of friction in the extensometer apparatus became evident by small vertical offsets in the digital hourly record. The friction likely was caused by contact between the extensometer cable and the down-hole casing, and has been noted in many extensometer records (Riley, 1986). The friction is often overcome (at least partially), but results in a frictional deadband in the extensometer record. Consequently, the time delay between actual compaction and recording of the compaction is unknown.

Panoche Site

At the Panoche extensometer/well, hourly data collection of water levels began April 19, 2012, and aquifer-system compaction data collection began April 5, 2012, in well 14S/13E-11D6 screened below the Corcoran Clay (*http://waterdata.usgs.gov/ca/nwis/inventory/?site_no=364358120314906&agency_cd=USGS&amp*; table E-1*B*). The Panoche extensometer measures aquifer-system compaction above 414 m (1,358 ft). The water-level record was dominated by a linear decline of more than 7.6 m (25 ft) through mid-June 2012; short-term fluctuations were not evident in the record (fig. E-2*A*). The extensometer indicated diurnal fluctuations (fig. E-2*B*) superimposed on a very small amount of aquifer-system expansion (1 mm or 0.003 ft). The apparent discordance between the measured water-level declines and the small measured aquifer-system expansion is hypothesized to occur because water-level changes measured in this depth interval (345–365 m) were not the dominant stresses causing the strain measured by the extensometer or because there was friction, which became evident in mid-June 2012.

DWR Yard Site

At the DWR Yard extensometer/well, hourly data collection of water levels and aquifer-system compaction began March 1, 2012, in well 18S/16E-33A1 screened below the Corcoran Clay (*http://waterdata.usgs.gov/ca/nwis/inventory/?site_no=361935120134501&agency_cd=USGS&amp*; table E-1*C*). The DWR Yard extensometer measures aquifer-system compaction above 314 m (1,029 ft). The water-level record showed several cycles of water-level declines followed by water-level recoveries, ranging in duration from 2 days to 2 weeks that probably are the result of nearby pumping (fig. E-3*A*). From March 2012 through mid-April 2012 water-levels declined about 7.6 m (25 ft). By mid-June 2012, water levels declined about 12 m (40 ft). The extensometer record showed small diurnal fluctuations (fig. E-3*B*) superimposed on overall compaction of 3 mm (0.01 ft) through mid-June 2012, when friction became evident that created deadband in the extensometer record.

Rasta Site

At the Rasta extensometer/well, hourly data collection of water levels began February 14, 2012, and aquifer-system compaction began April 4, 2012, in well 20S/18E-6D1 screened below the Corcoran Clay (*http://waterdata.usgs.gov/ca/nwis/inventory/?site_no=361334120035101&agency_cd=USGS&amp*; table E-1*D*). The Rasta extensometer measures aquifer-system compaction above 264 m (867 ft). The water-level record was dominated by a rapid water-level decline of about 35 m (115 ft) between mid-March and mid-June 2012 (fig. E-4*A*). The extensometer recorded small diurnal fluctuations (fig. E-4*B*) superimposed on overall compaction of 15 mm (0.05 ft) through mid-June 2012. Unlike the other extensometers discussed in this section, friction was not apparent in the Rasta extensometer record.

Summary of Preliminary Extensometer Data

The data collected since early 2012 through mid-June 2012 at the four refurbished extensometer sites indicated that further adjustments to the extensometers are needed to reduce friction. Additional data collection at these sites will help discriminate between various extensometric responses to aquifer-system processes and other environmental variables, which will be used to correct the preliminary data presented here. In addition to measurement of the magnitude of aquifer-system compaction and water-level elevations, the concurrent recording of hourly compaction and water-level data will be useful for detection of the change in the relationship between aquifer-system compaction and water levels if water levels fall below the preconsolidation head. The paired data collected at these sites also will be useful in determining aquifer-system storage properties (Riley, 1969).

References Cited

Riley, F.S., 1969, Analysis of borehole extensometer data from central California, *in* Tison, L.J., Land Subsidence: International Association of Hydrological Sciences Publication 89, v. 2, p. 423–431.

Riley, F.S., 1986, Developments in borehole extensometry, *in* Johnson, I.A., Carborgnin, Laura, and Ubertini, L., eds., Land subsidence: International Association of Scientific Hydrology Publication 151, p. 169–186.

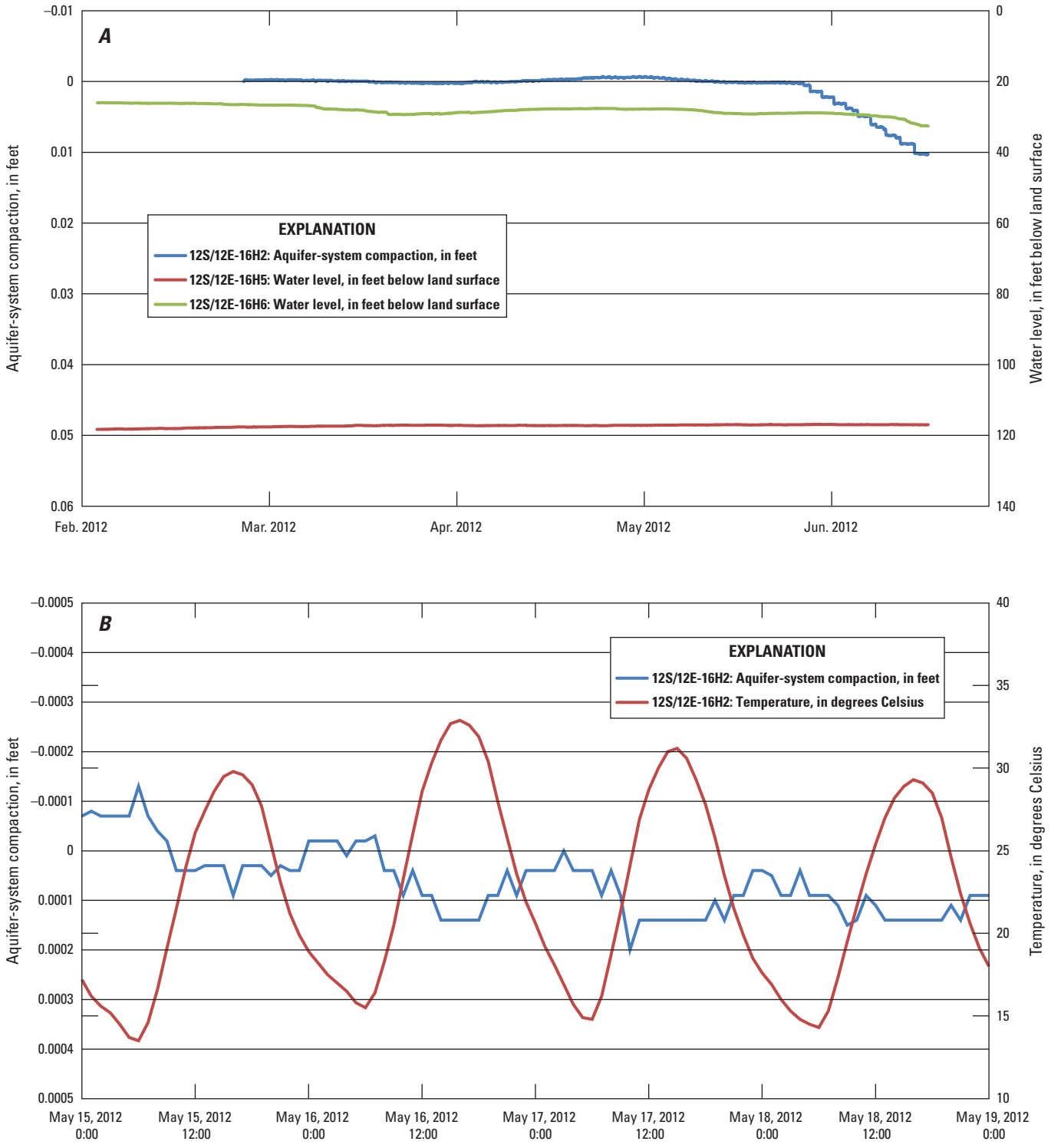

Figure E-1. *A*, Aquifer-system compaction measured using the Oro Loma Deep extensometer (12S/12E-16H2) and groundwater levels measured in wells 12S/12E-16H5 and -16H6 at the Oro Loma site, February–June, 2012 and *B*, Aquifer-system compaction and shelter temperature at the Oro Loma site, May 15–19, 2012.

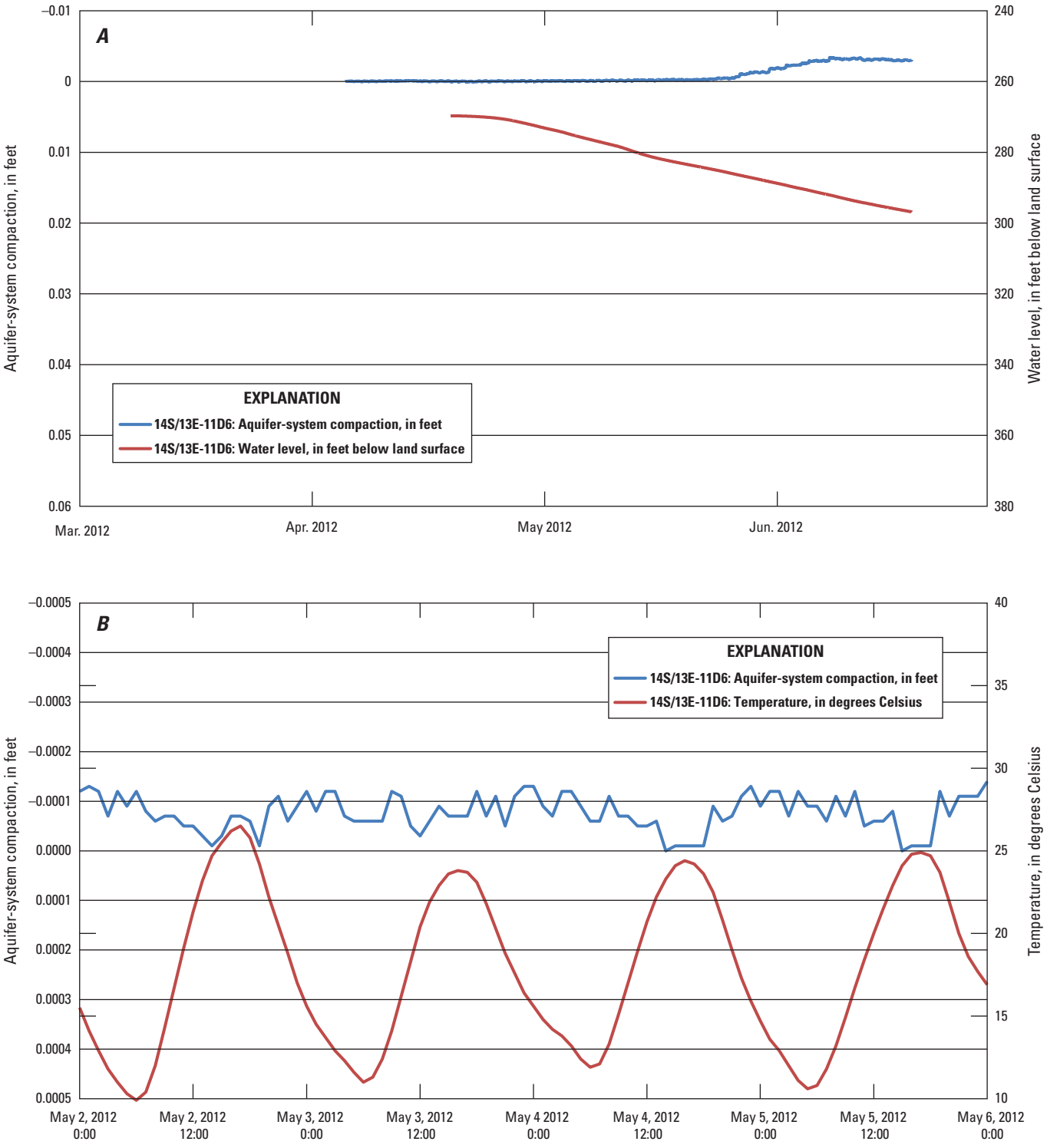

Figure E-2. *A*, Aquifer-system compaction and groundwater levels measured using the Panoche extensometer/well (14S/13E-11D6), April–June, 2012 and *B*, Aquifer-system compaction and shelter temperature at the Panoche site, May 2–6, 2012.

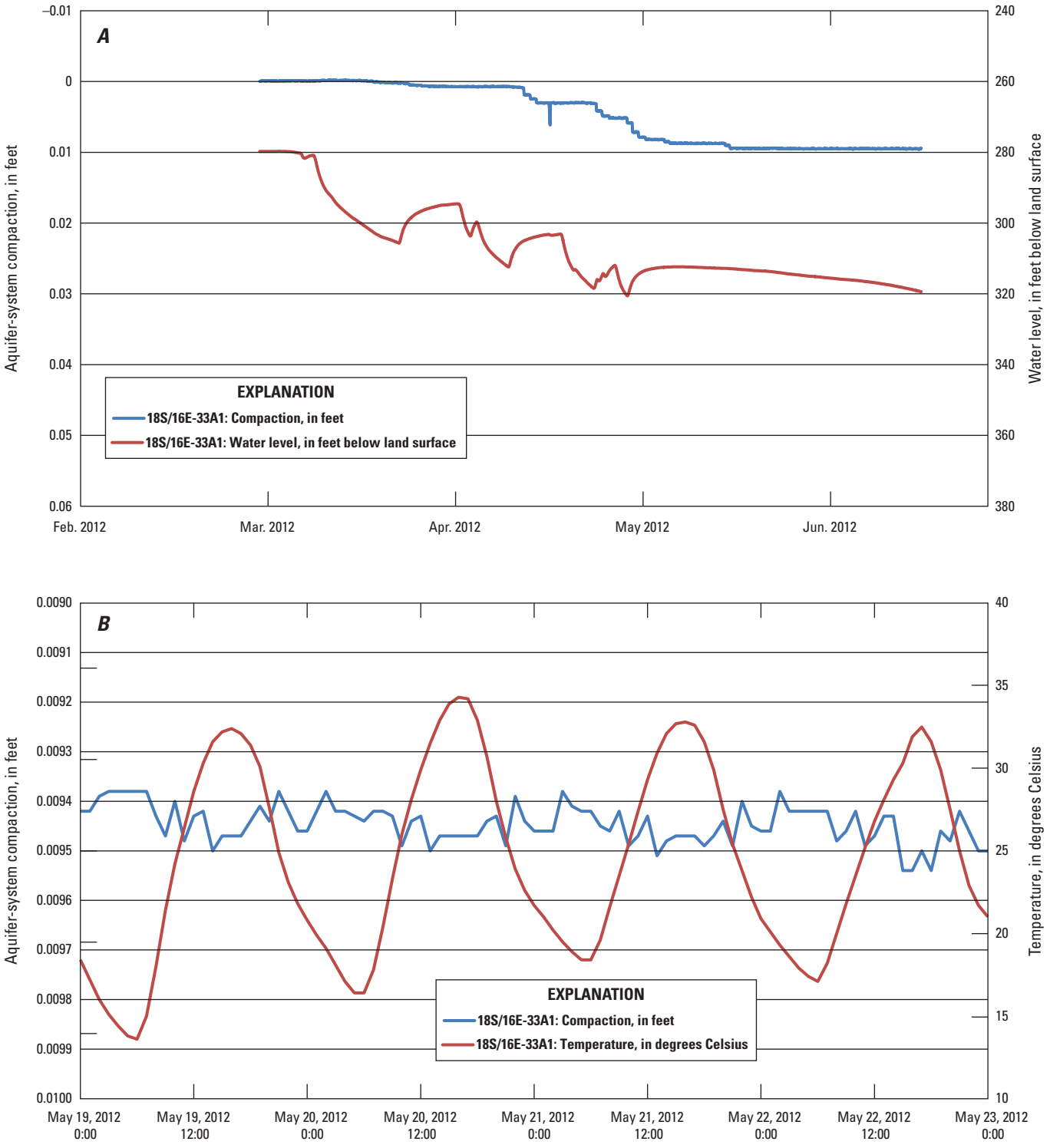

Figure E-3. *A*, Aquifer-system compaction and groundwater levels measured using the California Department of Water Resources (DWR) Yard extensometer/well (18S/16E-33A1), March–June, 2012 and *B*, Aquifer-system compaction and equipment temperature at the DWR Yard site, May 19–23, 2012.

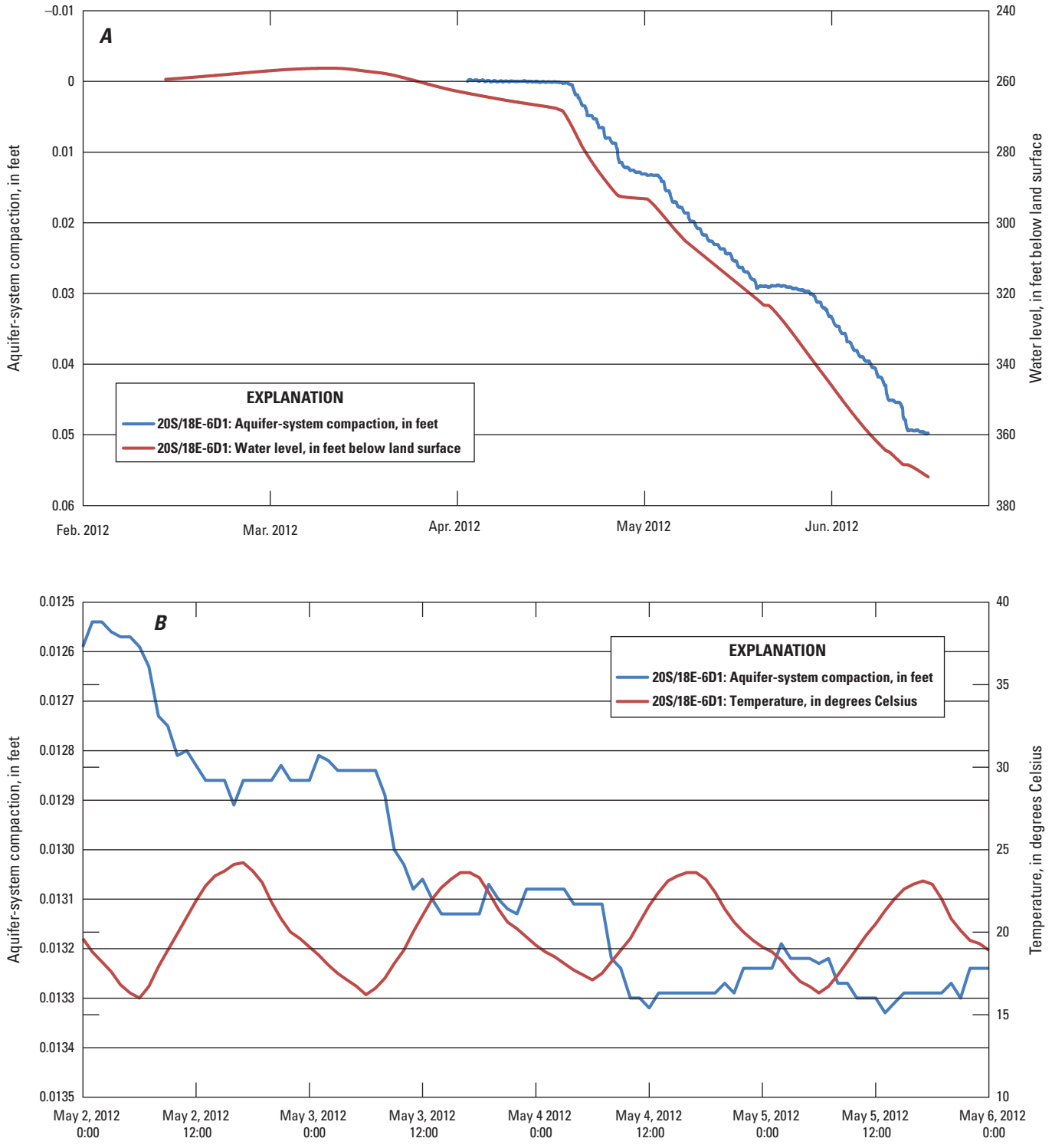

Figure E-4. *A*, Aquifer-system compaction for April–June, 2012, and groundwater levels for February–June, 2012 measured using the Rasta extensometer/well (20S/18E-6D1), and *B*, Aquifer-system compaction and equipment temperature at the Rasta site, May 2–6, 2012.

Prepared by the Sacramento Publishing Service Center.

For more information concerning this report, contact:

Director
U.S. Geological Survey
California Water Science Center
6000 J Street, Placer Hall
Sacramento, CA 95819
dc_ca@usgs.gov

or visit our Web site at:
http://ca.water.usgs.gov

ISSN 2328-0328 (online)
http://dx.doi.org/10.3133/sir20135142